DISSERTATION

APPLICATION OF THE VARIATIONAL METHOD FOR CORRECTION OF WET ICE ATTENUATION FOR X-BAND DUAL-POLARIZED RADAR

Submitted by

Leonid Tolstoy

Department of Electrical and Computer Engineering

In partial fulfillment of the requirements

For the Degree of Doctor of Philosophy

Colorado State University

Fort Collins, Colorado

Fall 2011

Doctoral Committee:

Advisor: V. N. Bringi
Co-Advisor: V. Chandrasekar

C.D. Kummerow
B. Notaros

ABSTRACT

APPLICATION OF THE VARIATIONAL METHOD FOR CORRECTION OF WET ICE ATTENUATION FOR X-BAND DUAL-POLARIZED RADAR

In recent years there has been a huge interest in the development and use of dual-polarized radar systems operating at X-band (~10 GHz) region of the electromagnetic spectrum. This is due to the fact that these systems are smaller and cheaper allowing for a network to be built, for example, for short range (typically < 30-40 km) hydrological applications. Such networks allow for higher cross-beam spatial resolutions while cheaper pedestals supporting a smaller antenna also allows for higher temporal resolution as compared with large S-band (long range) systems used by the National Weather Service.

Dual-polarization radar techniques allow for correction of the strong attenuation of the electromagnetic radar signal due to rain at X-band and higher frequencies. However, practical attempts to develop reliable correction algorithms have been cumbered by the need to deal with the rather large statistical fluctuations or “noise” in the measured polarization parameters. Recently, the variational method was proposed, which overcomes this problem by using the forward model for polarization variables, and uses iterative approach to minimize the difference between modeled and observed values, in a least

squares sense. This approach also allows for detection of hail and determination of the fraction of reflectivity due to the hail when the precipitation shaft is composed of a mixture of rain and hail. It was shown that this approach works well with S-band radar data.

The purpose of this research is to extend the application of the variational method to the X-band dual-polarization radar data. The main objective is to correct for attenuation caused by rain mixed with wet ice hydrometeors (e.g., hail) in deep convection. The standard dual-polarization method of attenuation-correction using the differential propagation phase between H and V polarized waves cannot account for wet ice hydrometeors along the propagation path. The ultimate goal is to develop a feasible and robust variational-based algorithm for rain and hail attenuation correction for the Collaborate Adaptive Sensing of the Atmosphere (CASA) project.

TABLE OF CONTENTS

List of Figures

List of Tables

Chapter 1

INTRODUCTION

The development of meteorological radars, operating at high frequency range (X-band, 8-12 GHz), began in the early 1950's. Because of high attenuation of the electromagnetic energy by liquid hydrometeors, mostly high power and long range, lower frequency radars, operating at C- (4-8 GHz) and S-band (2-4 GHz) were used by National Weather Service for weather observation purposes until recent times. With the invention of the dual-polarization technology which allows for correction of the strong attenuation of the radar signal due to rain at high frequencies, the development of X-band radars became feasible. A good example of application of these radars is the Collaborate Adaptive Sensing of the Atmosphere (CASA) project. Its goal is to create a distributed network of small, cheap, short-range X-band radars to overcome the Earth-curvature blockage and to allow for higher cross-beam spatial resolutions in the lower troposphere. Also, cheaper pedestals supporting a smaller antenna allows for higher temporal resolution as compared with large S-band (long range) systems used by the National Weather Service at the present time (McLaughlin et al. 2005, Brotzge et al. 2005).

Conventional radars cannot distinguish hail from heavy rain, and the measurements are very difficult to correct for attenuation. Dual-polarization

radars can overcome these problems via the measurement of differential propagation phase (e.g., chapter 7 of Bringi and Chandrasekar, 2001).) There are several well developed methods to correct for rain attenuation using polarimetric algorithms (Park et al. (2003a), Liu et al. (2006)). But attenuation due to wet ice was ignored in much of the previous studies because of the complexity of the problem. Mie theory was used by Battan (1971) and Atlas et al. (1960) to calculate the radar attenuation of wet ice spheres for S-, C- and X-bands, and it was found that thin water layer surrounding the hail particle can cause a significant attenuation, especially at X-band. While methods to correct for rain attenuation make use of the close relation between the differential propagation phase (Φ_{dp}) and path integrated attenuation (or PIA), when wet ice is present along the path, differential propagation phase is not affected by the isotropic wet hail, but reflectivity is affected. Hail detection is possible due to the fact that when hail is present, differential reflectivity (Z_{dr}) and specific differential phase shift (K_{dp}) provide complementary information (Smyth et al 1999). Hailstones are usually close to spherical, and they usually tumble during the fall, so their intrinsic Z_{dr} and K_{dp} are close to zero. Besides, hail has considerably lower Z_{dr}, compared to the rain of the same reflectivity. Hence the combination of Z, Z_{dr} and K_{dp} can be used to detect hail (e.g., chapter 7 of Bringi and Chandrasekar 2001 and references contained therein). Another problem is that there are large statistical fluctuations or “noise” in the measured polarization parameters, so practical attempts to develop reliable correction algorithms have been cumbered by the need to deal

with it. It is necessary to average K_{dp} and Z_{dr} over several kilometers, which leads to ”over-smoothing” of the retrieved parameters and loss of resolution.

Recently, the variational method was proposed by Hogan (2007) , which overcomes these problems by using the forward model for polarization variables, and uses iterative approach to minimize the difference between modeled and observed values, in a least squares sense. This approach also allows for detection of hail and determination of the fraction of reflectivity due to the hail when the precipitation shaft is composed of a mixture of rain and hail. It was shown that this approach works well with S-band radar data.

Research objectives

The research objectives are focused in two general directions:

- Tune the forward model (FM) used in the variational algorithm for better performance at X-band, and specifically for CASA radars. It can be achieved by fine tuning of the observational errors for CASA radars, and fine tuning *a priori* values of coefficient *a* in the $Z_h=aR^b$ relationship. Also it might be feasible to add to the set of the input variables in the state vector.
- Extend the variational method to handle cases with wet ice and hail in deep convection with focus on CASA applications (hail attenuation correction). It can be achieved by improving the hail detection (by using other methods for “initial guess” of hail location and estimation of

reflectivity fraction due to hail). This initial data can be supplied to the algorithm to improve its convergence to an “optimal” state.

Chapter 2

THEORETICAL BACKGROUND

2.1 Interaction of electromagnetic wave with hydrometeors

The radar is the principal device that is used for weather observation. The principle is based on the interaction of the electromagnetic energy emitted by the radar with the scatterers (e.g. hydrometeors – rain drops, hail stones, etc). The energy reflected back from the scatterer to the receiving antenna depends on the backscatter cross section (or radar cross section) σ_b of the reflecting particle. The σ_b is defined as an apparent area that intercepts a power σS_i , which if scattered isotropically, produces at the receiver a power density

$$S_r = \frac{S_i \sigma_b}{4\pi r^2} \tag{2.1}$$

equal to that scattered by the actual hydrometeor (Doviak and Zrnic, 1993). For the small spherical water drop of diameter D, if D is small compared to electromagnetic incident wavelength λ (Rayleigh's approximation $D < \lambda/16$), backscattering cross section can be approximated by

$$\sigma_b = \frac{\pi^5 |K|^2 D^6}{\lambda^4} \tag{2.2}$$

where $|K|^2 = \left|\frac{(\varepsilon_r - 1)}{(\varepsilon_r + 2)}\right|^2$ (2.3)

is a dielectric factor, and ε_r – complex relative permittivity of the dielectric, or complex dielectric constant (exp(-*jωt*) time convention is used here):

$\varepsilon_r = \varepsilon' + i\varepsilon''$

Real part of ε_r is the relative permittivity, imaginary part is the loss factor, associated with wave attenuation (Sadiku 1985). The dielectric factor K depends on the wavelength and temperature. Complex refractive index N is related to ε_r, with $N = \sqrt{\varepsilon_r}$.

Table 2-1 Refractive index of water and ice for radar frequencies

Frequency, GHz	**Refractive index of water at temperature 0 C**	**Refractive index of ice at temperature 0 C**
3	9.035 + 1.394i	$1.783 + 5.474 * 10^{-3}$i
6	8.227 + 2.341i	$1.782 + 3.344 * 10^{-3}$i
10	7.089 + 2.907i	$1.781 + 2.325 * 10^{-3}$i

The dielectric factor K^2 (at 3 GHz and 0 C) for water is ~0.93 and for ice is ~0.17 (Bringi and Chandrasekar 2001, p. 433), which means that backscatter cross section for dry ice hydrometeor (like dry hail) of the same size as liquid or water-coated hydrometeor is about 5 times lower. However, numerical calculations and experiments confirm that ice spheres can have larger backscatter cross section than water spheres of the same diameter (Atlas et al.1960), because of the angle (θ,ϕ) dependence of the radiation pattern of the scattered energy (Luneberg lens mechanism). Scattered energy is more directive

in the back direction (to the radar antenna) for ice sphere than for water sphere of the same diameter.

An electromagnetic wave in air suffers power loss both due to energy absorption and scattering. Absorption of the hydrometeor depends on the absorption cross section σ_a, an apparent area that intercepts from the incident radiation a power equal to the power dissipated as heat. Scattered energy depends on the scattering cross section σ_s, an apparent area that, when multiplied by the incident power density, gives the power equal to that scattered by the particle. For small spheres $\sigma_s = 2\sigma_b /3$ (Battan 1973).

Total power loss due absorption and scattering is defined as the extinction cross section

$$\sigma_e = \sigma_a + \sigma_s \,, \tag{2.4}$$

$$\sigma_a \approx \frac{\pi^2 D^3}{\lambda} \mathrm{Im}(-K) \tag{2.5}$$

$$\sigma_s \approx \frac{2\pi^5 D^6}{3\lambda^4} |K|^2 \tag{2.6}$$

For low radar signal frequencies (~3 GHz), attenuation occurs because of absorption, as usually $\sigma_a >> \sigma_s$. For high frequencies (~ 30 GHz), σ_a can be less than σ_s. Also, comparing refractive indexes of water and ice, we can see that imaginary part of it (loss factor), is much higher for liquid water, so specific attenuation caused by liquid hydrometeors is much higher than specific attenuation due to dry hydrometeors:

$$A = 4.343 * 10^3 \int_D \sigma_e(D) N(D) dD \quad dB/km \tag{2.7}$$

where N(D) is drop size distribution, defines the number of drops per unit volume of each diameter within the interval D to D+dD.

The radar reflectivity (η) (Bringi and Chandrasekar, 2001) can be defined as: $\eta = \frac{\lambda^4}{\pi^5 |K|^2} \int_D \sigma_b(D) N(D) dD$ (2.8)

where σ_b is the back scatter cross-section.

2.2 Radar parameters of liquid and dry hydrometeors

The discrimination of liquid and dry hydrometeors is based on the size, shape, orientation and dielectric factor properties. Liquid drops are oblate spheroids, with a nearly vertical orientation of their symmetry axes. Drop size distribution in exponential form can be expressed as:

$$N(D) = N_0 \exp(-3.67 \frac{D}{D_0}); \ mm^{-1}m^{-3} \quad (2.9)$$

where N_0 is the intercept parameter. There are several models describing relationship between rain drop shape and size. In general drops can be approximated as a sphere for small D, and it becomes an oblate spheroid with increasing diameter D.

Hailstones are characterized by wide variability of their size and, even though assumed to be spherical, they can be oblate and tumbling or their

surfaces can have large protuberances. Their size distribution in exponential form can be expressed as (Cheng and English, 1983):

$$N(D) = N_0 \exp(-\Lambda D) = 115\Lambda^{3.63} \exp(-\Lambda D); \;\; mm^{-1}m^{-3} \qquad (2.10)$$

but this relationship is not valid for all cases. There is no well-defined relationship between hail shape and size so far. There are documented hailstones of non-spherical shape (Knight 1986), but most commonly observed shapes for large hailstones are oblate spheroids (longest dimensions ~ 20 mm) or even conical (longest dimensions ~ 20-30 mm). Hailstones tumble as they fall and melt as they fall below the 0 C level. The melt water often forms an oblate shell around the ice core, which greatly improves orientational stability (typically for sizes<10 mm or so; see figure 7.45 of Bring and Chandrasekar 2001). To the radar such melting hailstones will appear as a “giant raindrops” and most frequently so at C-band due to strong resonant scattering.

These change in size, form and electrical properties of the particles lead to changes in polarization properties of the reflected radar signal. For oblate and prolate spheroids there is a difference in backscattering cross sections for horizontally and vertically polarized electromagnetic waves, and hence there is a difference in the radar measured vertical and horizontal reflectivities η_v and η_h:

$$\eta_{h,v} = \int \sigma_{h,v}(D) N(D) dD \qquad (2.11)$$

The differential reflectivity is defined as:

$$Z_{dr} = 10 \log (\eta_h/\eta_v) \qquad (2.12)$$

In addition, there is a difference in the propagation constants for horizontally and vertically polarized waves, which creates a phase shift, or differential propagation phase Φ_{dp}:

$$\Phi_{dp} = \Phi_{hh} - \Phi_{vv} \tag{2.13}$$

Specific differential phase K_{dp} is defined for a homogeneous path as:

$$K_{dp} = \frac{\Phi_{dp}(r_2) - \Phi_{dp}(r_1)}{2(r_2 - r_1)} \tag{2.14}$$

where r_1, r_2 are two different distances along the beam path ($r_2 > r_1$). K_{dp} is, by convention, defined to be positive for horizontally oriented oblate particles and negative for vertically oriented prolates.

In general, liquid hydrometeors as oblate oriented particles will have large Z_{dr} values for large drops, and low Z_{dr} values for small nearly spherical drops. K_{dp} and Φ_{dp} are sensitive only to the oriented oblate raindrops, so randomly oriented hailstones does not change K_{dp} and Φ_{dp} parameters. The reflectivity factor Z itself increases many times because of the water phase change. It worth noting that Z_{dr} due to mixture of oblate raindrops and spherical hailstones will be ~ 0 dB, because larger hailstones with axis ratio close to 1 will dominate and bias the total Z_{dr} value (Bringi and Chandrasekar 2001, p.390). A good signature of the hailshaft below the melting layer is a vertical region of reduced Z_{dr} values (<1 dB),

the so-called "Z_{dr}-hole", collocated or located very close to the region of high reflectivity values.

2.3 Discrimination between liquid and dry ice hydrometeors

To better understand the principles of the storm and precipitation development and quantitative parameter estimation (like rain rate), one needs to have reliable methods for classification of the hydrometeors. Two polarimetric variables are important for these purposes: Z_{dr} and Φ_{dp}, and reflectivity at horizontal polarization Z_h. Aydin et al.(1986) have introduced the concept of H_{dr}, defined as

$$H_{dr}=Z_h-f(Z_{dr}) \tag{2.15}$$

where Z_h is the measured reflectivity, and $f(Z_{dr})$ defines a straight line on Z_h vs Z_{dr} plot,

$$f(Z_{dr})=\left\{\begin{array}{ll} 27; & Z_{dr}\le 0 \ \ dB \\ aZ_{dr}+27; & 0<Z_{dr}\le b \\ 60; & Z_{dr}>b \end{array}\right\} \tag{2.16}$$

For 3 GHz frequency and equilibrium rain drop shape model give values a=16.5, b=2 dB.

This method allows for discrimination between pure rain and hail, it is simple and works well for altitudes below the melting level. Above approximately the -5 C level, frozen hydrometeors usually have Z_{dr}~0 dB and H_{dr} becomes

strictly proportional to Z_h. The magnitude of the H_{dr} itself can not be used to estimate the damage potential of the hailstorm, but there is some correlation with the maximum hail diameter (Depue et al. 2007; Bringi and Chandrasekar 2001, p 455). In particular for hailstorms in NE Colorado, Depeu et al. (2007) found that H_{dr}>20 dB was a reasonable threshold for detecting damaging hail (size>20 mm or so). This method does not work in case when hailstones fall in a mode which yields positive Z_{dr} in the same range as observed for oblate raindrops (Smyth et al. 1999).

For mixed-phase precipitation (where hail and rain coexist) another method was proposed by Golestani et al. (1989). The concept of Z_{dp} was introduced, defined as

$$Z_{dp}=10 \log_{10}(Z_h- Z_v) , \quad Z_h> Z_v , \text{ mm}^6 \text{ m}^{-3} \tag{2.17}$$

Z_{dp} is used to estimate the fraction of rain in the mixed precipitation, and works for the case when hail is nearly spherical in shape. The Z_{dp} here is due solely to rain, so there will be a straight line for pure rain on Z_{dp} vs Z_h plot. Given Z_h, Z_{dp} and the rain line, this method allows estimating contribution of rain Z_R to the total reflectivity Z, and so the fraction *f* is:

$$f= Z_R/(Z_R+ Z_H) \tag{2.18}$$

and the ratio of hail to rain reflectivity is

$$Z_H / Z_R=(1-f)/f \tag{2.19}$$

$$Z_H/Z= f_{hail}=1-f = 1 -10^{-0.1(\Delta Z)} \tag{2.20}$$

where ΔZ is horizontal deviation from the rain line in dB.

There is another simple method for estimation of fraction of ice in a rain/hail mixture, which uses reflectivity Z and specific differential phase K_{dp}. The K_{dp} is affected only by anisotropic rain drops, but not by isotropic hailstones.
The empirical relationship which distinguishes the boundary between pure rain from mixed phase and hail is given by (Doviak and Zrnic 1993, p. 261):

$$Z=8 \log_{10}(2K_{dp}) + 49 \quad (2.21)$$

For a given Z, the lower the measured K_{dp} from that calculated in (2.21), the higher the probability that precipitation contains hail (Doviak and Zrnic 1993). The fraction of reflectivity factor which is due to hail,

$$f_{hail} = Z_H/(Z_R+ Z_H) = (Z - Z_R)/ Z \quad (2.22)$$

and Z_R can be obtained from $Z_R – K_{dp}$ relationship. For 3 GHz radar, for example the mean relationship is given by (Doviak and Zrnic 1993, p. 262):

$$Z_{hR}=65800(K_{dp})^{1.386} , mm^6 m^{-3} \quad (2.23)$$

There are limitations of this method as the above relationship depends on the rain DSD. Also, the K_{dp} can only be obtained as a path average whereas the reflectivity is measured at each range gate. Balakrishnan and Zrnic (1990) provide a good overview.

There are also several more complicated methods for discrimination between liquid and dry ice hydrometeors, which are based on fuzzy logic, neural networks, and their combinations, and also dual-wavelength methods (see Chapter 7 of Bringi and Chandrasekar 2001).

Chapter 3

METHODOLOGY

In Hogan (2007), a method was described, which applies the variational approach to rainfall rate retrieval from the polarization radar variables Z, Z_{dr} and Φ_{dp}. This methodology, also known as “optimal estimation theory”, was used mostly in satellite retrievals, but has only recently been applied to radar applications (e.g., Austin and Stephens 2001; Löhnert et al. 2004). This method was shown to successfully overcome problems with other techniques, which appear due to inherent measurement fluctuations or “noise” in radar variables (Z_{dr} and K_{dp}). The K_{dp}, as the range derivative of an already noisy Φ_{dp}, can become negative, which is physically impossible in rain. The Z_{dr} and K_{dp} have to be averaged over some distance, so some sharp changes appear in the final field between averaged regions. Furthermore, it is difficult to design conventional algorithms to make use of Z_{dr} and Φ_{dp} simultaneously in all rain/hail regimes, so the most appropriate one usually has to be chosen (Hogan 2007).

The variational method overcomes these regime transitions by explicit treatment of the errors, includes attenuation correction to the forward modeling of Z and Z_{dr}, and allows for hail detection as well as retrieves the fraction of the reflectivity that is due to hail. It is designed to work for the following regimes:

- Very light rain: Rain drops are spherical, Z_{dr}, K_{dp} are ~0. Use a priori values of *a* and *b* in $Z_h=aR^b$ to estimate rain rate
- Light to moderate rain: Z_{dr}>0 dB, K_{dp} close to 0 deg/km. Z_{dr} provides information on *a*.
- Heavier rain: K_{dp}>0 deg/km, and so K_{dp} also has information on *a*. Method uses the known errors in Z_{dr} and Φ_{dp} to use both variables by weighting the information from both appropriately.
- Significant attenuation: Use Φ_{dp} for attenuation correction.
- Strong attenuation: It can result in differential attenuation, when Z_h is attenuated more than Z_v, and Z_{dr}, becomes negative at the far side of a region of heavy rain.
- Hail is present: Z_{dr} and K_{dp} of hail ~0. Combination of Z, Z_{dr}, K_{dp} is used to identify hail regions, and retrieve the fraction of the reflectivity that is due to hail. When there is a mixture of rain and hail, the rain rate can be estimated from K_{dp} alone, and fraction of the reflectivity that is due to hail can be estimated.

In general, for this algorithm to work, measurements have to be “cleaned” of noise and pixels below melting layer selected for the input, which is organized ray-by-ray. The forward model H(**x**), which is the essence of the variational method, will use the first guess of state vector **x** to predict the observations at each gate (vector **y**). The difference between predicted and observed variables is used to change state vector **x** for better fit with the observations **y** in a least

squares sense. This process would be repeated until convergence is reached. In state vector **x** we need to put variable that describes the rain rate, which in Hogan's (2007) formulation is the coefficient *a* between reflectivity and the rainrate R:

$$Z_h = aR^b, \tag{3.1}$$

b usually equals to 1.5 (for normalized gamma DSDs).

To guarantee the smooth variation in range and avoid "noise" problems, the coefficient *a* is represented by a set of *n* basis functions. Typically

$$n \sim m/10, \tag{3.2}$$

where *m* is number of the input gates in the beam.

By using ln(*a)* instead of just *a,* unphysical negative *a* values can be avoided; also more rapid convergence is realized, so the state vector for the single ray is given by:

$$\mathrm{x} = \begin{pmatrix} \ln a_1 \\ \vdots \\ \ln a_n \end{pmatrix} \tag{3.3}$$

It can be assumed that the error in Z_h is much less than the errors in Z_{dr} and Φ_{dp}, so Z_h can be omitted from the observation vector **y**:

$$\mathrm{y} = \begin{pmatrix} Z_{dr,1} \\ \vdots \\ Z_{dr,m} \\ \phi_{dr,1} \\ \vdots \\ \phi_{dr,m} \end{pmatrix} \tag{3.4}$$

One caveat is that the absolute calibration of the radar is accurate to within an uncertainty of 1 dB while the Z_{dr} is calibrated to within an uncertainty 0.2 dB.

Hogan (2007) has defined the cost function J as:

$$2J = \sum_{i=1}^{m} \frac{(Z_{dr,i} - Z'_{dr,i})^2}{\sigma^2_{Z_{dr}}} + \frac{(\phi_{dp,i} - \phi'_{dp,i})^2}{\sigma^2_{\phi_{dp}}} + \sum_{i=1}^{n} \frac{(x_i - x^a{}_i)^2}{\sigma^2_{x^a}} \quad (3.5)$$

where first summation represents the deviation of the observations Z_{dr} and Φ_{dp} from the values predicted by the forward model Z'_{dr} and Φ'_{dp}, and the second summation represents the deviation of the elements of the state vector from some a priori estimate x^a (a priori *a*=200 $mm^6m^{-3}(mm\ h^{-1})^{-1.5}$). The terms σ_{Zdr} and $\sigma_{\Phi dp}$ are the root-mean-square observational errors, and $\sigma_x{}^a$ is the error in the *a priori* estimate.

$$2J = \delta y^T R^{-1} \delta y + (x - x^a)^T B^{-1} (x - x^a) \quad (3.6)$$

where $\delta\mathbf{y} = \mathbf{y} - H(\mathbf{x})$, R and B are the error covariance matrices of the observations and the *a priori*. Hogan (2007) used the Gauss-Newton method to iteratively minimize the cost function. At iteration *k* an estimate of the state vector $\mathbf{x_k}$ and the corresponding forward-model estimate of the observations $H(\mathbf{x_k})$ are

obtained. The forward-model operator H(x) is nonlinear. The linearized cost function J_L is obtained by replacing H(x) in (3.6) by

$$H(\mathbf{x_k}) + H \times (\mathbf{x} - \mathbf{x_k}), \tag{3.7}$$

where H is the Jacobian, a matrix containing the partial derivative of each observation with respect to each element of the state vector. In this case it is a 2m - by - n matrix given by

$$H = \begin{pmatrix} \partial Z'_{dr,1}/d\ln a_1 & \ldots & \partial Z'_{dr,1}/d\ln a_n \\ \ldots & \ldots & \ldots \\ \partial Z'_{dr,m}/d\ln a_1 & \ldots & \partial Z'_{dr,m}/d\ln a_n \\ \partial \phi'_{dp,1}/d\ln a_1 & \ldots & \partial \phi'_{dp,1}/d\ln a_n \\ \ldots & \ldots & \ldots \\ \partial \phi'_{dp,m}/d\ln a_1 & \ldots & \partial \phi'_{dp,m}/d\ln a_n \end{pmatrix} \tag{3.8}$$

The state vector at the minimum of J_L is

$$\mathbf{x}_{k+1}=\mathbf{x}_k+A^{-1}[H^T R^{-1}\delta\mathbf{y} - B^{-1}(x_k-x^a)] \tag{3.9}$$

Here A is Hessian:

$$A=H^T R^{-1}H + B^{-1} \tag{3.10}$$

The forward model and H are recalculated for each iteration step until convergence (usually there are around 4 iterations).

The correction for attenuation is achieved within the forward model by using ln*a* and Z_h at a particular gate to estimate the associated attenuation, and then using it to correct Z_h at all subsequent gates. The possible instability due to

accumulation of small errors (scattering model errors or radar calibration errors) is fixed by the iterative nature of the method. If the first guess of ln*a* is too low then it will lead to an overestimate of the attenuation for a given measured Z_h, and hence the correction applied to Z_h will be increasingly overestimated at the gates after current. This will lead to the forward model overestimating both Z_{dr} and Φ_{dp} at these gates. When compared with the observed values, the scheme will know that it needs to increase ln*a* at the earlier gates to get a better fit to the observations, and the subsequent iterations will converge on a retrieval of ln*a* that is consistent with them.

If there is a hail segment in the ray, this scheme cannot find a solution for ln*a* that, when used in the forward model, can closely predict both Z_{dr} and Φ_{dp}, so it is done in 2 passes. The first pass is used for detection of the gates with the hail, and second is used for estimation of the fraction of the measured reflectivity due to hail.

At the first pass the σ_{Zdr} is increased (10 times), to make the solution to be consistent with the measured Φ_{dp} only. If hail is present in the gate it will appear as an overestimate of the Z_{dr} predicted by the forward model, so this gate will be marked as the one with hail.

The ad hoc criteria for the hail detection is that after correction for attenuation (and when $Z_h > 35$ dB) the Z_{dr} is overestimated by 1.5 dB (comparing measured and modeled values). At the second pass the σ_{Zdr} is returned to its original value and state vector is changed, to include the fraction *f* (in range 0 - 1) of the reflectivity factor that is due to hail for each gate marked as having hail. In

this way the scheme is able to find a combination of ln*a* and *f* that enable both Z_{dr} and Φ_{dp} to match the observed values. If the hail flag is triggered incorrectly than the second pass should retrieve low values of hail fraction *f*. The rainrate R is calculated from the rain part of the reflectivity:

$$R = [(1 - f)10^{0.1A_h} Z_h / a]^{1/b} \tag{3.11}$$

where A_h is the total 2-way attenuation at horizontal polarization in dB.

The flowchart of the variational scheme is shown next:

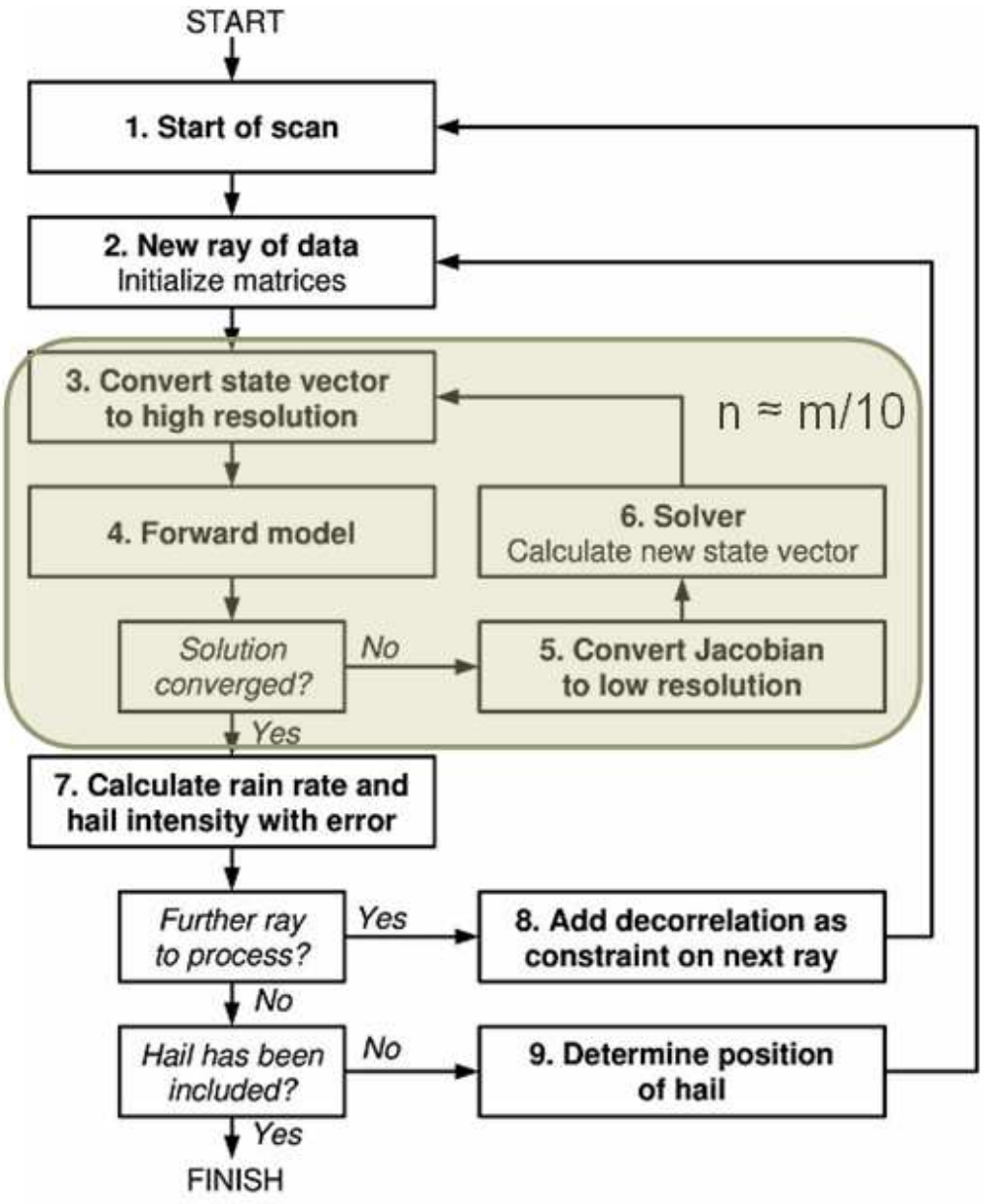

Figure 3-1. Flowchart of the variational scheme. Adapted from Hogan (2007).

3.1 Forward model

The forward model (FM) should predict values of Z'_{dr} and Φ'_{dp}, and the elements of the state vector ln*a*, having correct observed Z_h values. For this the scattering properties of oblate raindrops have been calculated using the T-matrix method (Waterman 1969) for equivalent-volume drop diameters between 0.1 and

10 mm. The Andsager et al. (1999) relationship for drop axial ratio as a function of diameter has been used. However, above 4.5 mm this relationship is not constrained by observations and predicts unrealistically low axial ratios, and therefore the axis ratio is seamlessly adjusted to the Goddard et al. (1995) shapes. Also, the temperature-dependent refractive index of liquid water is needed, which is calculated following Liebe et al. (1989) (Hogan 2007).

Lookup tables (LUT) for rain are constructed to relate Z_{dr} and K_{dp}/Z_h to the ratio Z_h/R. They are calculated from gamma DSD with a range of D_0 (median volume diameter), using T-matrix method. These LUT are shown in figure 3-2.

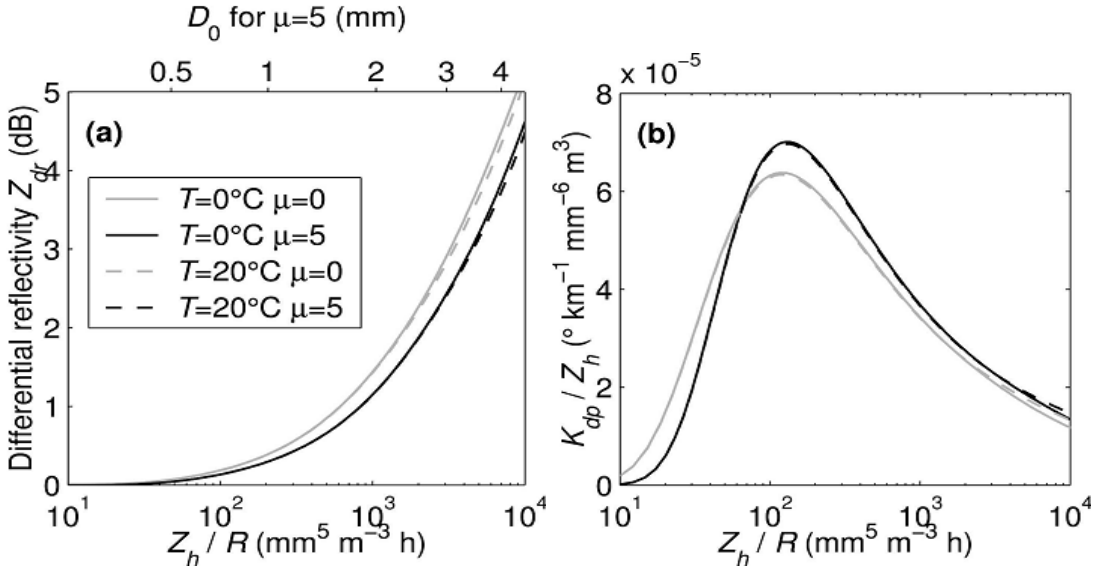

Figure 3-2. (a) Differential reflectivity Z_{dr} vs the ratio of reflectivity factor to rain rate Z_h/R for two values of temperature and two gamma-distribution shape parameters μ. The corresponding median volumetric diameter D0 for μ= 5 is shown on the upper axis.
(b) The ratio of one-way specific differential phase shift to reflectivity factor (K_{dp}/Z_h) vs Z_h/R. The calculations have been performed at S band (3 GHz) using the T-matrix method. (Adapted from (Hogan 2007)).

Then Z_h and ln*a* are used to calculate ln(Z_h/R) (from eq.3.1), and use ln(Z_h/R) to obtain Z_{dr} and K_{dp}/Z_h at each gate, and then calculate Φ'_{dp} by multiplying K_{dp}/Z_h by Z_h and integrating K_{dp} in range.

To calculate the attenuation, the estimate of the one-way specific attenuations for horizontal and vertical polarizations α_h, α_v (dB/km) are needed. This is done by using another set of lookup tables, which relate the ratio α_h/Z_h and $(\alpha_h-\alpha_v)/ Z_h$ to the ratio Z_h/R (figure 3-2). In the figure, (α_h, α_v) are referred to as *(a_h,a_v),* respectively. Attenuation depends on the imaginary part of the refractive index which strongly depends on the temperature, whereas Z_{dr} and K_{dp} depend on the real part, which does not depend on the temperature that much, so the LUT in figure 3-3 shows greater dependence on the temperature.

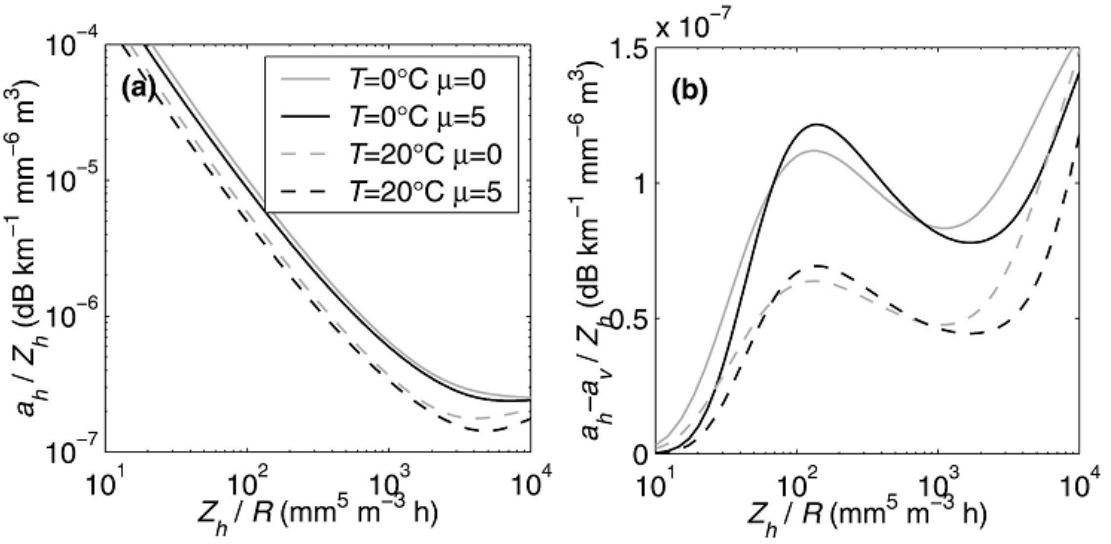

Figure 3-3. (a) The ratio of one-way specific attenuation at horizontal polarization to reflectivity factor (a_h /Z_h) vs Z_h/R for two values of temperature and two gamma-distribution shape parameters μ.
(b) The ratio of one-way specific differential attenuation to reflectivity factor (a_h-a_v)/Z_h vs Z_h/R. The calculations have been performed at S band (3 GHz) using the T-matrix method. (Adapted from (Hogan 2007)).

The forward model considers each range gate of the input radar beam in turn. At each gate *i* , the values of $Z_{h,i}$, ln(a_i), f_i, and total 2-way attenuations $A_{h,i}$, $A_{v,i}$ (dB) from LUT are available. The unattenuated reflectivity factors for rain and hail are calculated as:

$$\begin{aligned} Z_{h,i}^{rain} &= (1-f_i)10^{0.1A_{h,i}} Z_{h,i} \\ Z_{h,i}^{hail} &= f_i 10^{0.1A_{h,i}} Z_{h,i} \end{aligned} \tag{3.12}$$

Then $Z_{h,i}^{rain}$, ln(a_i) are used to calculate ln($Z_{h,i}^{rain}$/R), and LUT (figure 3-2.a) are used to obtain $Z_{dr,i}^{rain}$. The measured differential reflectivity is affected by hail, which is assigned an intrinsic differential reflectivity $Z_{dr,i}^{hail}$=0 dB, and differential attenuation, which is estimated as:

$$Z'_{dr,i} = Z_{dr,i}^{all} - A_{h,i} + A_{v,i} \tag{3.13}$$

where unattenuated differential reflectivity of the rain-hail mixture

$$Z_{dr,i}^{all} = -10 \log_{10}[f_i 10^{-0.1Z_{dr,i}^{hail}} + (1-f_i)10^{-0.1Z_{dr,i}^{rain}}] \tag{3.14}$$

The LUTs are used to calculate K_{dp}/Z_h, α_h/Z_h, α_v/Z_h from ln($Z_{h,i}^{rain}$/R_i), then recover $K_{dp,i}^{rain}$, $\alpha_{h,i}^{rain}$, $\alpha_{v,i}^{rain}$. Then forward model (FM) estimates the phase shift and total 2-way attenuations (V, H polarizations) in next gate *i+1* by accounting for contributions from rain and hail from the current gate:

$$\phi''_{dp,i+1} = \phi''_{dp,i} + 2\Delta r(K_{dp,i}^{rain} + K_{dp,i}^{hail}), \tag{3.15}$$

$$A_{h,i+1} = A_{h,i} + 2\Delta r(\alpha_{h,i}^{rain} + \alpha_{h,i}^{hail}) \tag{3.16}$$

$$A_{v,i+1} = A_{v,i} + 2\Delta r(\alpha_{v,i}^{rain} + \alpha_{v,i}^{hail}) \tag{3.17}$$

where Δr is range-gate spacing. The intrinsic attenuation of the hail $\alpha_{h,i}^{hail}$, $\alpha_{v,i}^{hail}$ are assumed to be small relative to rain attenuation.

Since the total attenuation and differential phase at the current gate are known, the algorithm proceeds to the next gate and repeats the procedure, thus obtaining Z_{dr}, Φ_{dp} at each gate of the beam.

The elements of the Jacobian matrix (3.7) are partial derivatives with respect to each element of the state vector:

$$\frac{\partial Z'_{dr,j}}{\partial \ln a_i} = 0.1\ln(10)(1-f_i)10^{0.1(Z^{all}_{dr,j}-Z^{rain}_{dr,j})}(1-1/b)\left[\frac{\partial Z_{dr}}{\partial \ln(Z_h/R)}\right]_j^{rain}\frac{\partial A_{h,j}}{\partial \ln a_i} - \frac{\partial A_{h,j}}{\partial \ln a_i} + \frac{\partial A_{v,j}}{\partial \ln a_i} \tag{3.18}$$

and

$$\frac{\partial \phi'_{dr,j+1}}{\partial \ln a_i} = \frac{\partial \phi'_{dr,j}}{\partial \ln a_i} + 0.2\ln(10)\Delta r \frac{Z_{h,i}^{rain}}{b}\frac{\partial A_{h,j}}{\partial \ln a_i}\left\{\frac{Kdp}{Z_{h,j}^{rain}} + (1-1/b)\left[\frac{\partial(Kdp/Z_h)}{\partial \ln(Z_h/R)}\right]_j^{rain}\right\} \tag{3.19}$$

Chapter 4

DATA SOURCES

To review this variational method, to see how well it works for different weather conditions, and find its advantages and drawbacks, it was applied to datasets from different radars, operating at S- and X-bands. These data sources are briefly described here:

CP2 radar

This is a dual-wavelength system, working at S-band (with polarimetric capabilities) and an X-band radar whose main beam is matched with the S-band beam (S and X-band antennas are mounted on the same pedestal). The CP2 radar is located at Redbank Plains (coordinates: Latitude 27°40.0' S, Longitude 152°51.5' E, altitude 15 m asl) near Brisbane, Australia, in a subtropical environment on the coastal zone of eastern Australia.

Table 4-1 Some technical details of the CP2 radar at Brisbane, Australia.

Characteristic of the CP2 radar	CP2 S-Band	CP2 X-band
Wavelength (cm)	10.7	3.2
Peak Power (kW)	1000	200
Beamwidth (degrees)	0.93	0.94
Polarizations radiated	LIN H, LINV	LIN H
Doppler Capability	Y	N
Number of Range Gates	1024	1024
Range Resolution (m)	> 30 typically 150	> 30 typically 150
Polarization Quantities measured	Z, Z_{DR}, Φ_{dp}, ρ_{HV}	Z, LDR

IHOP (International H2O Project)

This data comes from year 2002 summer (13 May–25 June) field campaign of the International H2O Project (IHOP2002), which was based in Oklahoma, northern Texas, and southern Kansas. The operations center was set in Norman, OK. This experiment involved six aircraft, 9 radars (2 fixed, 5 mobile, and 2 airborne), and a number of other weather instruments.

CASA KCYR

This data set was obtained from the CASA X-band radar network, operating in Oklahoma. There are four radar nodes operational now, located at Chickasha (KSAO; 35.0314^o lat., -97.9561^o lon., 355 m alt.), Rush Springs (KRSP; 34.8128^o, -97.9306^o, 436), Cyril (KCYR; 34.8740^o, -98.2512^o, 445), and Lawton (KLWE; 34.6239^o, -98.2708^o, 396)

.

Chapter 5

CASE STUDIES

The results of application of this variational algorithm to datasets from the aforementioned radars will be described now.

5.1 CP2 data

This S-band dataset was obtained from CP2 radar on March 26, 2008, 053922 UTC. It includes 16 PPI sweeps at different elevation angles. The 0.4 degree elevation angle sweep was analyzed first since no hail was detected. Hence, the variational method of Hogan (2007) which has been “tuned” for S-band is expected to work well in this situation. Figure.5-1 shows the PPI of input variables:

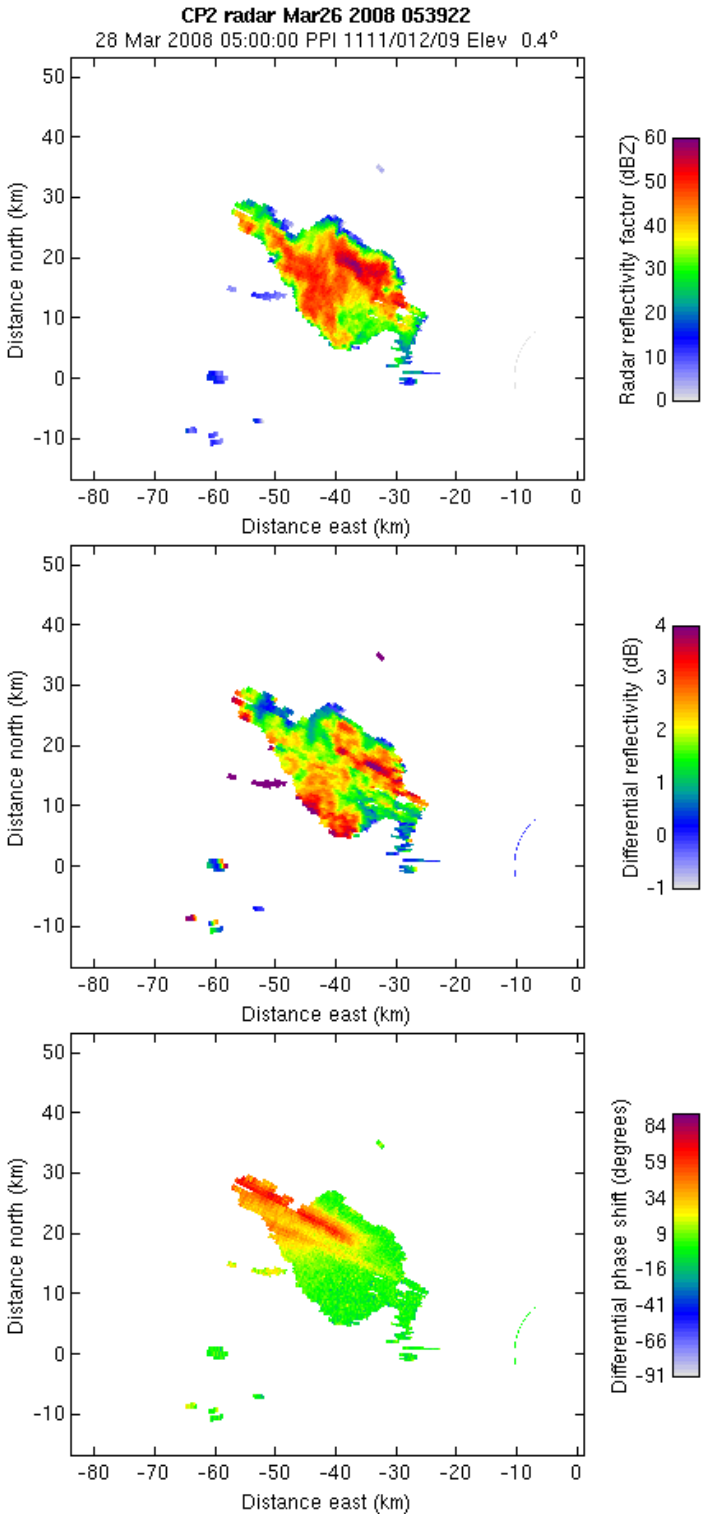

Figure 5-1. CP2 radar dataset, the 0.438 deg elevation angle. The input data to the variational algorithm: Z_h, Z_{dr}, Φ_{dp}.

The output of the variational algorithm is shown on the Figure 5-2:

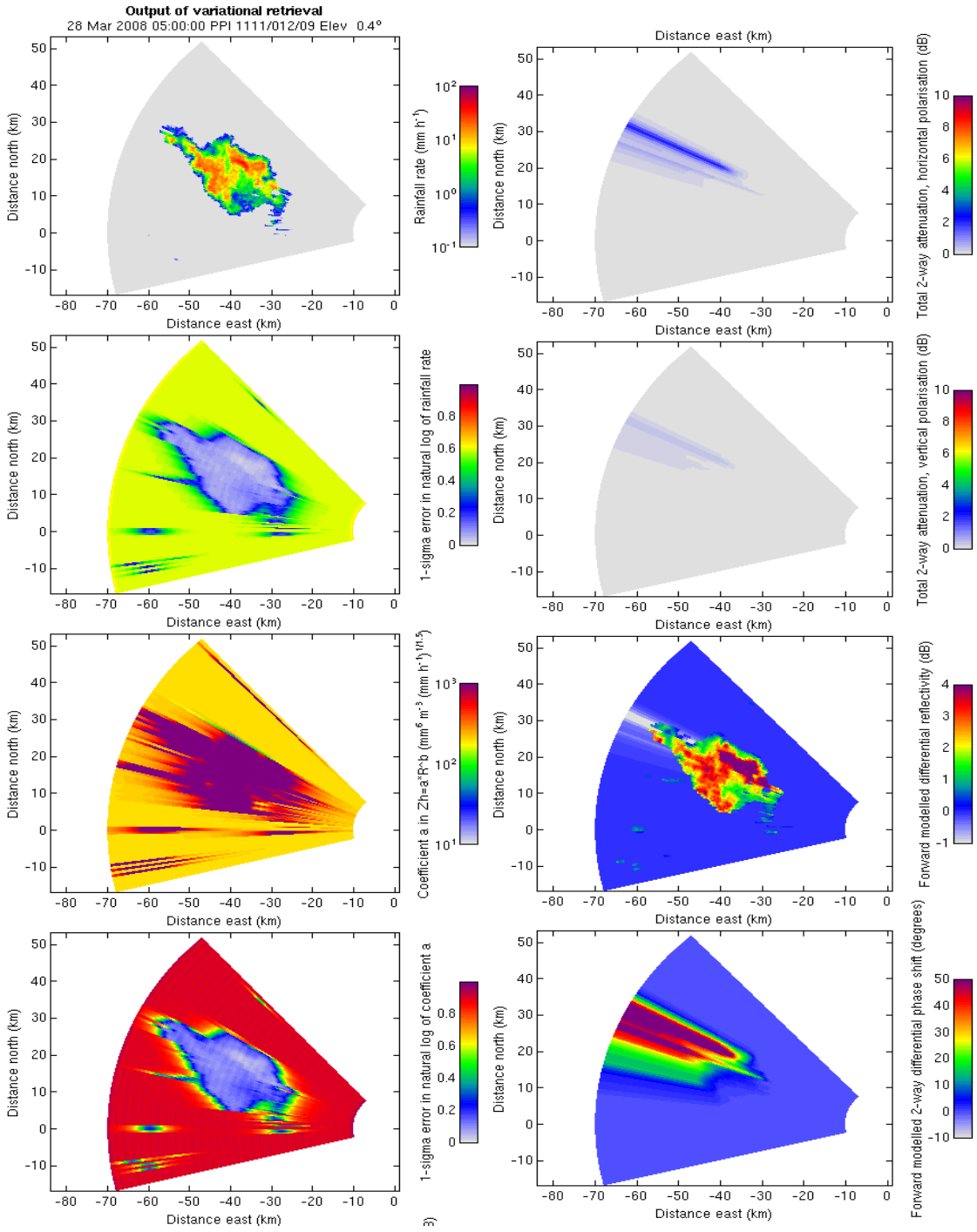

Figure 5-2. CP2 radar dataset, the 0.438 deg elevation angle. The output of the variational algorithm: rainrate R, 1-sigma error in natural log of R, coefficient *a* (from the $Z_h=aR^b$ relationship), 1-sigma error in natural log of *a*, total 2-way attenuation in vertical and horizontal polarizations, forward-modeled Z_{dr}, forward-modeled 2-way Φ_{dp}.

We now compare forward modeled variables with the input variables gate-by-gate for several beams:

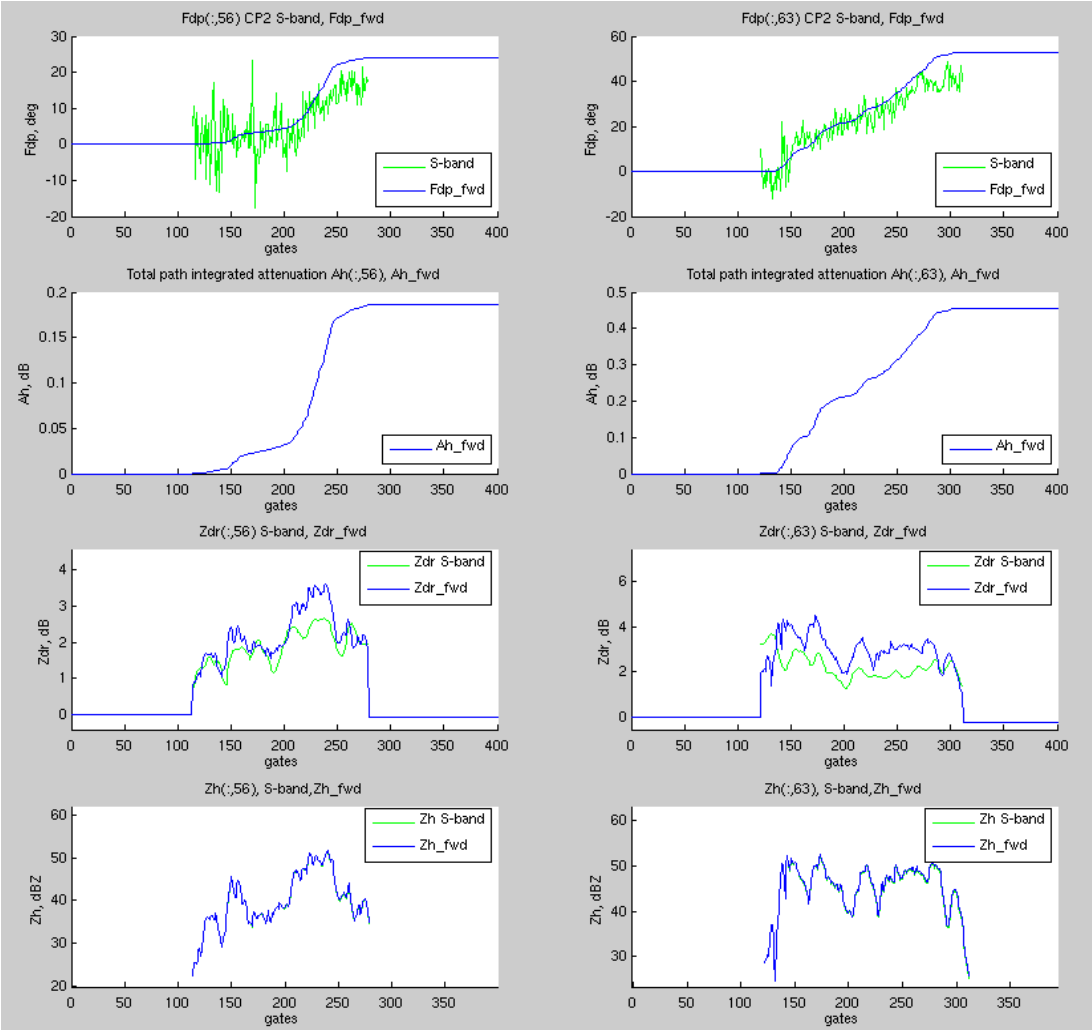

Figure 5-3. CP2 radar dataset, the 0.438 deg elevation angle. Gate-by-gate variables comparison for beams #56, #63.

The coefficient α is the multiplicative coefficient of the power-law of the form:

$$A_h = \alpha K_{dp}^{b} \qquad (5.1)$$

On average the coefficient α is near 0.017 and the exponent *b* is 0.84 at S-band (Bringi and Chandrasekar 2001). Here we see that Z_h from FM is very

close to Z_h observed, and Z_{dr}, Φ_{dp} values predicted by FM are in good agreement with observed values. It can be seen also by the histograms of the differences between observed and FM modeled values for the whole sweep (Figure 5-4):

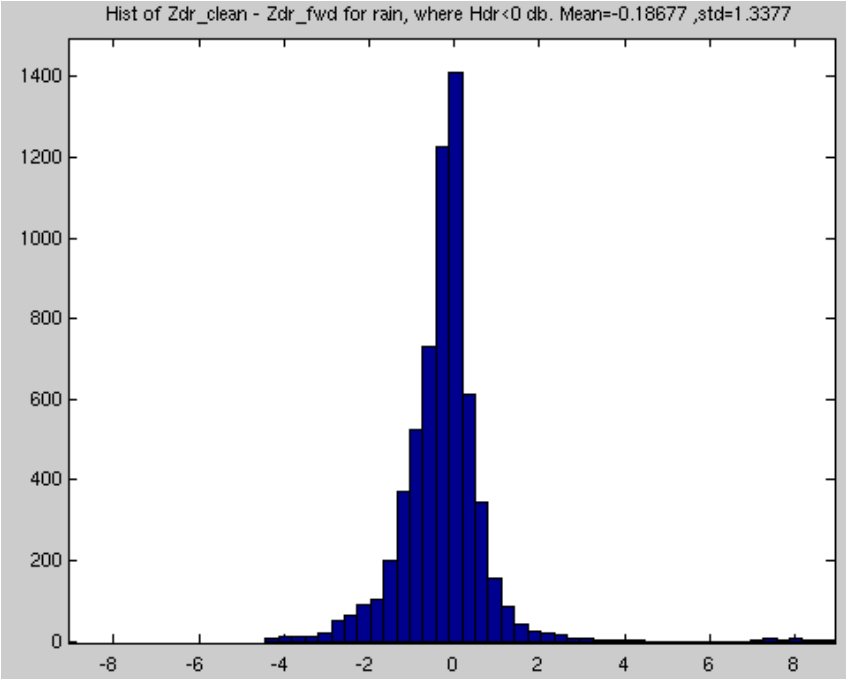

Figure 5-4. CP2 radar dataset, the 0.438 deg elevation angle. Histogram of the difference between observed and FM-modeled values for Z_{dr}, dB.

Another set of data from the CP2 radar from the same day but higher elevation angle of 4.6 deg is now considered since there was substantial areas where H_{dr}>5 dB indicative of hail. The PPI of the input variables is shown on the next figure:

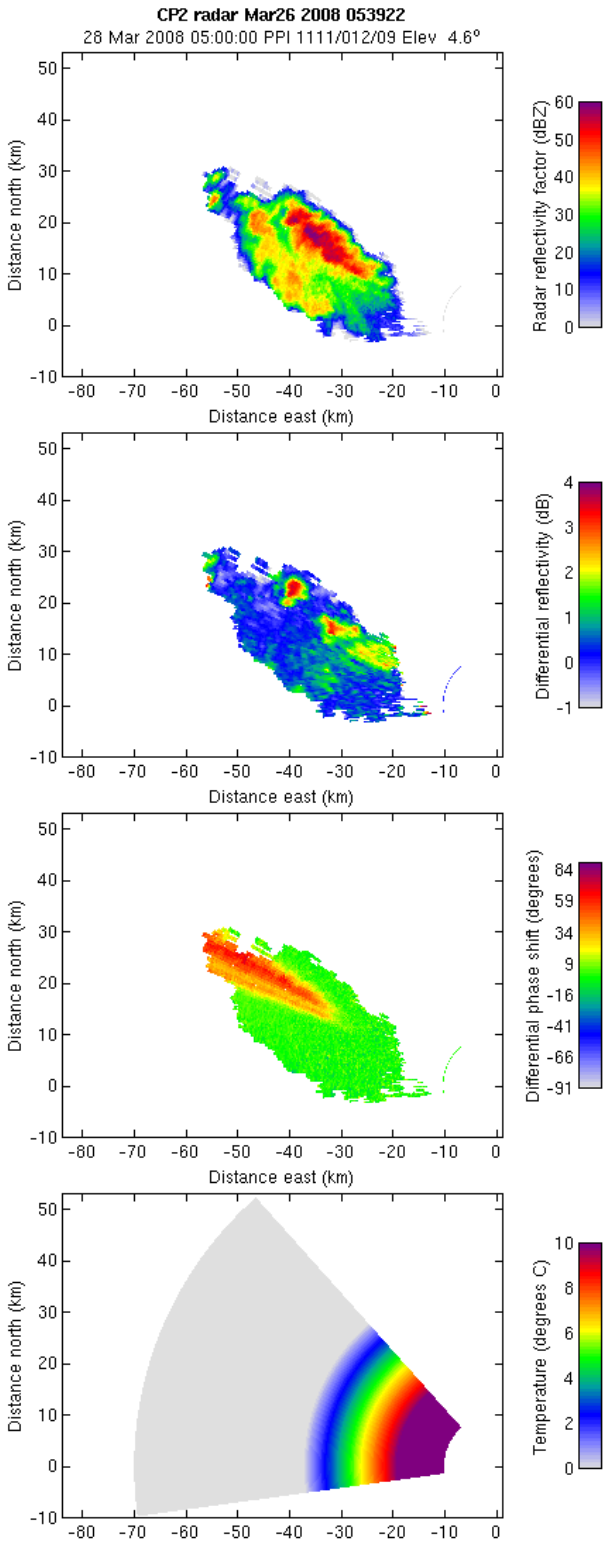

Figure 5-5. CP2 radar dataset, the 4.593 deg elevation angle. The input data to the variational algorithm: Z_h, Z_{dr}, Φ_{dp}. Also, approximate temperature variation is shown in the last panel.

The calculated H_{dr} values show gates where there is a high probability of hail:

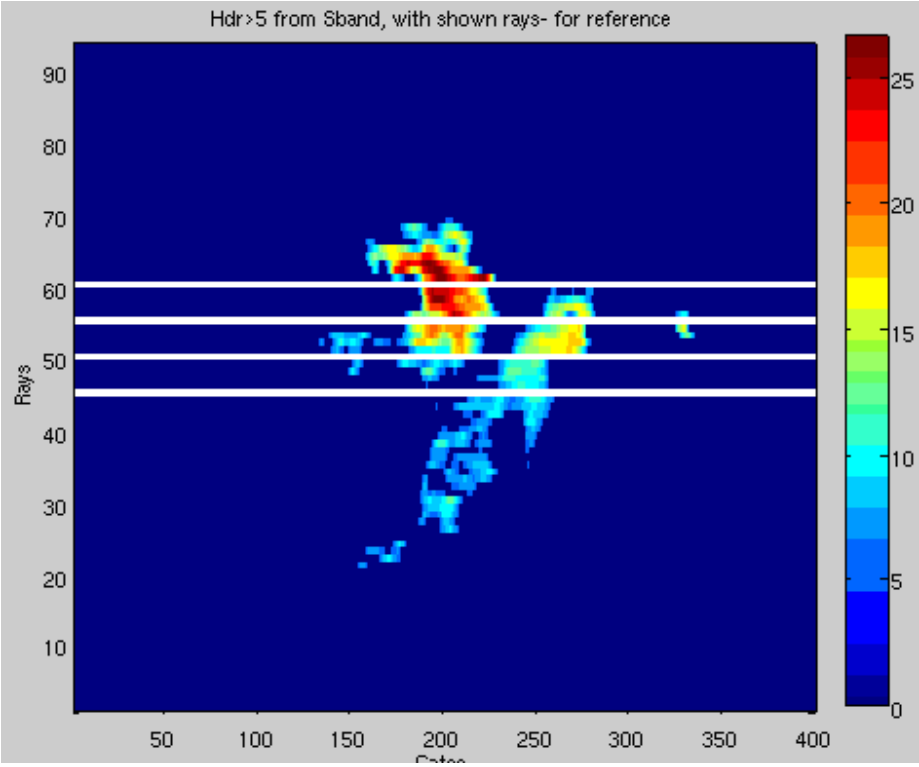

Figure 5-6. CP2 radar dataset, the 4.6 deg elevation angle. High values of H_{dr} (> 5 dB) indicate high probability of hail.

The next figure shows the output of the variational algorithm:

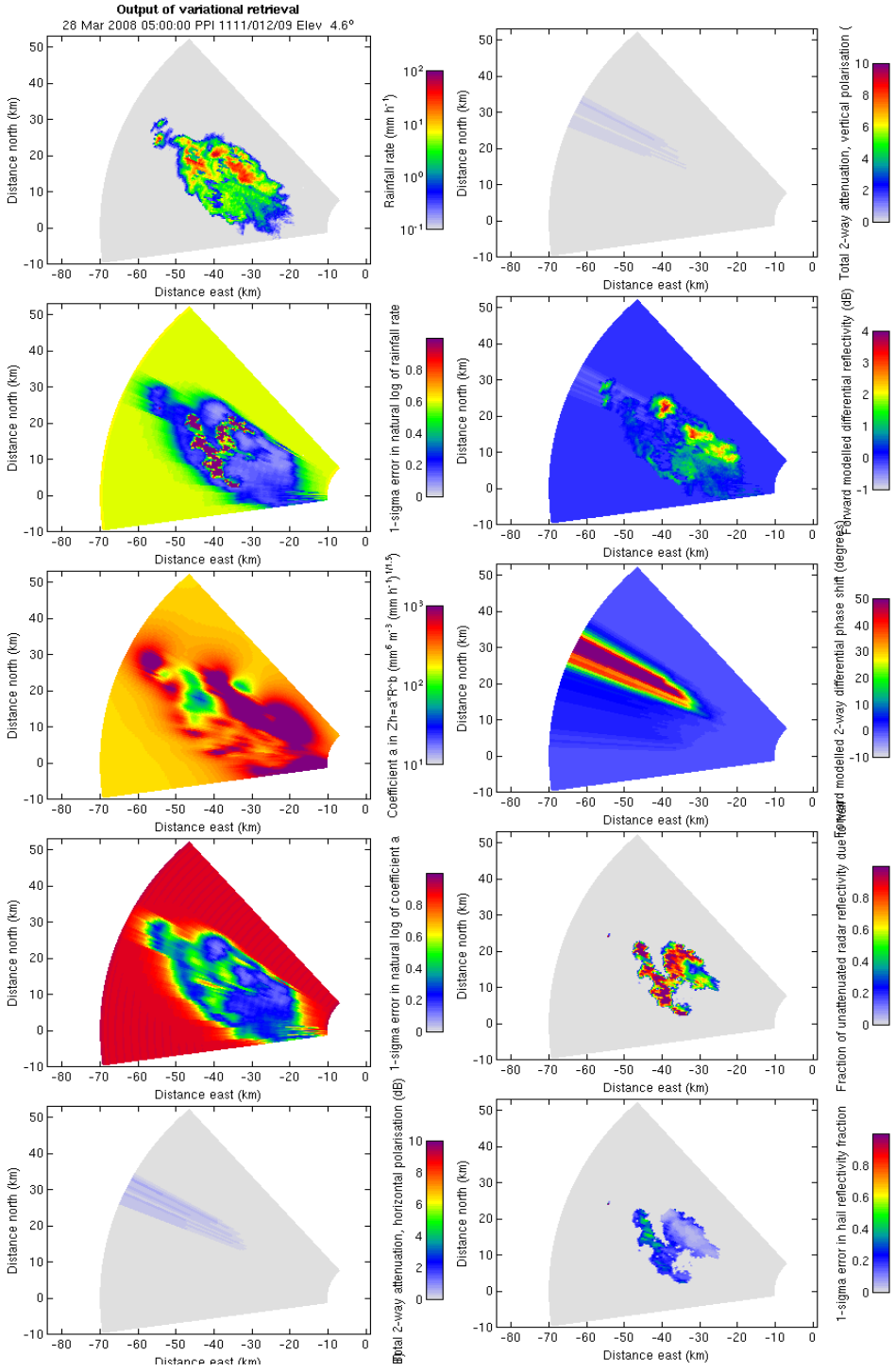

Figure 5-7. CP2 radar dataset, the 4.6 deg elevation angle. The output of the variational algorithm: rainrate R, 1-sigma error in natural log of R, coefficient *a* (from the $Z_h=aR^b$ relationship), 1-sigma error in natural log of *a*, total 2-way attenuation in vertical and horizontal polarizations, forward-modeled Z_{dr}, forward-modeled 2-way Φ_{dp}, fraction of unattenuated radar reflectivity due to ice *f*, 1-sigma error in hail reflectivity fraction.

We can compare forward modeled variable with the input variables gate-by-gate for several beams for this elevation angle. Here the algorithm takes 2 passes to find hail and estimate the fraction of reflectivity due to hail *f*. The next figure shows also H_{dr} values, calculated from S-band data:

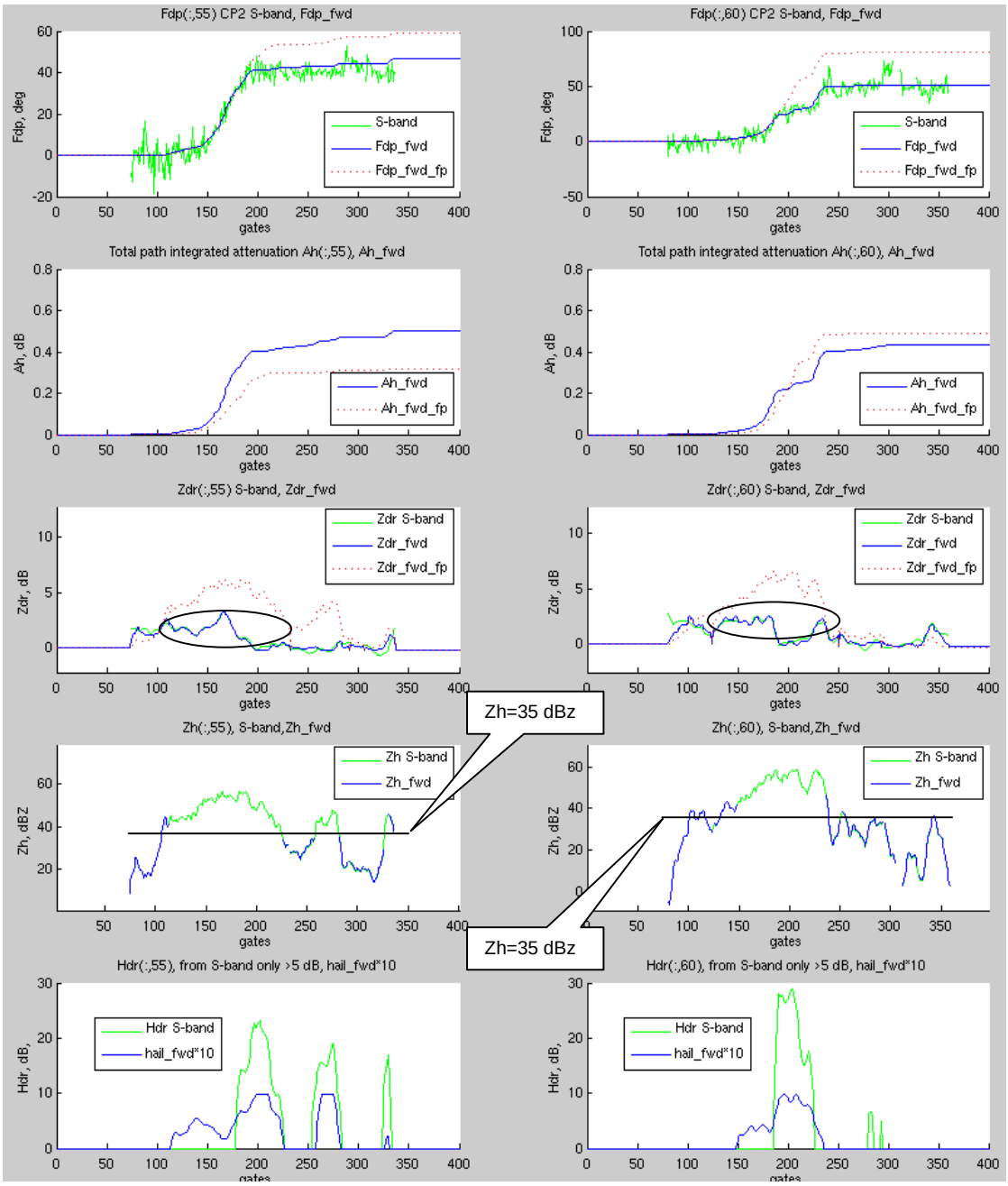

Figure 5-8. CP2 radar dataset, the 4.6 deg elevation angle. Gate-by-gate variables comparison for beams #55, #60.

The coefficient α in power-law relationship (5.1) is for this case α= 0.018 (recall that the average value is close to 0.017 according to Bringi and Chandrasekar 2001). It can be seen how ad hoc criteria for detection of gates with hail is working (marked areas). Hail is detected where Z_h > 35 dB and Z_{dr} at first pass is overestimated by 1.5 dB. We can see that Z_{dr}, Φ_{dp} values predicted by FM are in good agreement with observed values. It can be seen also on the histograms of the differences between observed and FM modeled values for the whole sweep:

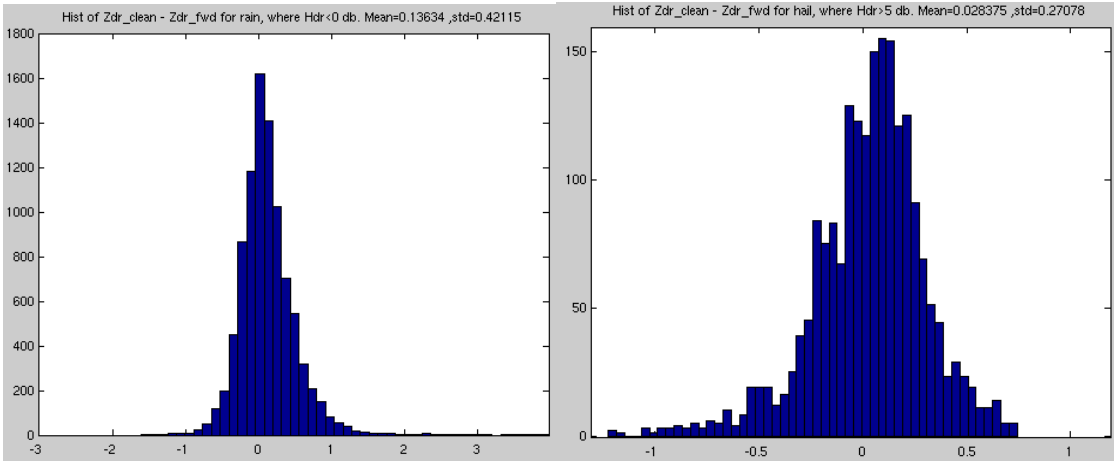

Figure 5-9. CP2 radar dataset, the 4.6 deg elevation angle. Histogram of the difference between observed and FM-modeled values for Z_{dr}, dB, for rain (left panel) and hail (right panel) regions.

5.2 IHOP 2002 data

Data from IHOP 2002 experiment are available for both S- and X-bands. The SPOL radar is the S-band dual-polarized radar. A separate dual-polarized X-band radar was located next to SPOL. While the beam widths of the two antennas are 1 deg, they are on different pedestals and so it is more difficult to match the beams as the radars scan in either azimuth or elevation. Also, some radar variables were corrected by other methods (dual-frequency method), so we can compare with the variational method. The data from IHOP experiment appears to be noisier than CP2 radar data, so it has to be carefully "cleaned" and calibrated before entering into the variational method. The Φ_{dp} values have to begin from ~0 degrees at the beginning of the beam, so we need to eliminate radar system phase offset. Z_{dr} values for low rain rate (Z_h < 10 dBz) have to be around 0 dB, as drops are small and approximately spherical.

The next figure shows the PPI of input variables for S-band, for 2 degrees elevation:

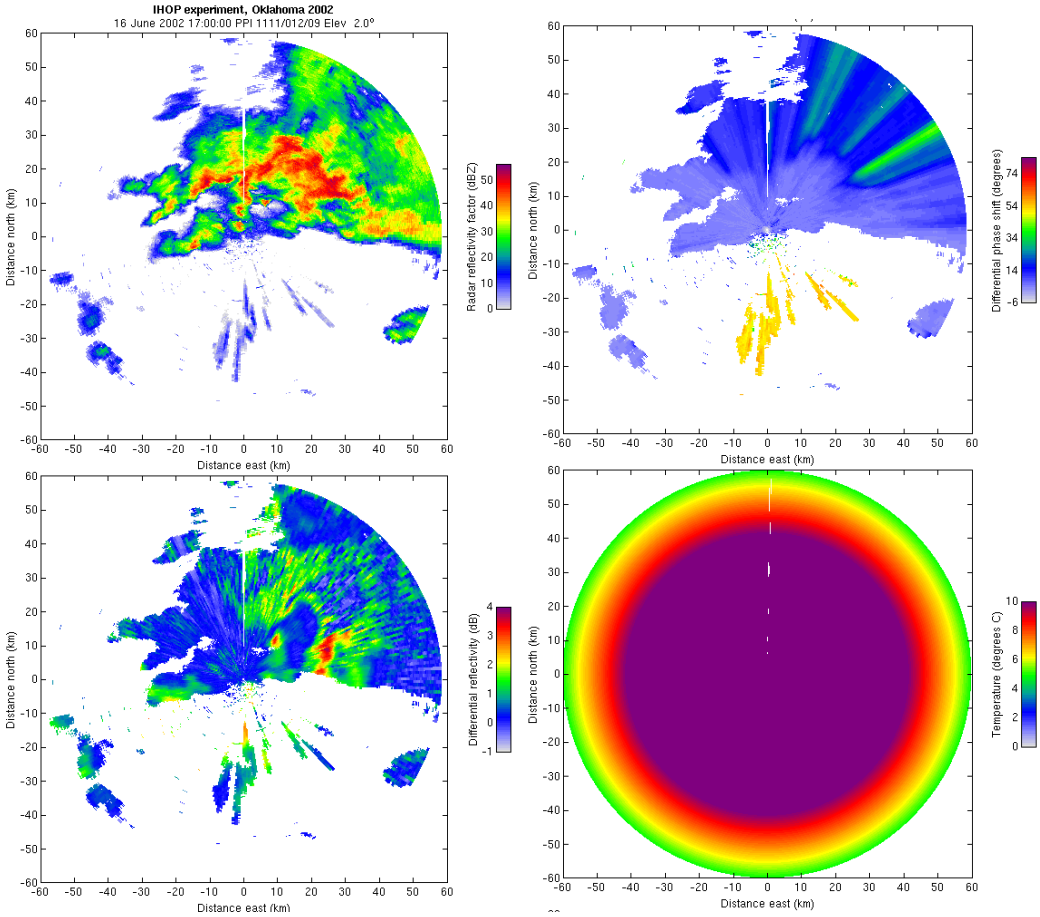

Figure 5-10. IHOP dataset, the 2 deg elevation angle. The input data to the variational algorithm: Z_h, Z_{dr}, Φ_{dp}, temperature.

The output of the variational algorithm is shown on the next figure:

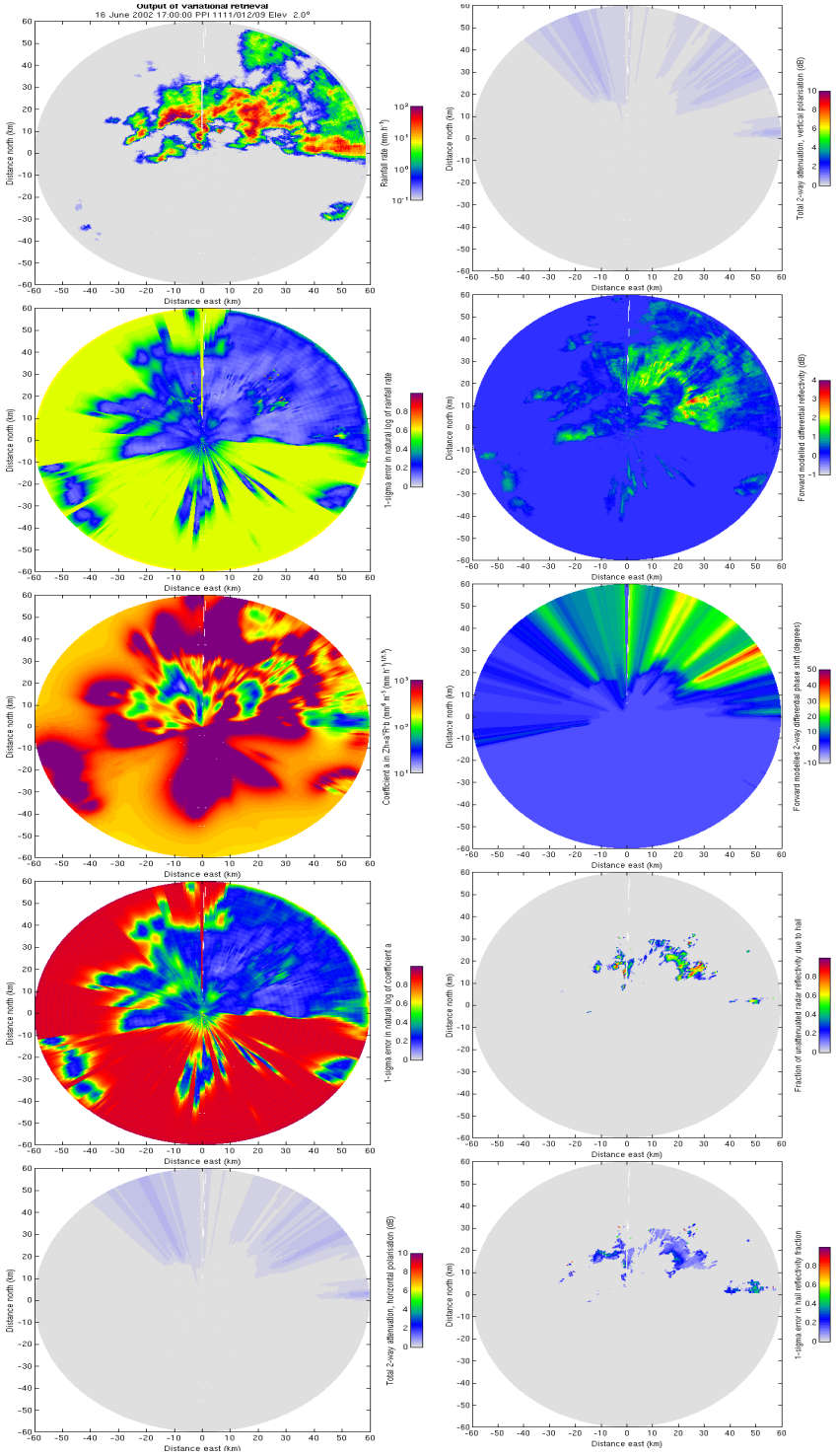

Figure 5-11. IHOP dataset, the 2 deg elevation angle, S-band. The output of the variational algorithm: rain rate R, 1-sigma error in natural log of R, coefficient *a* (from the $Z_h=aR^b$ relationship), 1-sigma error in natural log of *a*, total 2-way attenuation in vertical and horizontal polarizations, forward-modeled Z_{dr}, forward-modeled 2-way Φ_{dp}, fraction of unattenuated radar reflectivity due to ice *f*, 1-sigma error in hail reflectivity fraction.

The first image of figure 5-11 shows the modeled rain rate R, mm/hr. In some parts of the storm (range around 20 km and az around 300°) values of rain rate are high, around 100 mm/hr. It must be noted that values of the coefficient *a* (shown on the image 3) near the high rain rate core are having low values, around 30-40, and they reach much higher values (around 300-1000) for the zones where rain rate is lower. It appears that the *a* values in the high R regions are much lower (by a factor of 3) than expected for the mid-latitudes whereas at low rain rates the *a* values are much more reasonable and representative of stratiform rain. The second image shows the 1-sigma retrieval error in ln(R), this error is low (0.1-0.2) where signal-to-noise ratio is high (at the storm core) and grows higher when signal-to-noise ratio becomes lower. The fourth image shows the 1-sigma retrieval error in ln(*a*), which includes random errors in the measurements of Z_{dr} and Φ_{dp} but not forward model errors. This error is low for high signal-to-noise ratio areas. The image ten of the figure shows that FM detected hail in the core of the storm, which well correlates to the areas of high rain rate values.

At S-band attenuation is low, so we can use it to calculate H_{dr} and thereby locate gates where there is a high probability of hail (and then use these results to compare to the output of the X-band version of the algorithm, to see if the hail will be found on the same regions).

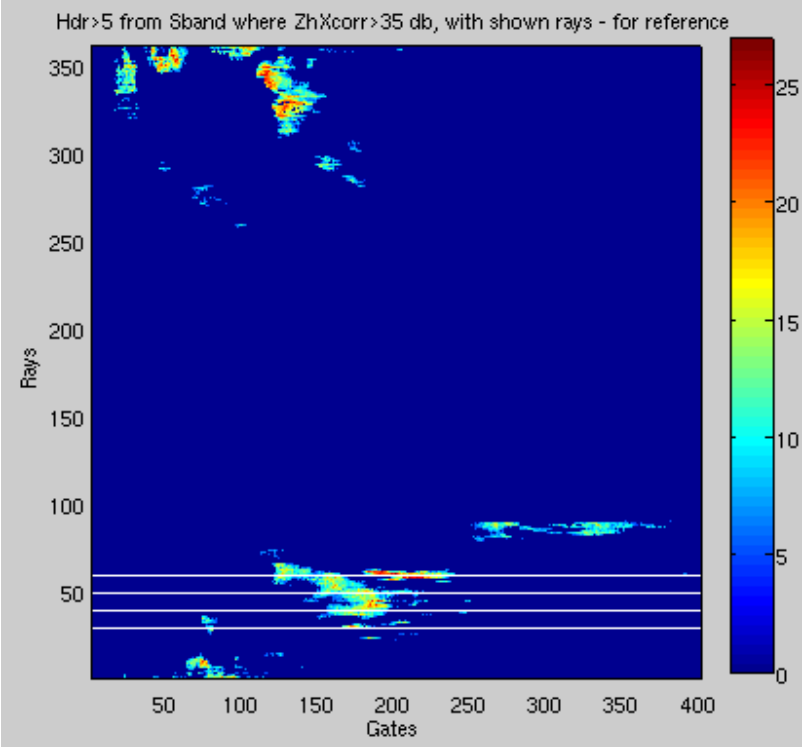

Figure 5-12. IHOP dataset, the 2 deg elevation angle, S-band. High values of Hdr (> 5 dB) indicate high probability of hail.

The gate-by-gate comparison for S-band is shown on the next figure:

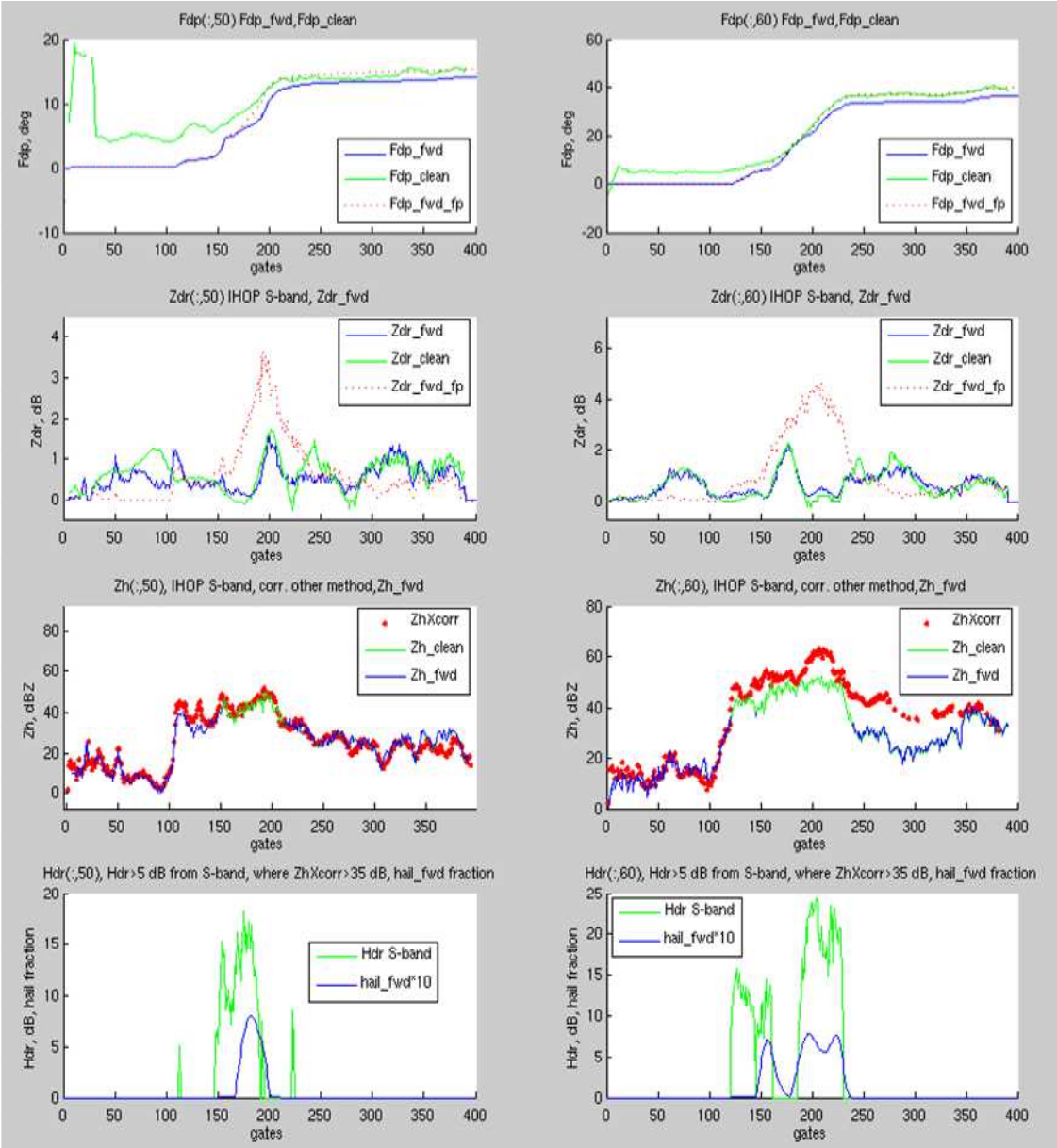

Figure 5-13. IHOP dataset, the 2 deg elevation angle, S-band. Gate-by-gate variables comparison for beams #50, #60.

The coefficient α in power-law in relationship (eq. 5.1) is for this case α= 0.02 (0.017 according to Bringi 2001). For this case some tuning of the input to the variational method was needed to achieve reasonable outputs. Hail is detected where Z_h > 35 dB and Z_{dr} at first pass is overestimated by 0.5 dB

(instead of 1.5 dB). There is good agreement between gates with high H_{DR} values and gates marked as having hail by FM, although at some gates even with tuning is not sensitive enough to locate hail as robustly as H_{DR}.

We can see that Z_{dr} values predicted by FM are in good agreement with observed values. The Φ_{dp} values can be followed by FM too; FM expects it to start from about 0 degree, that is why at the beginning of the beam #50 there is a difference.

For X-band, the output of the algorithm is shown in the next Figure 5-14. Comparing S-band and X-band outputs, we see that the variational method is still able to find hail at the same position. But it is lower, in terms of area covered by hail, and in terms of fraction of reflectivity due to hail.

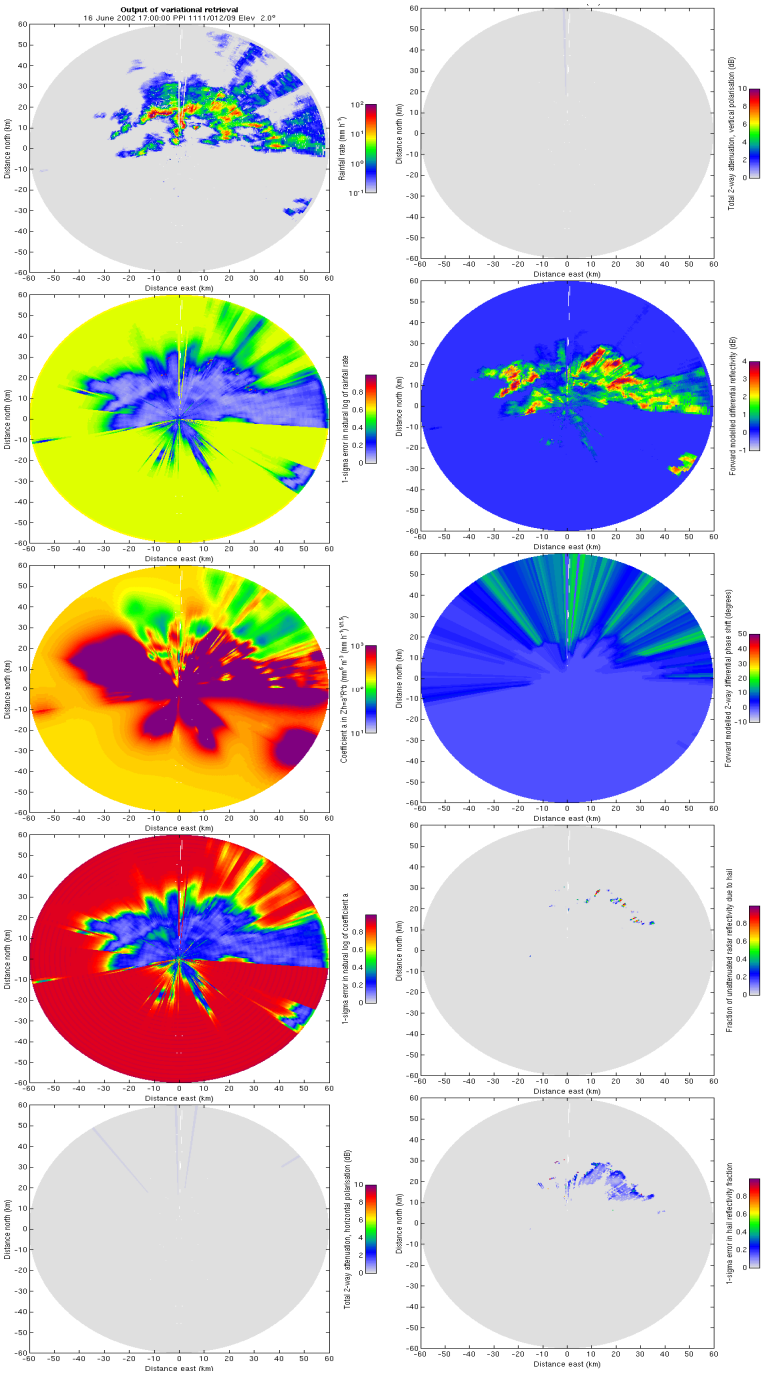

Figure 5-14. IHOP dataset, the 2 deg elevation angle, X-band. The output of the variational algorithm: rainrate R, 1-sigma error in natural log of R, coefficient *a* (from the $Z_h=aR^b$ relationship), 1-sigma error in natural log of *a*, total 2-way attenuation in vertical and horizontal polarizations, forward-modeled Z_{dr}, forward-modeled 2-way Φ_{dp}, fraction of unattenuated radar reflectivity due to ice *f*, 1-sigma error in hail reflectivity fraction.

If we compare forward modeled variable with the input variables gate-by-gate for several beams (as shown on Figure 5-15), we can see that for X-band this model does not work well. The Φ_{dp} values predicted by FM are different from observed and the 2-way total attenuation is different too. The other (dual-frequency) method also cannot find hail at the positions predicted by high H_{dr} values, for example (beam #50). It is interesting to note that “something” actually was detected by the algorithm at the areas where there are high H_{dr} values, but iterations converged to some very small values of hail fraction *f* (gates 150-200 beam #50, #60). Definitely this model has to be tuned for X-band data for this particular radar.

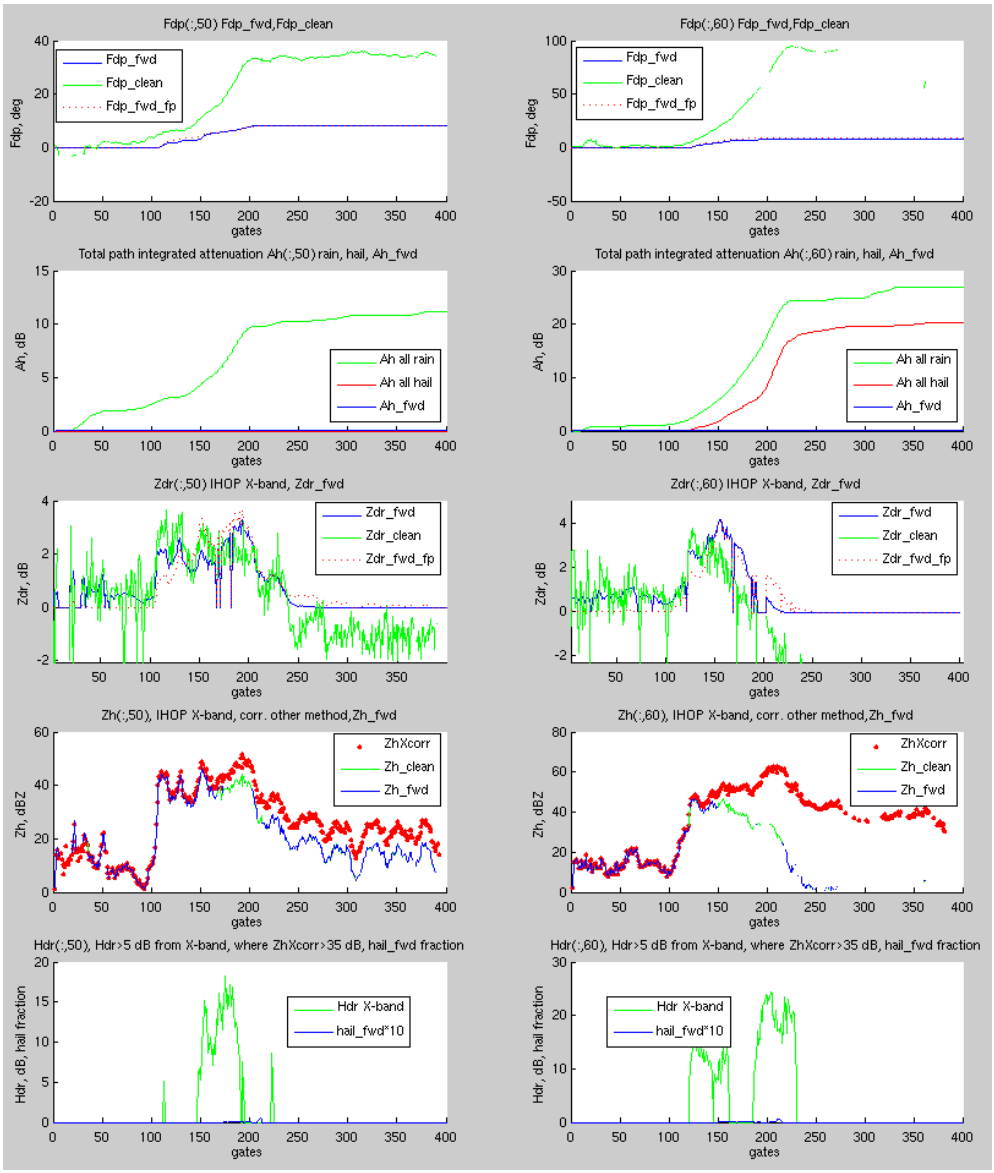

Figure 5-15. IHOP dataset, the 2 deg elevation angle, X-band. Gate-by-gate variables comparison for beams #50, #60.

5.3 CASA data from 10 June 2007

The data from CASA radar KCYR from storm event of June 10, 2007 (22:15:47), 2 degrees elevation, was used to test the performance of the algorithm. This data is noisy hence it was extensively “cleaned” and calibrated before variational method was applied. To eliminate the system offset Φ_{dp} values were shifted up to 60 degrees. As the maximum altitude of the beam at the distance of 30 km is about 1 km, so one can hypothesize that hail is unlikely (i.e. full melted) and run the algorithm with hail detection turned off.

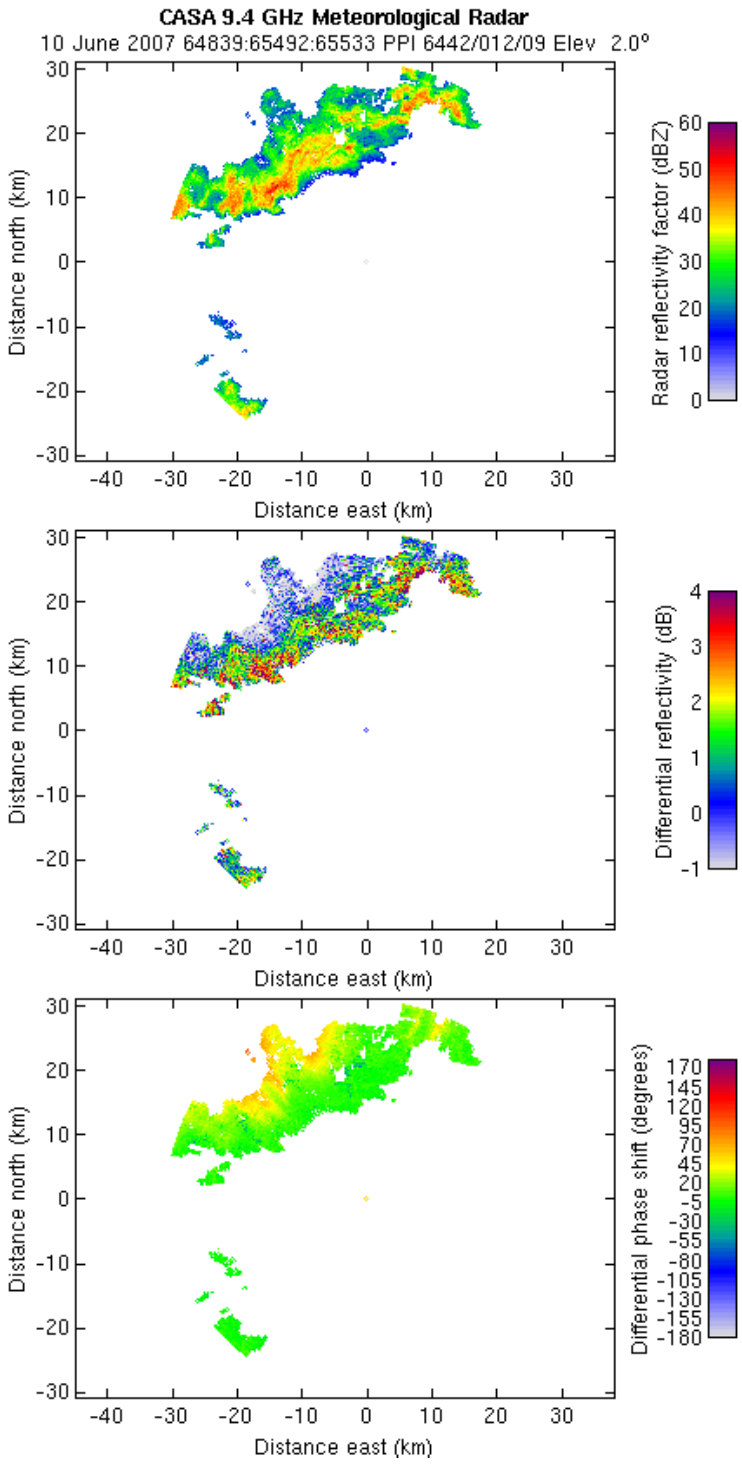

Figure 5-16. CASA KCYR 20070610 dataset, the 2 deg elevation angle. The input data to the variational algorithm: Z_h, Z_{dr}, Φ_{dp}.

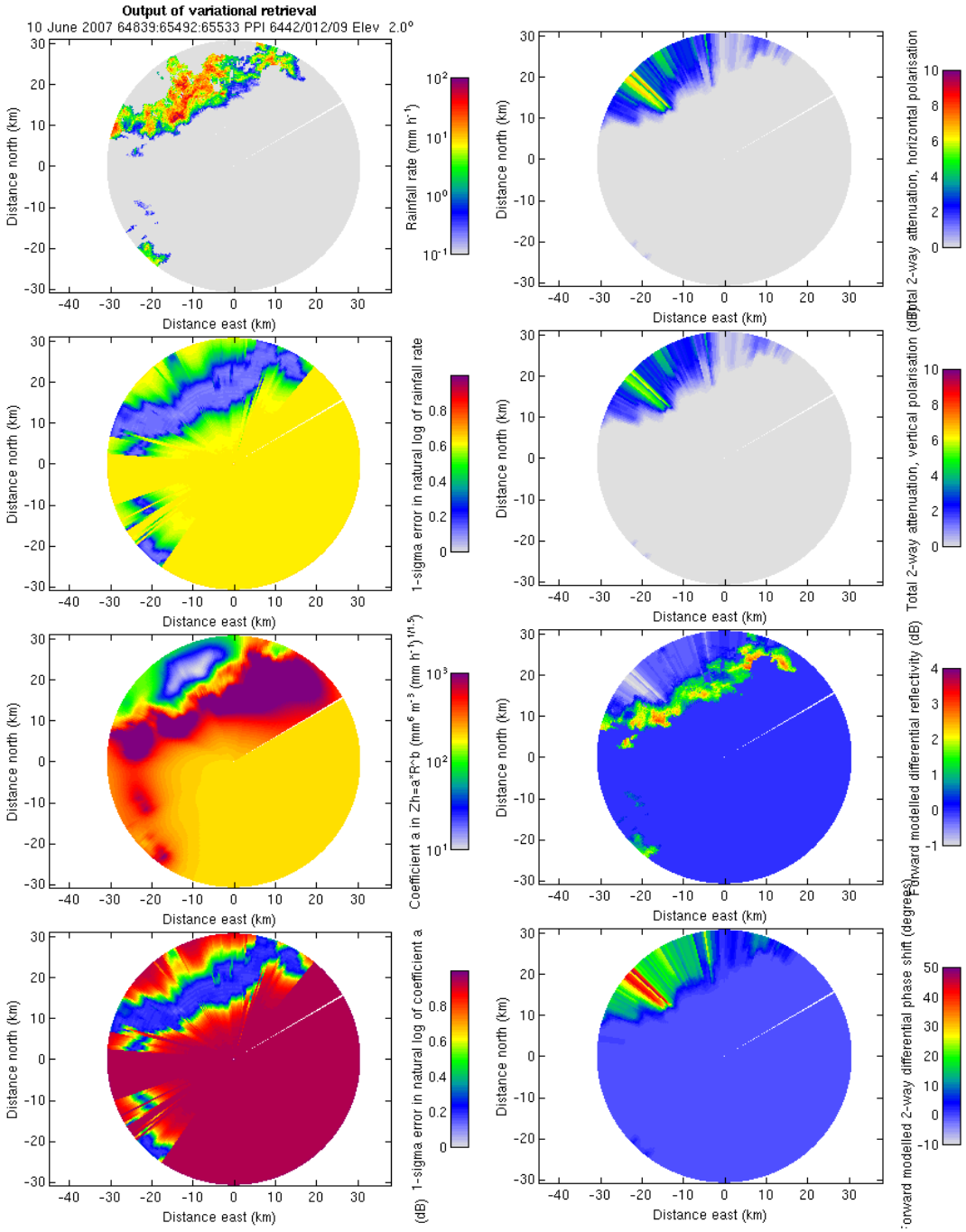

Figure 5-17. CASA KCYR 20070610 dataset, the 2 deg elevation angle. The output of the variational algorithm: rainrate R, 1-sigma error in natural log of R, coefficient *a* (from the $Z_h=aR^b$ relationship), 1-sigma error in natural log of *a*, forward-modeled Z_{dr}, forward-modeled 2-way Φ_{dp}.

If we compare forward modeled variables with the input variables gate-by-gate for several beams, we can see that for CASA radars this model still needs some improvements. The Φ_{dp} values predicted by FM are different from that observed in some cases and 2-way total attenuation values are too low. The Z_{dr} values are predicted very well though, at least for positive Z_{dr}. Coefficient α in power-law relationship (eq. 5.1) is for this case α= 0.15 (beam #258), α= 0.19 (beam #278) (mean value is around 0.233 at X-band according to Bringi and Chandrasekar 2001):

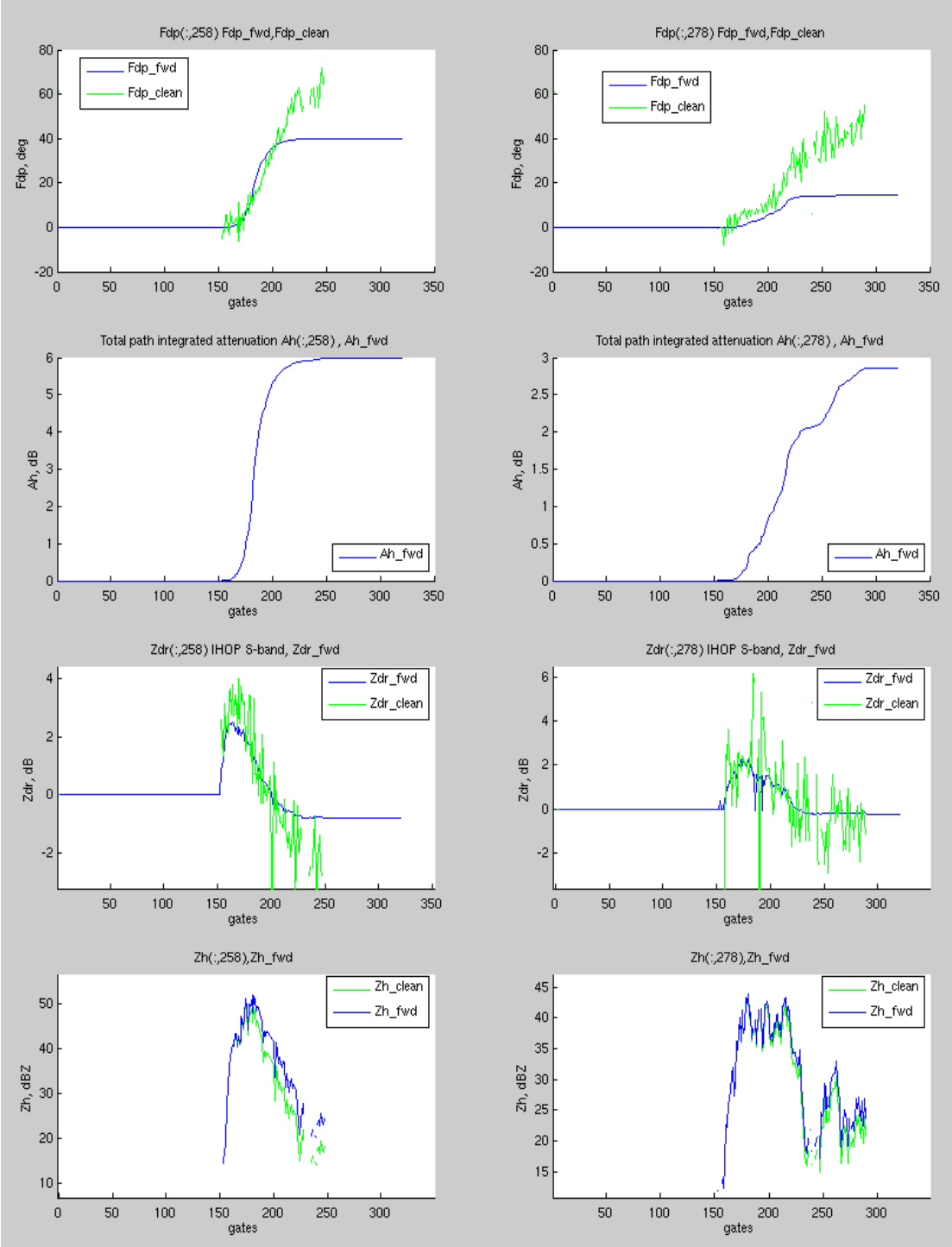

Figure 5-18. CASA KCYR 20070610 dataset, the 2 deg elevation angle. Gate-by-gate variables comparison for beams #258, #278.

Chapter 6

VARIABLE OBSERVATIONAL ERRORS IN THE COST FUNCTION

To achieve better performance of the optimal estimation scheme (OES) for the X-band CASA data, one need adjust the default errors assigned to Φ_{dp} and Z_{dr} values, which are used as an input data into FM.

As it was stated (Hogan, 2007), "the retrieval in low-rain-rate regions has been found to be very sensitive to the calibration of Z_{dr}. A simple solution would be to manipulate the elements of the observational error covariance matrix R, by simply increasing the error assigned to the Z_{dr} measurements at low values of Z."

For CASA radars the root-mean-square observational error for Z_{dr} data, i.e., σ_{Zdr} has a default value of 0.5 dB. For low rain rate areas (drizzle) the values of Z_h are less expected to be less than 20 dBz, and there the observational error should be higher then this default value.

After radar data examination and some numerical experiments it was found that value of σ_{Zdr} in first approximation could be changed according to the empirical formula

$$\sigma_{Zdr}(Z_h) = 0.5 * \begin{Bmatrix} -0.05Z_h(dBz) + 2, & Z_h < 20dBz \\ 1, & Z_h > 20\ dBz \end{Bmatrix} \qquad (6.1)$$

where 0.5 dB is the default value of the observational error. The next figure shows the dependency $\sigma_{Zdr}(Z_h)$.

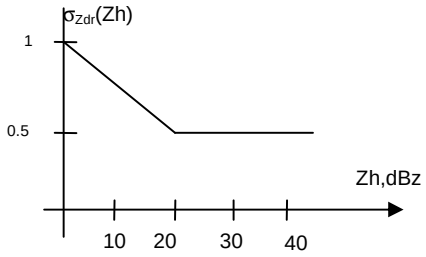

Figure 6-1. Empirically based dependency of σ_{Zdr} on Z_h

We note that from theory σ_{Zdr} should be dependent on the intrinsic copolar correlation coefficient and the SNR according to eq (6.115) of Bringi and Chandrasekar (2001). The empirical equation in (6.1) only approximates the dependence on SNR.

From (Hogan, 2007), "…in intense convection it would be desirable to increase the error in Φ_{dp} due to possibility of backscatter differential phase".

The default value of root-mean-square observational error ($\sigma_{\Phi dp}$) for Φ_{dp} for CASA data is 3 deg. This default value should be increased for the gates where signal-to-noise ratio is lower. These gates normally have lower values of the copolar correlation coefficient between horizontally polarized weather signals and vertically polarized weather signals ρ_{hv}, which changes in the range 0-1.

After examination of radar data and some numerical experiments it was found that value of $\sigma_{\Phi dp}$ in first approximation could be changed according to the formula

$$\sigma_{\Phi_{dp}}(\rho_{hv}) = 3 * \begin{cases} -4.44\rho_{hv} + 5, & \rho_{hv} < 0.9 \\ 1, & \rho_{hv} \geq 0.9 \end{cases} \qquad (6.2)$$

where 3 deg is the default value of the observational error for Φ_{dp} CASA data.

The next figure shows the dependency $\sigma_{\Phi dp}(\rho_{hv})$:

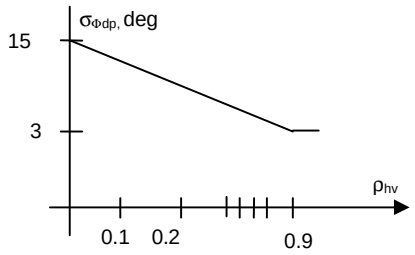

Figure 6-2. Empirically based dependency of $\sigma_{\Phi dp}$ on the copolar correlation coefficient, ρ_{hv}.

We note that from theory $\sigma_{\Phi dp}$ should be dependent on the intrinsic copolar correlation coefficient and the SNR according to eq (6.143) of Bringi and Chandrasekar (2001). The empirical equation in (6.2) only approximates the dependence on ρ_{hv}.

For the CASA data file KCYR_20070610-221257.netcdf these observational errors, changed according to the Z_h and ρ_{hv} values are depicted in Figs. 6-3.

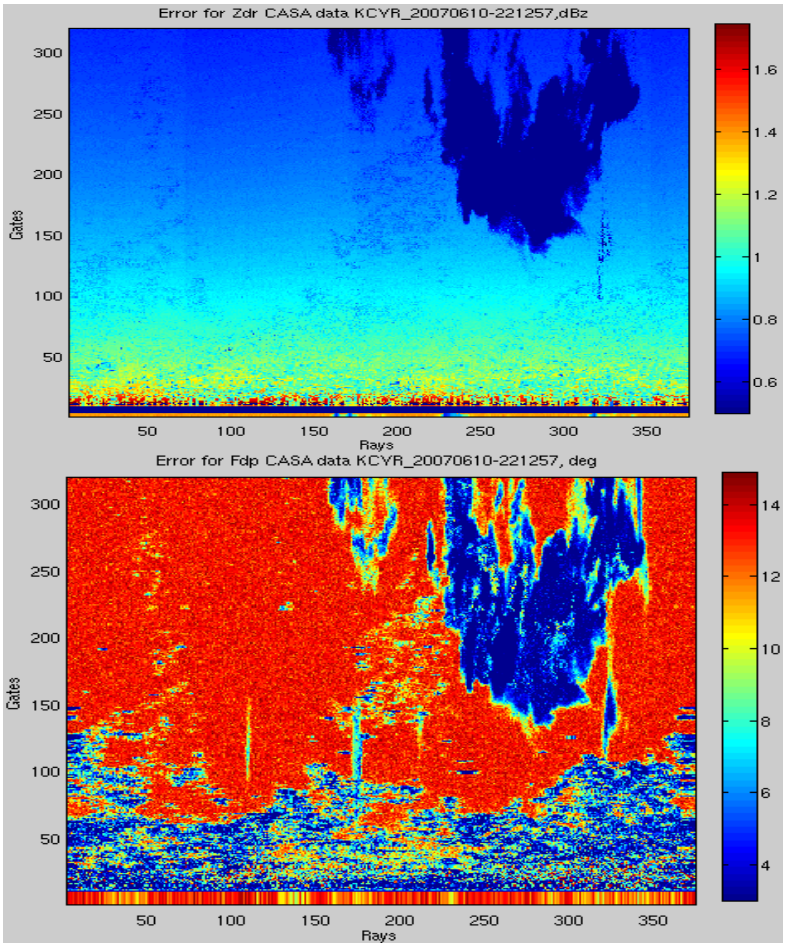

Figure 6-3. Observational errors σ_{Zdr} and $\sigma_{\Phi dp}$ changed according to the Zh and ρ_{hv} values, for CASA KCYR 20070610-221257 dataset.

For reference the GateFlags variable from the same CASA data file is shown on the next figure. This variable was used for the discrimination between "good gates" with useful weather information and noisy gates. It is to show that even for "good gates" these observational errors change in pretty wide range.

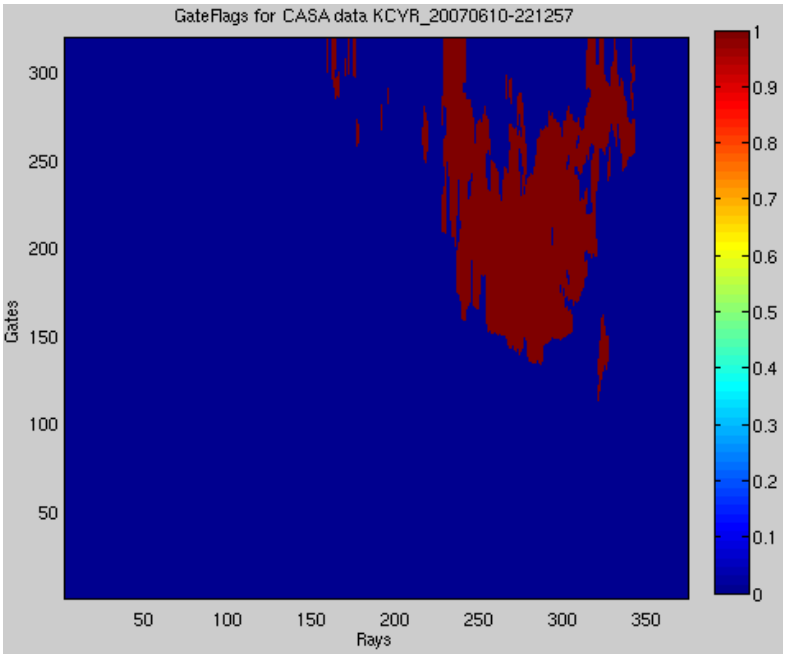

Figure 6-4. GateFlags variable used for data cleaning as a "good gates" mask, for CASA KCYR 20070610-221257 dataset.

The next figure shows the values of CrossPolCorrelation (which is ρ_{hv}) variable of the same CASA data file. It shows that even for "good gates" ρ_{hv} changes significally, so $\sigma_{\Phi dp}$ changes too, and in this way changes the weight of the components of the minimization function of the FM described earlier (see eq. 3.5):

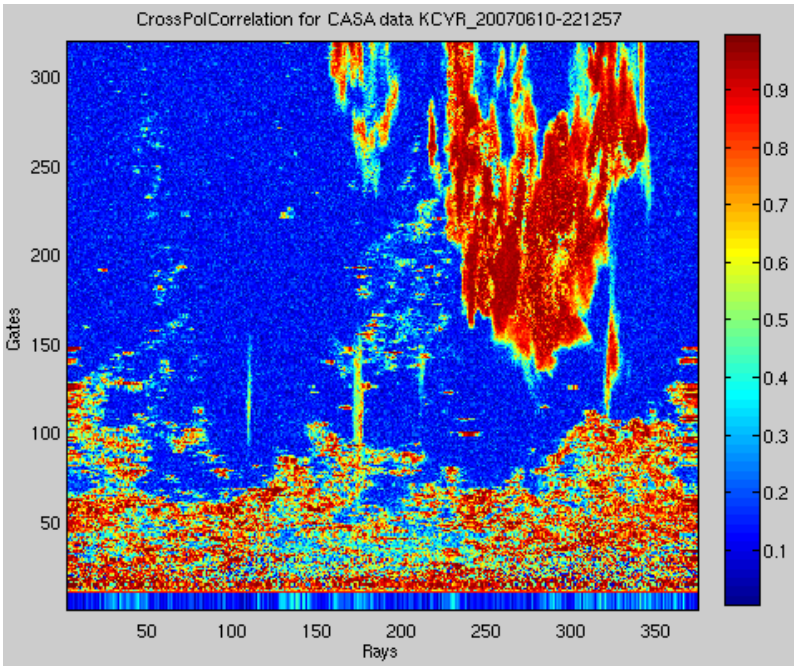

Figure 6-5. CrossPolCorrelation variable (ρ_{hv}), for CASA KCYR 20070610-221257 dataset.

As the result of the above procedure of changing the default values of observational errors σ_{Zdr}, $\sigma_{\Phi dp}$ leads to the re-balancing the influence of that corresponding variable on the cost function. The overall effect is that corresponding forward-modeled range profile (Z'_{dr} or Φ'_{dp}) tends to be close to the input variable, as in case when only one variable (Z_{dr} or Φ_{dp}) was used in the input to the program (these variables can be used as an input to the modeling together or switched off if not available in the radar data).

This is illustrated in the following figures (6-6. 6-7), which show the gate-by-gate comparison of the CASA KCYR 20070610 dataset used above, data from the 2 deg elevation angle sweep, the beam #258 and #318 which were generated using constant observational errors (left panel) and variable observational errors (right panel).

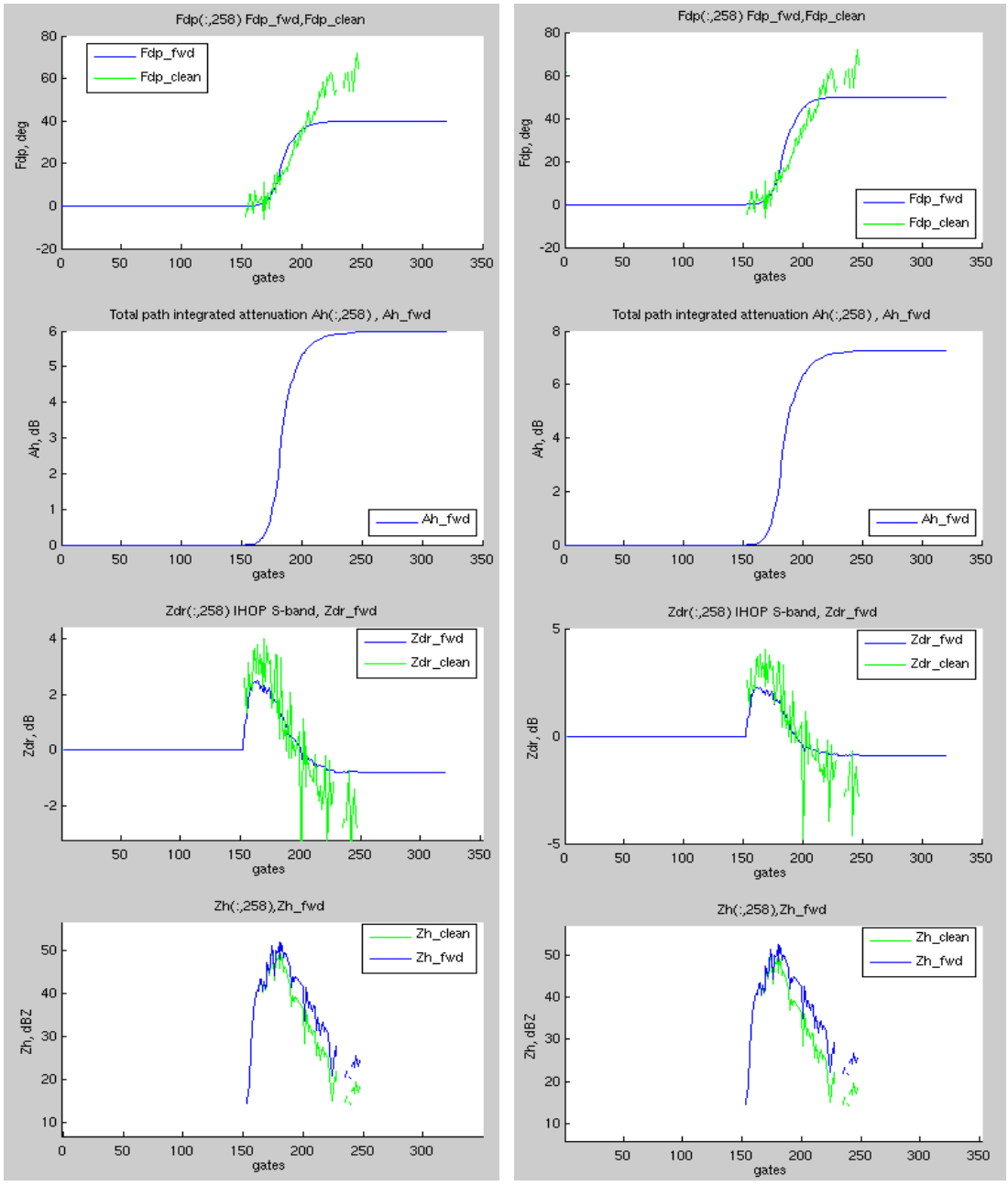

Figure 6-6. CASA KCYR 20070610 dataset, the 2 deg elevation angle. Gate-by-gate variables comparison for beams #258 generated using constant observational errors (left pane) and variable observational errors (right pane). Note how Φ_{dp} goes closer to the observed data, and attenuation Ah has more reasonable values.

The coefficient α in power-law in relationship (eq. 5.1) is for this case for constant errors α= 0.17 and for variable errors α= 0.14.

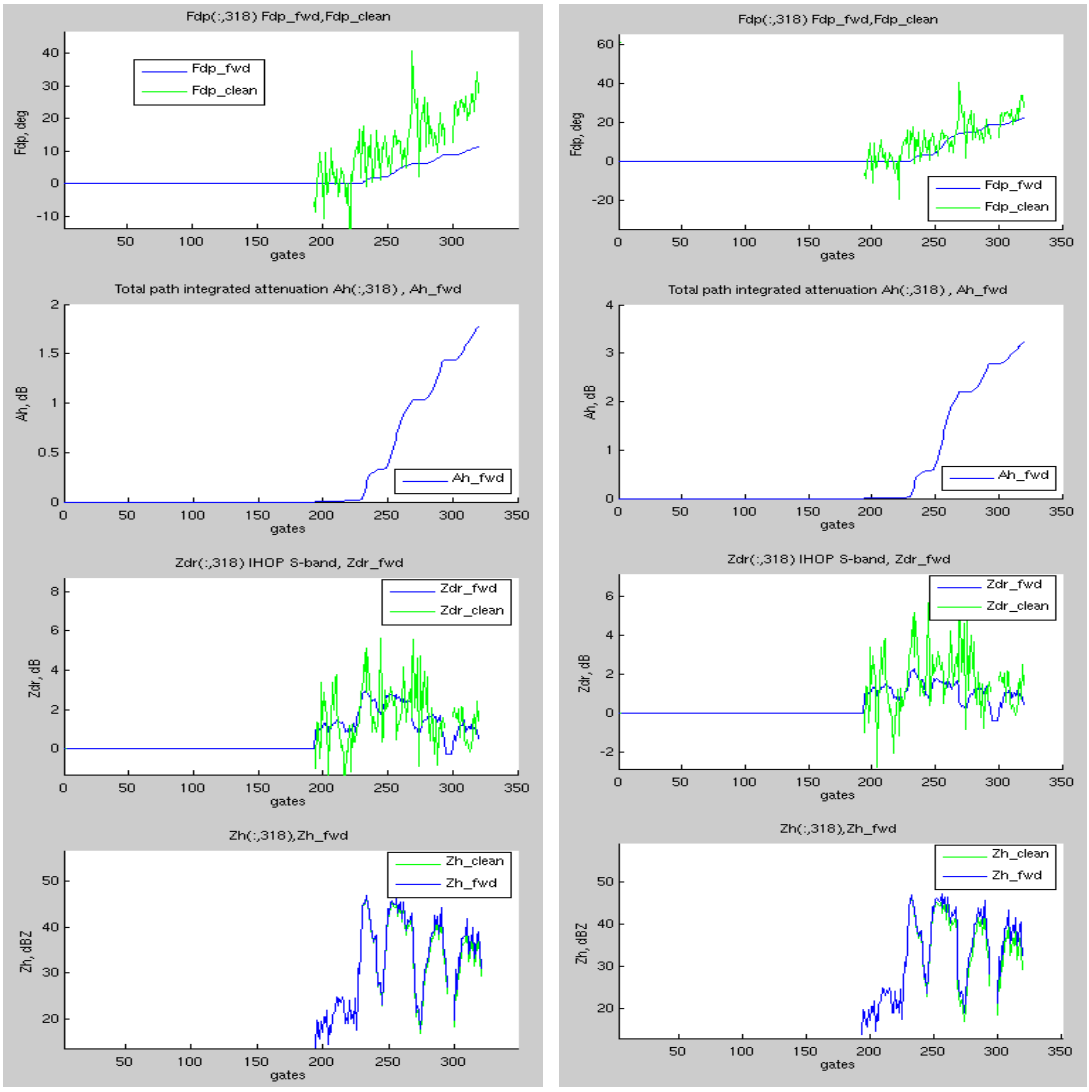

Figure 6-7.CASA KCYR 20070610 dataset, the 2 deg elevation angle. Gate-by-gate variables comparison for beams #318 generated using constant observational errors (left pane) and variable observational errors (right pane). Note how Φ_{dp} goes closer to the observed data, and attenuation Ah has more reasonable values.

The coefficient α in power-law in relationship (eq. 5.1) in this case for both constant and variable errors is α= 0.15. In both figures (6-6, 6-7), the improvement from variable observational errors mainly comes from the forward modeled Φ_{dp} being closer to the measured Φ_{dp}.

Chapter 7

ESTIMATION OF REFLECTIVITY-WEIGHTED FRACTION OF ICE IN A RAIN-HAIL MIXTURE

The forward model in the present state, when applied to the CASA X-band data, does not produce the good results when it comes to wet ice and hail detection. With the purpose to improve the output of the program, one can “help” the algorithm by detecting the gates with wet ice and hail and supply them to the program instead of just letting it to find these gates by itself, with ad hoc criteria described before. This new information should be used together with wet ice/hail found automatically by the algorithm.

To find the gates where the probability to find hail is high, one can use the H_{dr} (eq. 2.15) concept described by Aydin et al, (1986) and explained before in chapter 2.

To find the parameters of the $f(Z_{dr})$ for the X-band, the variables Z_h and Z_{dr} were simulated based on the one minute distribution data from pure rain from 2D video disdrometer installed near CP2 radar (Brisbane, Australia). These variables were simulated for pure rain event assuming the latest information on drop axis ratios and canting angles. One can make a plot similar to the one described in Aydin et al, (1986) paper, but this time for X-band, with the purpose to find the curve which is the rain-hail boundary. This simulated data together with the boundary line is shown on the next figure:

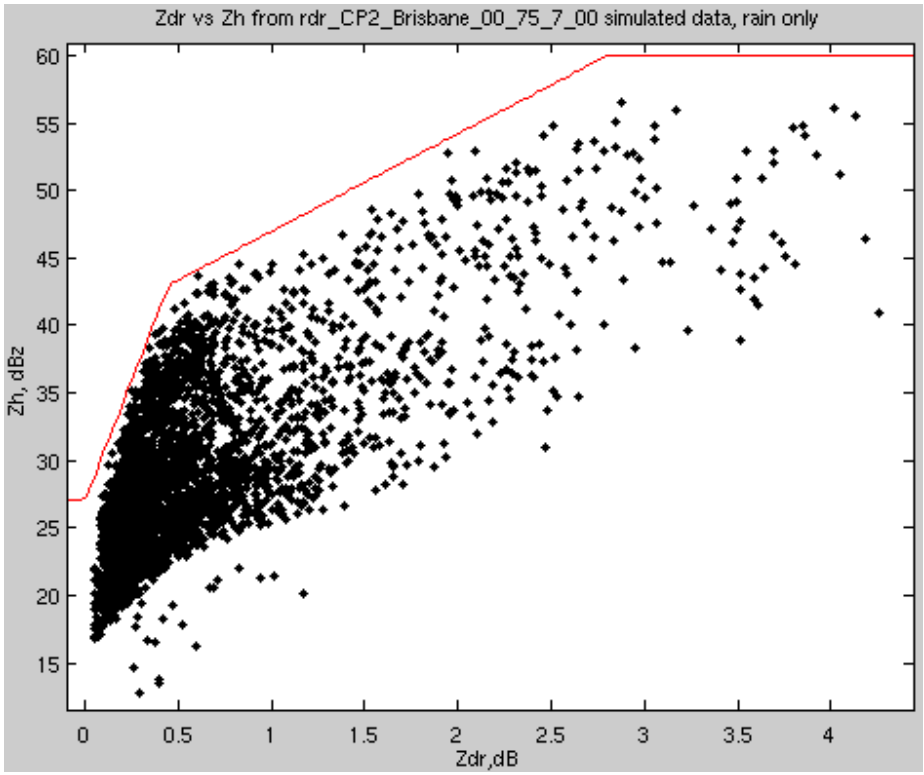

Figure 7-1. Zh vs Z_{dr} scatterplot representing simulated data for rain-only case at X-band, and rain-hail boundary line designed for X-band.

Even though the data used to create this curve was collected in subtropical coastal environment different from the continental environment of Oklahoma where CASA radars are installed, the boundary line separating rain from the rain-hail mixture should be fairly robust.

For X-band the $f(Z_{dr})$ is found to be the following:

$$f(Z_{dr}) = \begin{cases} 27; & Z_{dr} \le 0 \ \ dB \\ aZ_{dr} + 27; & 0 < Z_{dr} \le e \ \ dB \\ bZ_{dr} + c; & e < Z_{dr} \le g \ \ dB \\ 60; & Z_{dr} > g \ \ \ dB \end{cases} \qquad (7.1)$$

where a=35.56 , b=7.23, c=39.74, e=0.45 dB, g=2.8 dB.

When this boundary line is applied to the pure rain case discussed earlier (CASA data KCYR_20070610-221547), the result looks as shown on the next figure:

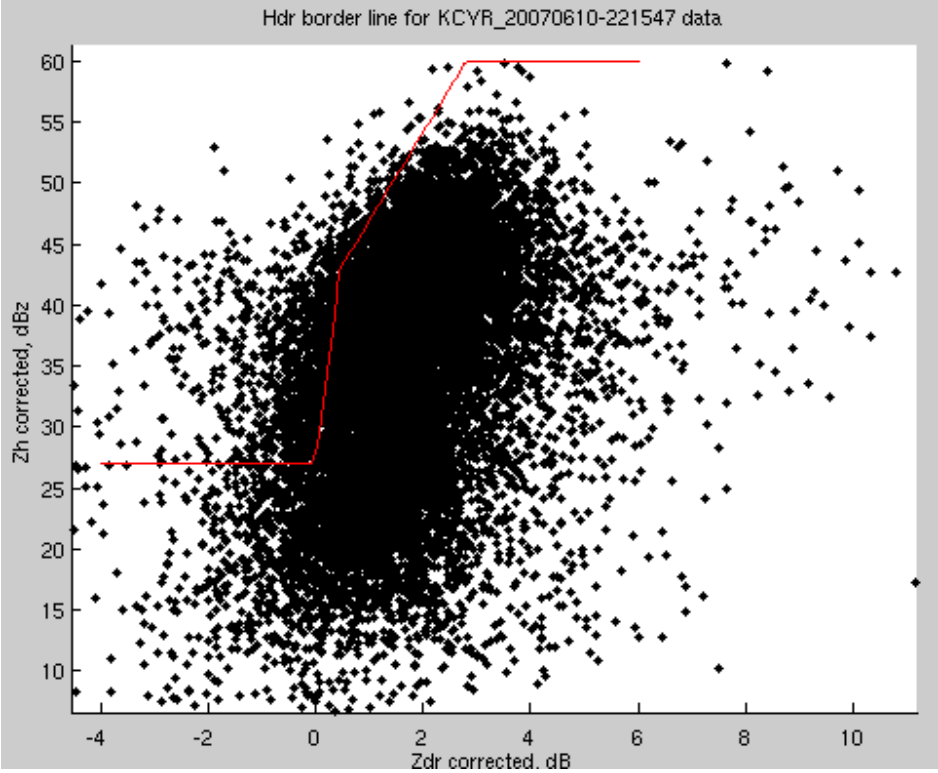

Figure 7-2. New rain-hail boundary applied to CASA KCYR_20070610-221547 "pure rain" case.

The CASA data file includes Z_h and Z_{dr} variables corrected for attenuation (by other algorithms) to find H_{dr} parameter. The values of H_{dr} found in this manner demonstrate spiky behavior, so one might need to apply FIR filter (in this case FIR filter of order 20 was used) before supplying these values into the OES. The following figure demonstrates H_{dr} data calculated for CASA

KCYR_20070610-221547 “pure rain” case before and after smoothing by FIR filter:

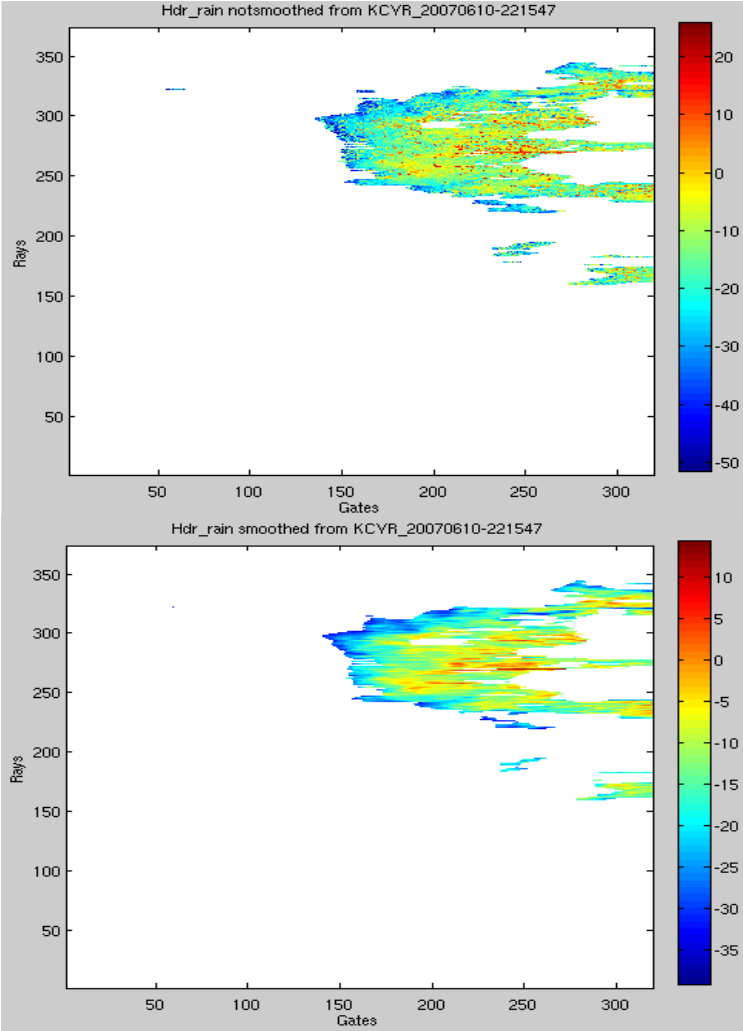

Figure 7-3. H_{dr} data calculated using corrected for attenuation Zh, Z_{dr} variables for CASA KCYR_20070610-221547 “pure rain” case. The gates with high probability of hail correspond to the H_{DR} values more than 3-5 dB.

This figure illustrates that “pure rain” case most probably still has some hail in the 2 deg elevation scan, but not significant amount.

The FM algorithm was modified to accept the H_{dr} data as an input, i.e. gates with high H_{dr} values (where H_{dr}>3 dB) were marked as having hail, and so

on the second pass FM is trying to calculate the hail fraction *f* for these gates, as it was described before in chapter 3.

After some experiments it was found that this method of selecting gates with high probability of hail and supplying this information to the FM does not produces sufficiently good results. The hail fraction *f* calculated by the program still demonstrates spiky, not smooth behavior.

With the purpose of farther improving the algorithm in part of recognizing gates with hail, one can use the difference reflectivity factor Z_{dp} as it was described in chapter 2, to estimate the fraction of reflectivity due to hail in the mixed rain and hail precipitation zone. The simulated (based on the data from 2D video disdrometer) variables Z_h and Z_v for pure rain case at X-band were used to find a "rain line" in Z_h vs Z_{dp} space:

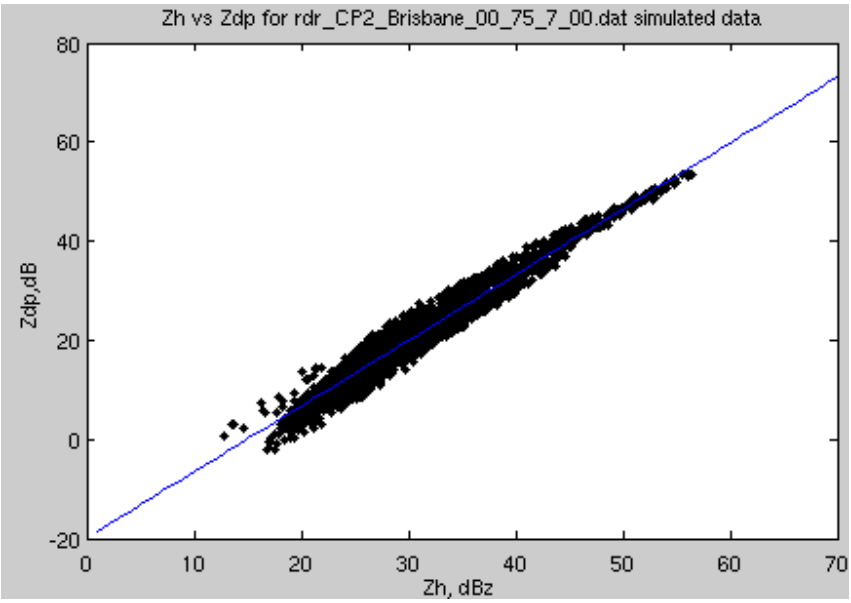

Figure 7-4. Z_h vs Z_{dp}, and found by data fitting the so-called "rain line".

The equation for the “rain line” which relates Z_h and Z_{dp} is

$$Z_{dp} = 1.327 Z_h - 19.82 \qquad (7.2)$$

One can use the corrected for attenuation by other algorithms variables Z_h, Z_v from CASA data files to calculate Z_{dp} and fraction of reflectivity due to hail f_{ice}. For example, for the described earlier “pure rain” case of June 10, 2007 (22:15:47), 2 degrees elevation (KCYR_20070610-221547.netcdf) Z_{dp} vs Z_h looks as follows:

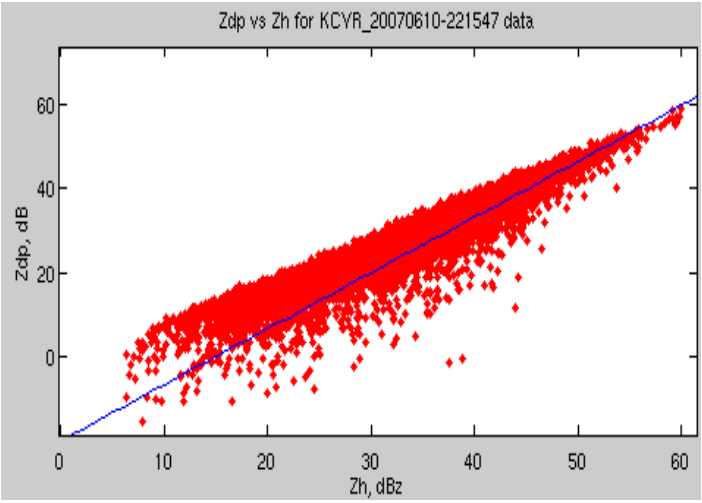

Figure 7-5. Z_{dp} vs Z_h for “pure rain” case of June 10, 2007 (22:15:47), 2 degrees elevation (KCYR_20070610-221547.netcdf) compared to the simulated data and “rain line”. It shows that there are some gates with hail (false detection of hail).

The next image shows the “mixed precipitation” case of April 24, 2007 (KSAO_20070424-172558.netcdf) together with the “rain line”:

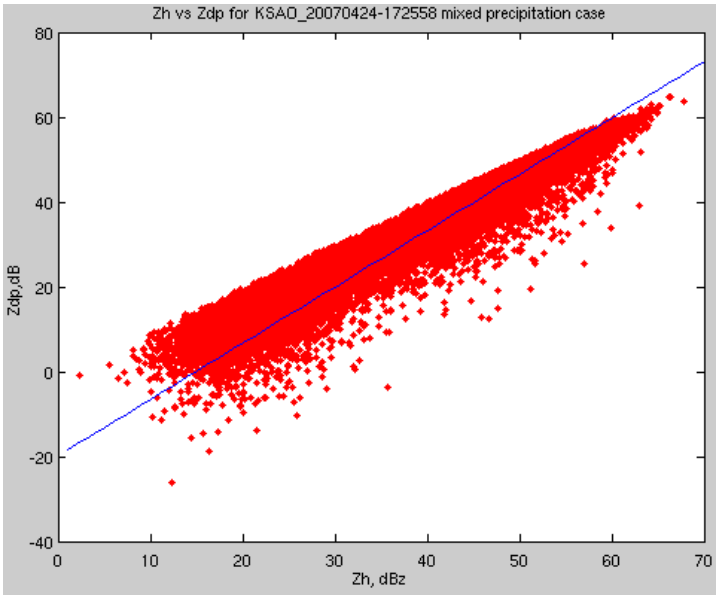

Figure 7-6. Z_{dp} vs Zh for "mixed precipitation" case of April 24, 2007 (KSAO_20070424-172558.netcdf), 2 degrees elevation compared to the "rain line". Many points here are below and to the right of the "rain line". It shows that there are much more gates with high f_{ice} compared to the "pure rain" case mainly for Z_h>45 dBZ

Even though the scatter plot of CASA variables Z_{dr} vs Z_h is not very tight and spreads more than the scatter plot based on the 2D video disdrometer simulated data, so there would be errors in f_{ice} values, it still can be used as the source of the "first guess" of fraction of ice for the OES algorithm. The algorithm then re-adjusts the final values of fraction of ice by minimizing the cost function.

One can build the f_{ice} map for the "mixed precipitation" case, and compare it to the calculated and smoothed H_{dr} values for the same case.

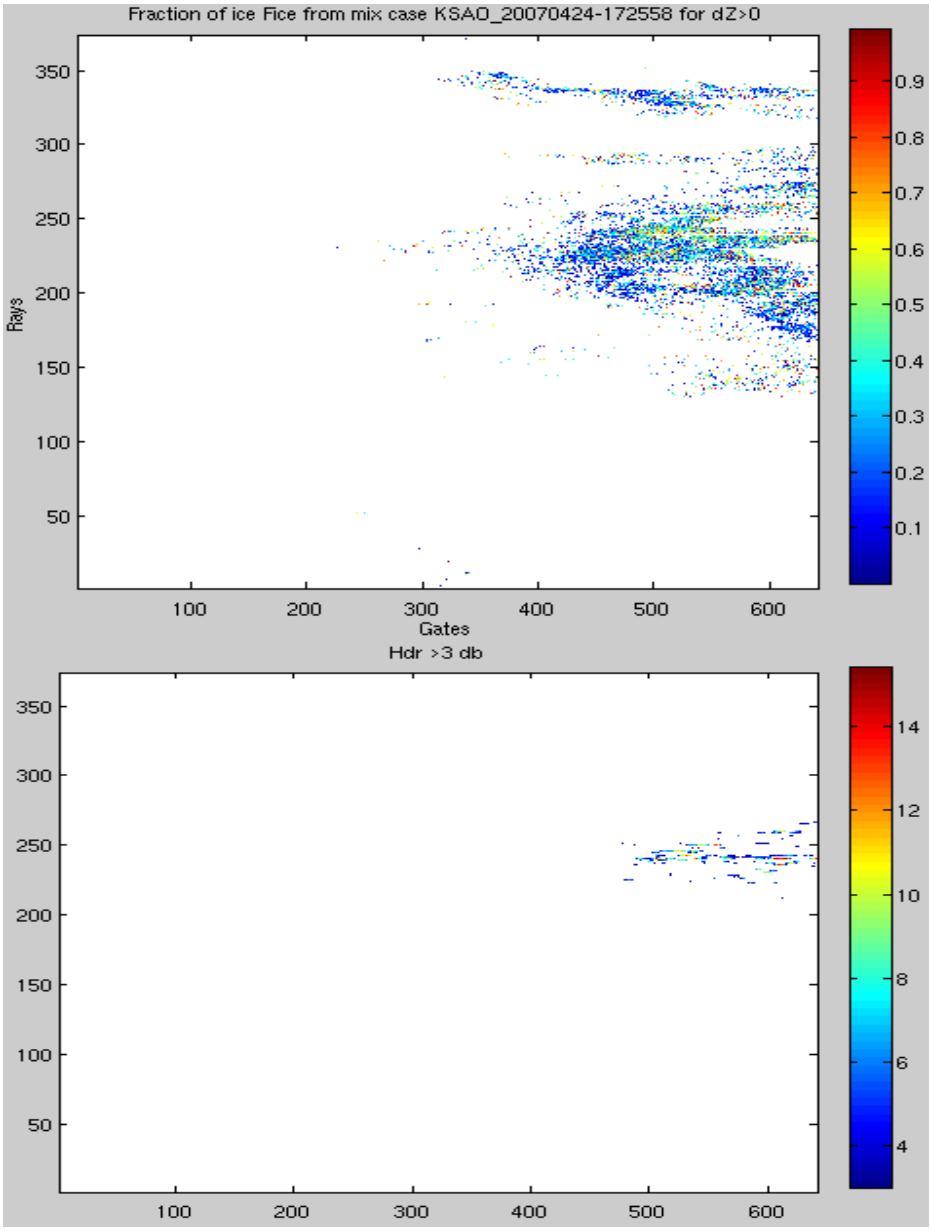

Figure 7-7.Fraction of ice f_{ice} for "mixed precipitation" case of April 24, 2007 (KSAO_20070424-172558.netcdf), 2 degrees elevation compared to the smoothed by FIR-filter H_{dr}>3 dB values for the same case. Note that high values of Hdr do not always correspond to the high values of f_{ice} .

One can note that high values of H_{dr} do not always correspond to the high values of f_{ice} . The map of f_{ice} looks scattered, for the purposes of achieving better

"first guess" it is desirable to use spatial averaging of the f_{ice} data, by using 5x5 smoothing window. The same matrix might be applied to the H_{dr} data:

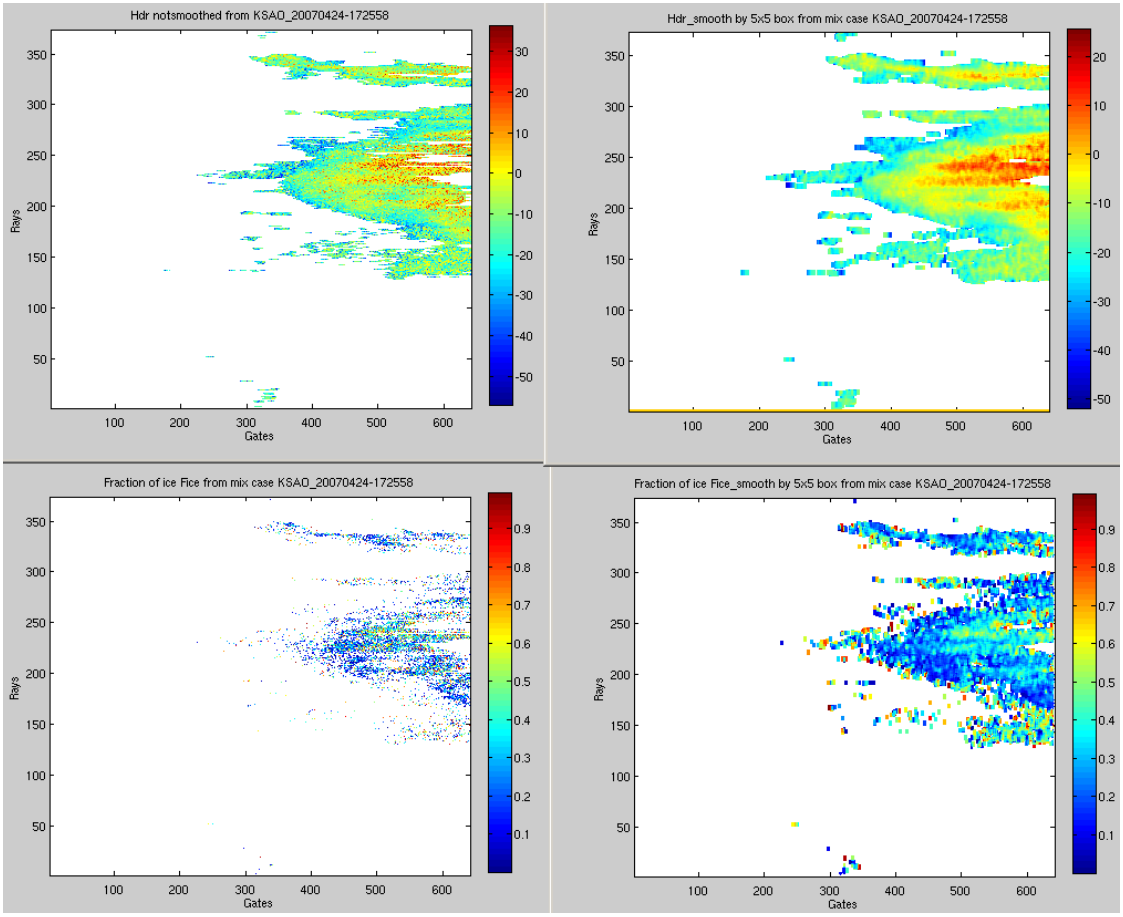

Figure 7-8. Fraction of ice f_{ice} for "mixed precipitation" case of April 24, 2007 (KSAO_20070424-172558.netcdf), 2 degrees elevation, before and after spatial smoothing by 5x5 averaging matrix, compared to the H_{dr} values before and after spatial smoothing by 5x5 averaging matrix.

This and previous figures show that spatially smoothed H_{dr} values are better correlated with the spatially smoothed f_{ice} values than simply FIR-filtered H_{DR} values. But still, high f_{ice} values can be seen at gates where H_{dr} values are low and would not pass the threshold limitation of the FM algorithm. It is shown on the next figure, where a few beams of the mixed precipitation case data are compared:

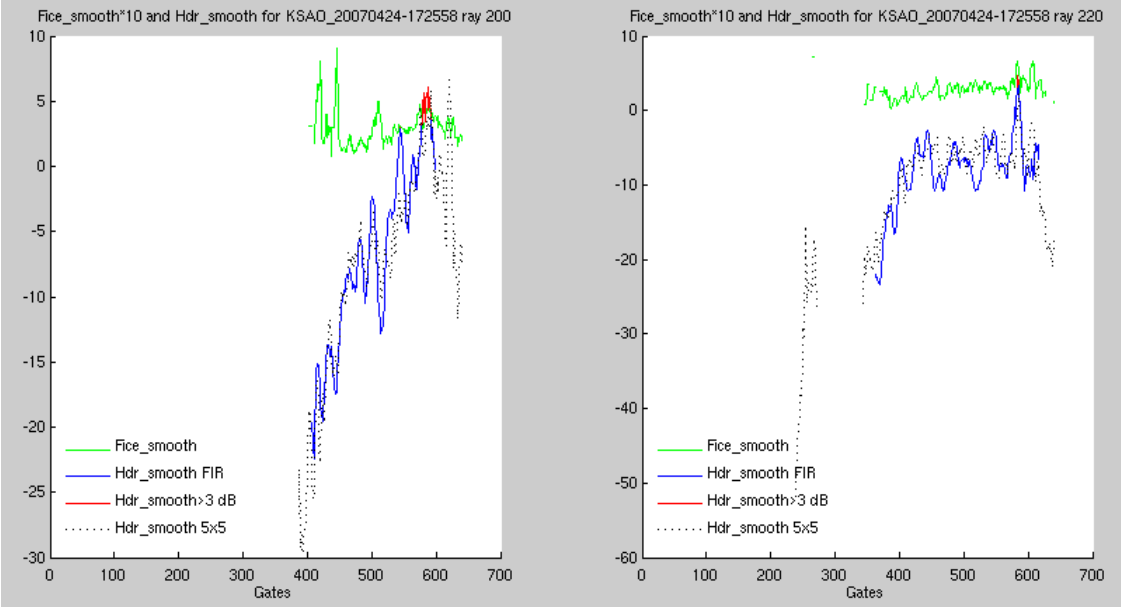

Figure 7-9. Beams #200 and #220 of the "mixed precipitation" case of April 24, 2007 (KSAO_20070424-172558.netcdf), 2 degrees elevation. Compared are spatially smoothed fraction of ice f_{ice} (values were multiplied by 10 for better visibility) and H_{dr} values after spatial smoothing by 5x5 averaging matrix and simple FIR-filtering. Red gates are the H_{dr} FIR-filtered ones that would pass the FM algorithm H_{dr}>3 db threshold and so would be marked as gates with hail. The spatially smoothed H_{dr} values (dotted line) are a little bit better, but still not good enough.

Based on this, the decision was made to supply FM algorithm with smoothed fraction of ice f_{ice} values as a "first guess", and for the gates where f_{ice} values exist simply assign the H_{dr}=6 dB values , with the purpose to pass H_{dr}>3 dB threshold of the FM algorithm. It should be noted that not all gates considered to be "good" based on the filtering techniques described before would have valid f_{ice} values, but this number is much larger than it was based on simply large H_{dr} values. It can significantly slow down the OES algorithm.

Chapter 8

SENSITIVITY OF THE VARIATIONAL SCHEME TO THE CASA REFLECTIVITY Z_h INPUT VARIABLE

The CASA SOCC website has a case study event of April 24, 2007 (p.m.) (http://socc.caps.ou.edu/cases_07.html), with the following description:

"A Tornado Watch was issued in anticipation of a significant severe wx outbreak. Instead, a severe squall line developed just west of IP1, and moved through the test bed from 17-20UTC. Large hail was prevalent along the line. Data were collected at three sites (KSAO, KCYR, and KLWE) in DCAS mode using the 20+40-sec heartbeat. Complete 360deg scans were collected at 2.0deg, and sector scans were collected at 1, 3, 5, 7, 9, 11, and 14 deg. "

One can use the radar data collected during this event to test the sensitivity of the FM model to the input Z_h data. It was stated at (Hogan 2007) that, "…We are effectively assuming that, in relative terms, the error in Z_h is much less than the errors in Z_{dr} and Φ_{dp} so that the retrieval should be forced to be exactly consistent with Z_h…" but the program might be sensitive to the absolute accuracy (absolute calibration) of the input variable Z_h. For this purpose the data from KSAO radar collected at April 24, 2007 at 17:25:58 (KSAO_20070424-172558.netcdf file) was selected. It was used as an input to the OES three times:

original variable representing reflectivity values and modified (increased by 3 dB and decreased by 3dB) values were used.

The next Figure 8-1 shows the original (not modified) input data:

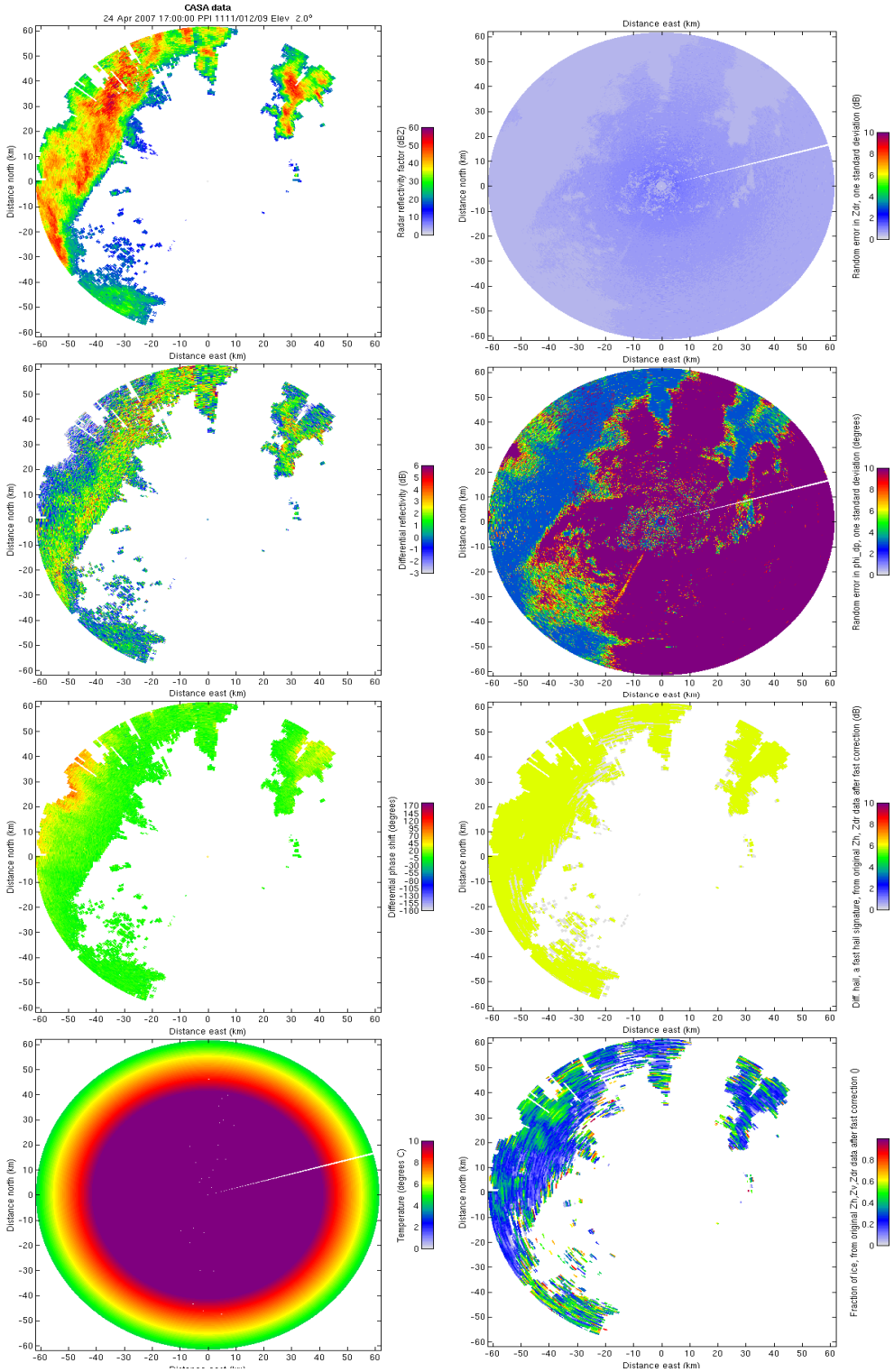

Figure 8-1. CASA April 24, 2007 case of mixed precipitation KSAO_20070424-172558, 2 deg scan. Data used as an input to FM algorithm.

The next Figure 8-2 shows the output of the OES algorithm:

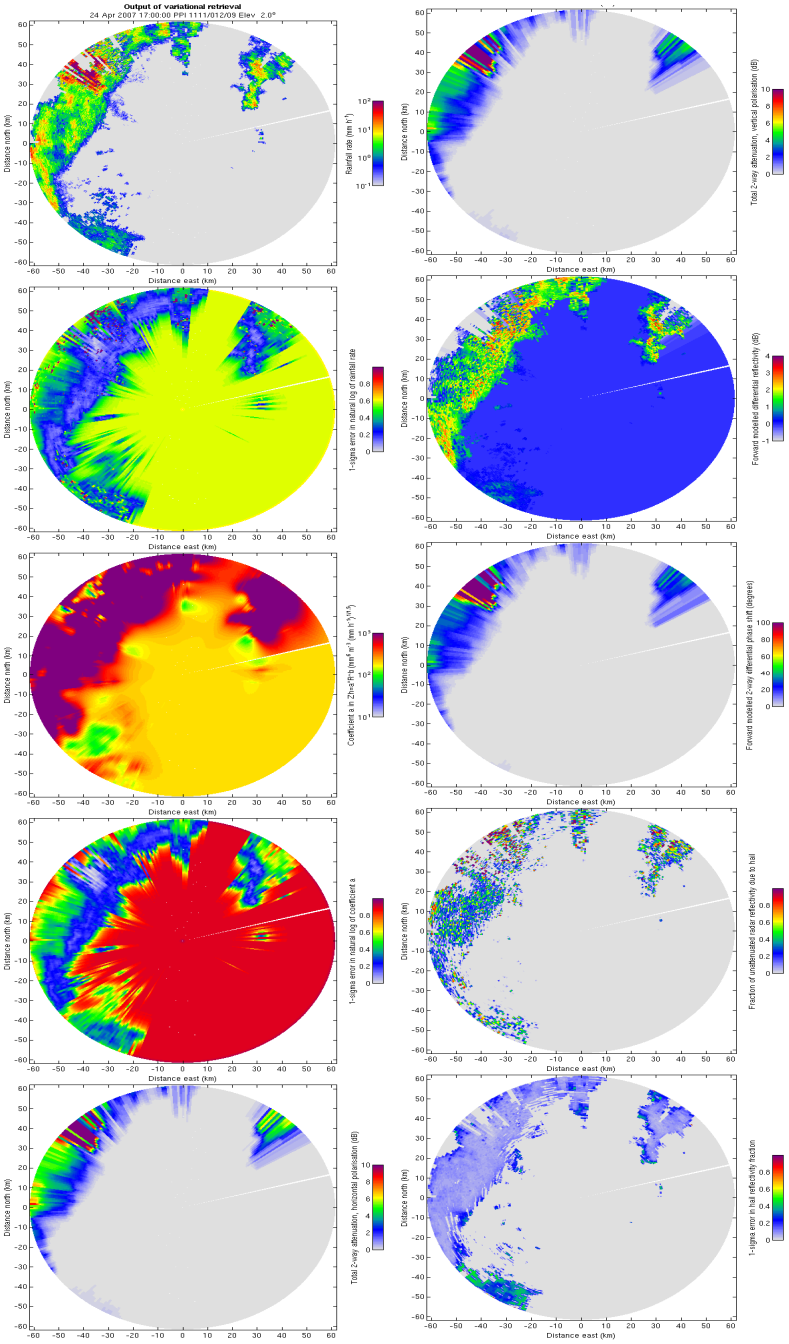

Figure 8-2. FM output for CASA April 24, 2007 case of mixed precipitation KSAO_20070424-172558, 2 deg scan. One can see the areas of the scan where output gets saturated (R, Φ_{dp}, Ah, Av values).

For the case where we increase the reflectivity values in the input data by 3 dB, the output looks as follows (Figure 8-3):

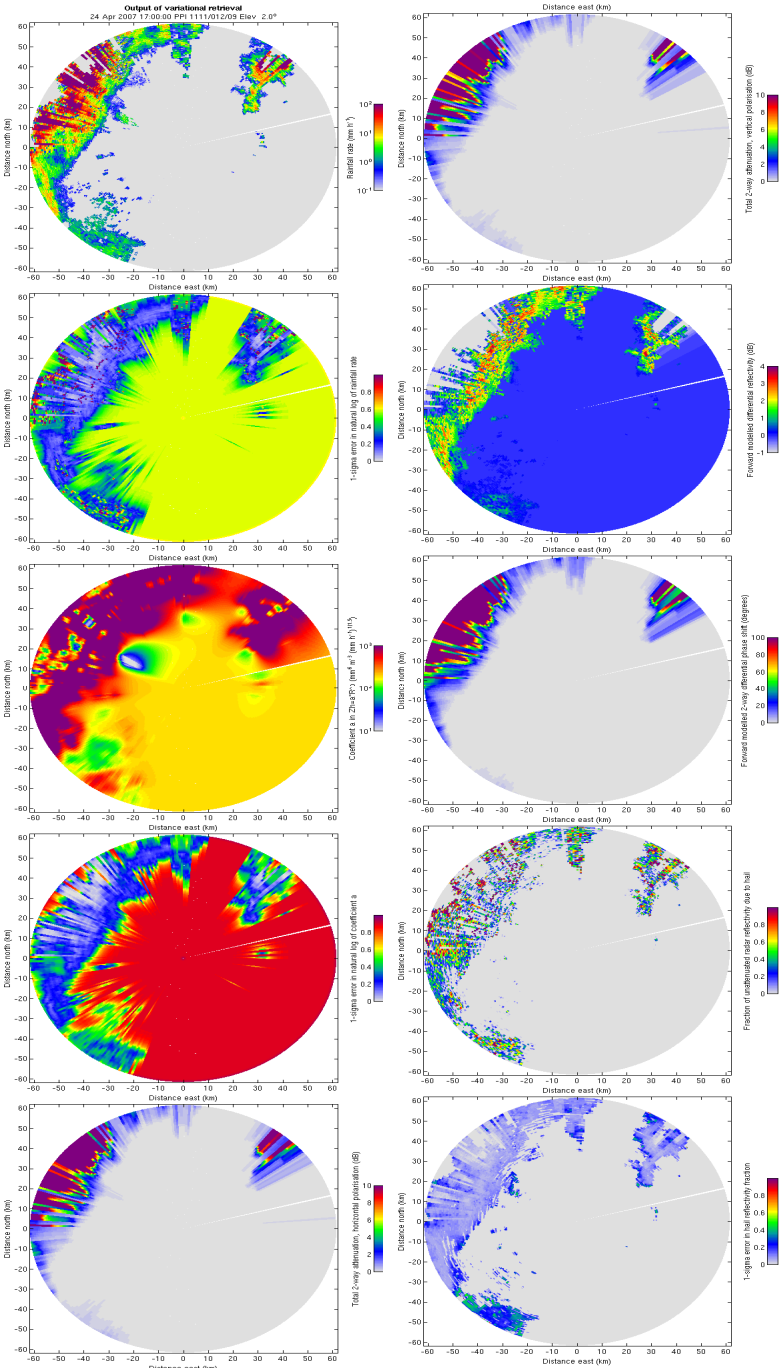

Figure 8-3. FM output for CASA April 24, 2007 case of mixed precipitation KSAO_20070424-172558, 2 deg scan. Zh input values were increased by 3dB. One can see the areas of the scan where output gets saturated (R, Φ_{dp}, Ah, Av values), even more than for original case of not-changed reflectivity.

The next Figure 8-4 shows the output for the reflectivity data decreased by 3dB:

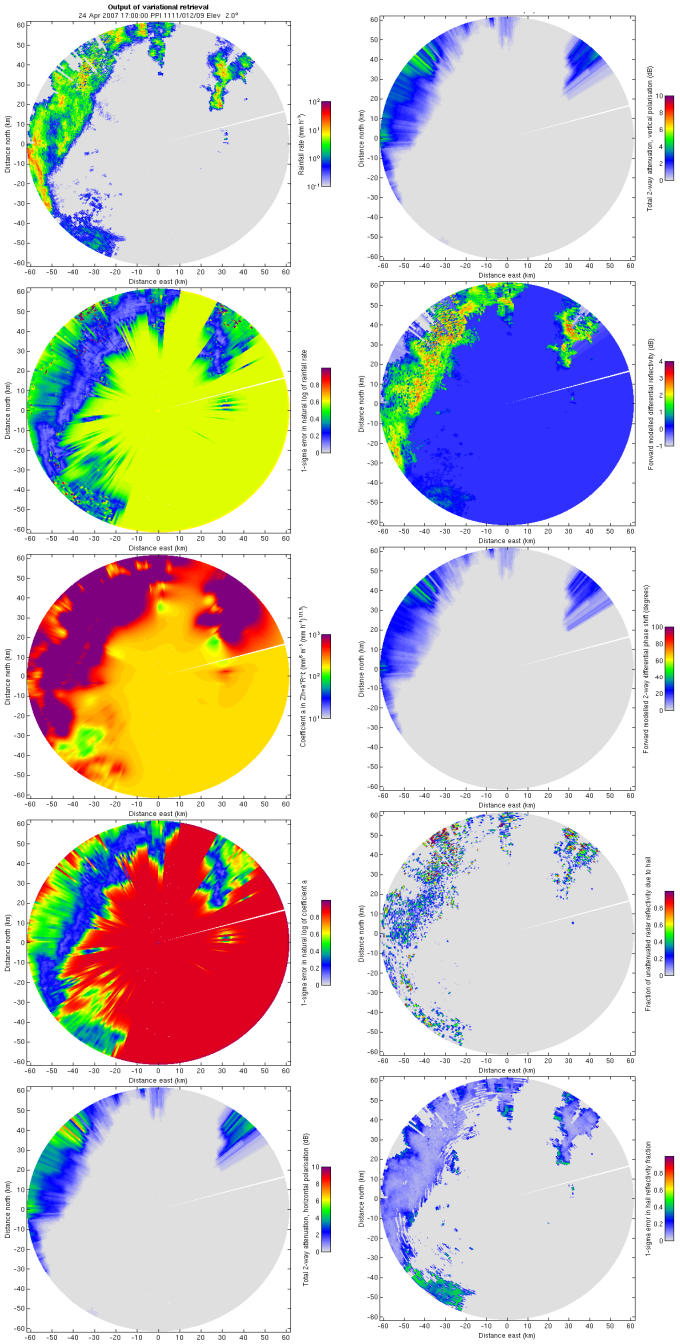

Figure 8-4. FM output for CASA April 24, 2007 case of mixed precipitation KSAO_20070424-172558, 2 deg scan. Zh input values were decreased by 3dB. One can see that there are no areas of the scan where output variables get saturated.

One can compare the maximum values of the Φ_{dp} and A_h variables for these 3 sets of data for each beam of the scan (at end of the beam).

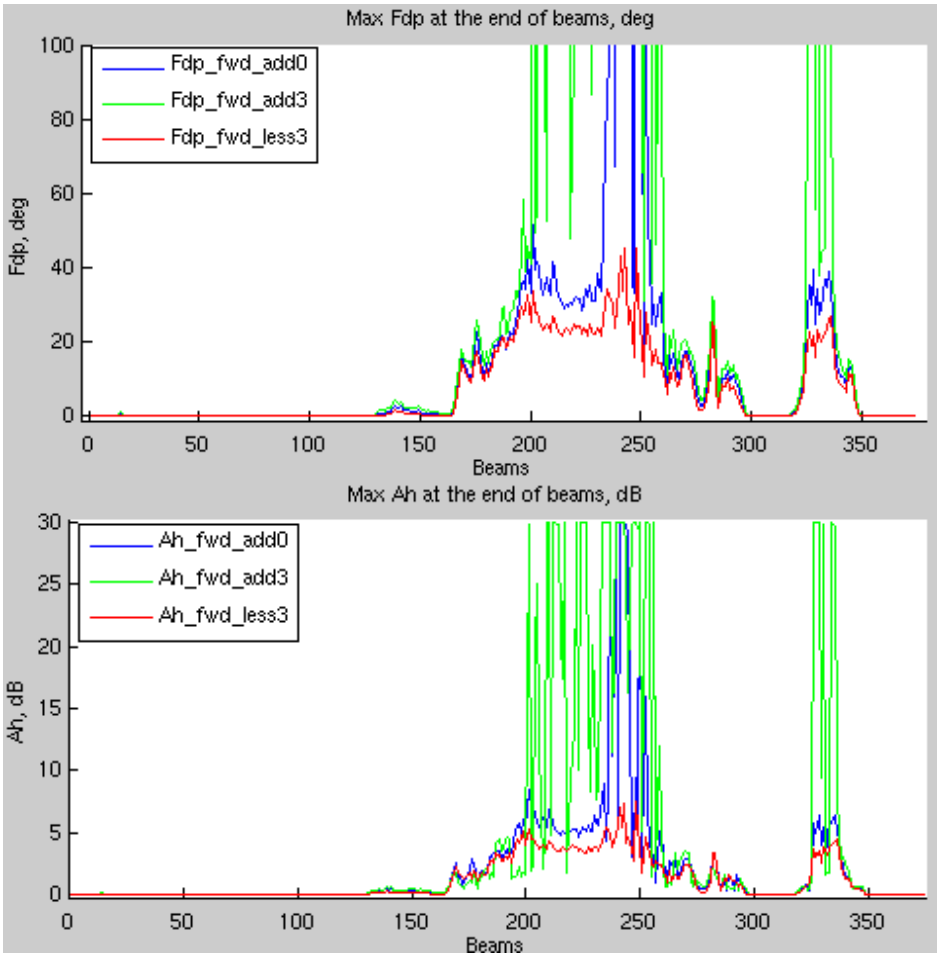

Figure 8-5. Maximum values of predicted by FM values of Φ_{dp} and Ah for 3 input data sets.

It can be seen from Figure 8-5 that for data sets where Z_h was increased by 3dB or even left at the original level, the values of Φ_{dp} and A_h tend to saturate for some beams, especially for ones that go through the core of the storm (beams around #230-250). For the dataset where reflectivity values were decreased by 3 dB there are no saturated Φ_{dp} and A_h data. It has to be noted that experiments were done for reflectivity decreased by 1 and 2 dB, and there were areas of saturated data in the FM output, so -3 dB seems to be the minimum for

decrease in input reflectivity to avoid spuriously large Φ_{dp} values (at least for this dataset).

One can compare these data sets beam-by-beam:

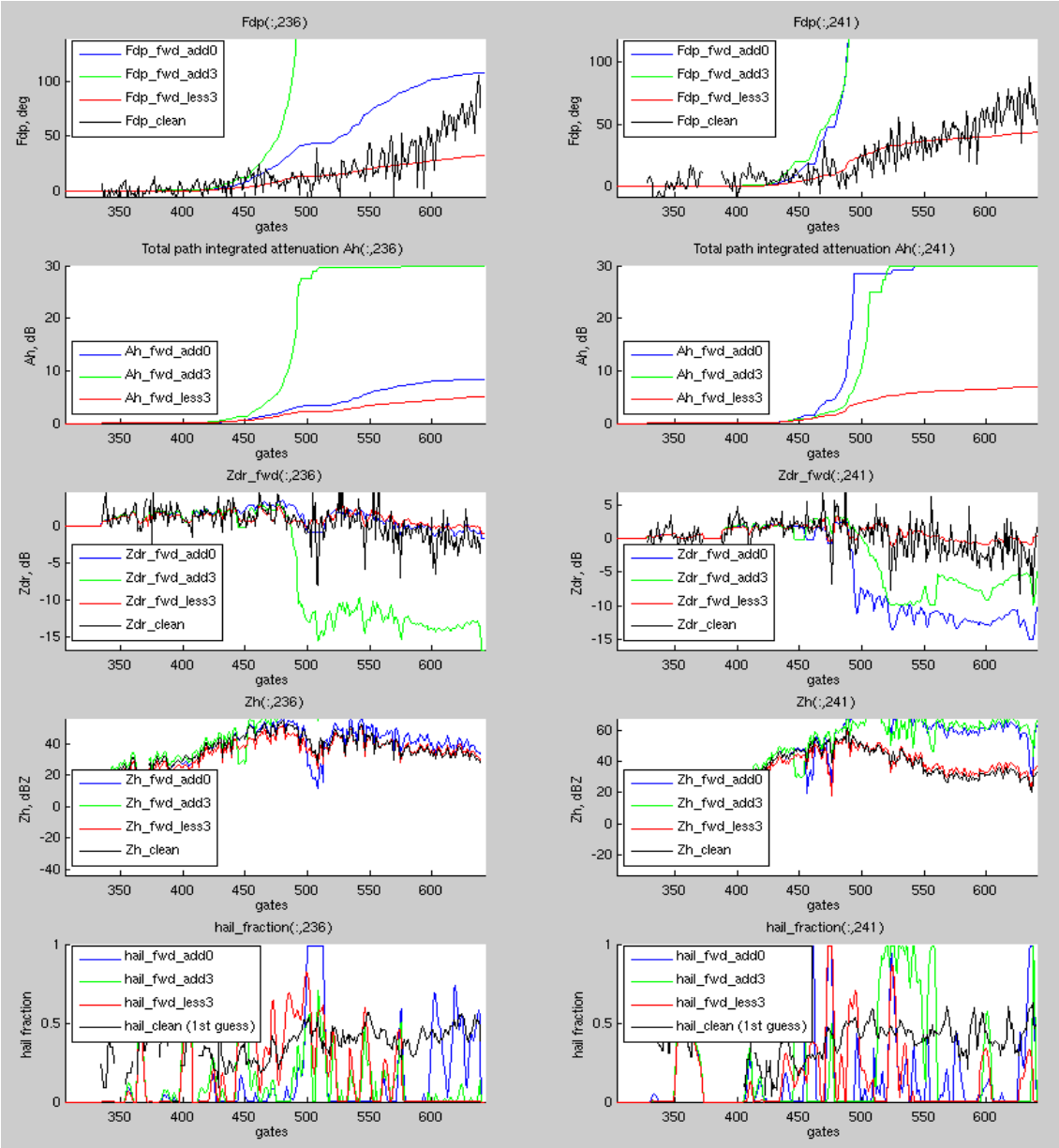

Figure 8-6. Three data sets. Beams #236 and #241 from the FM output for CASA April 24, 2007 case of mixed precipitation KSAO_20070424-172558, 2 deg scan. Shown are forward-modeled Φ_{dp}, Ah, Z_{dr}, Zh and f_{ice} variables, compared to the input variables.

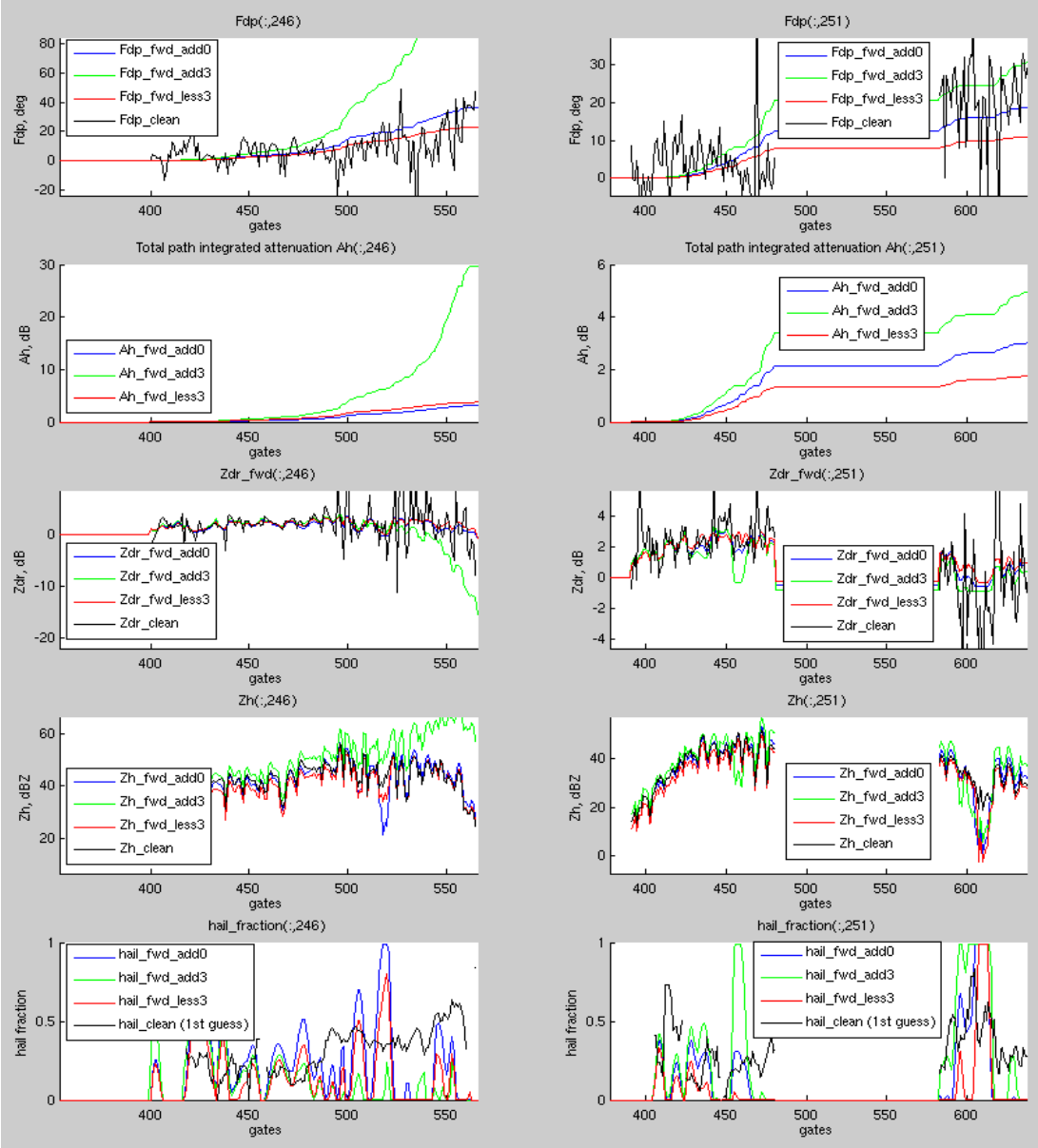

Figure 8-7. Three data sets. Beams #246 and #251 from the FM output for CASA April 24, 2007 case of mixed precipitation KSAO_20070424-172558, 2 deg scan. Shown are forward-modeled Φ_{dp}, Ah, Z_{dr}, Zh and f_{ice} variables, compared to the input variables.

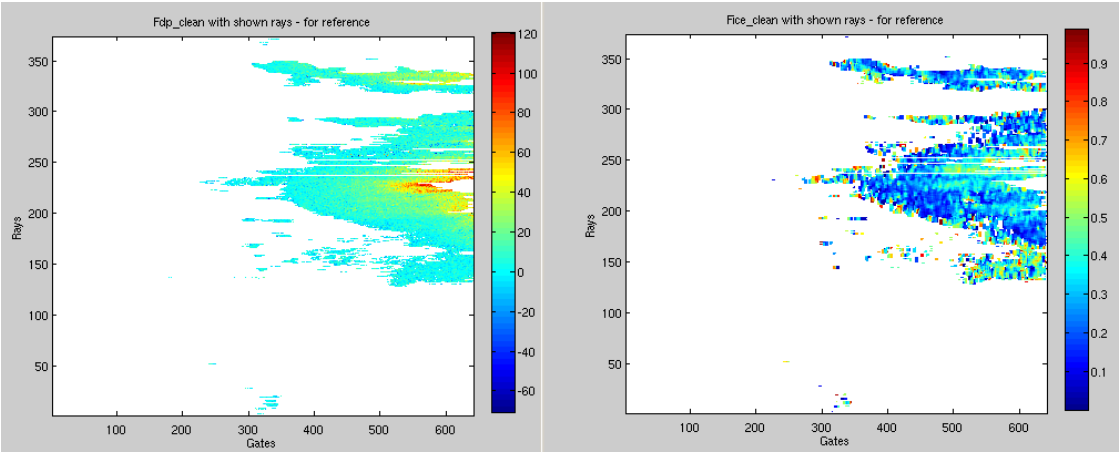

Figure 8-8. Shown are beams selected for beam-by-beam comparison, on Φ_{dp} and fraction of ice maps (for reference).

These selected beams go through the core area of the storm. One can see that this is the “difficult area“for the FM algorithm. From three datasets only one where reflectivity values were decreased by 3 dB (red line) can follow the input data (black line) with sufficient accuracy.

In FM, Z-R relation is used to compute rain rate, and K_{dp} is calculated and used to compute Φ_{dp} values for each gate. So if the input variable Z_h, which is assumed to be measured by CASA radars (to within an uncertainty of 1 dB) is in error (i.e., too “hot” by 3 dB) all calculated variables (like Φ_{dp}, attenuation A_h, A_v) achieve unrealistically high values, and FM cannot correct for this.

Chapter 9

CONTINUITY IN VERTICAL PROFILE

With the purpose to check the consistency of the results of FM in space, one can create the 3-dimensional dataset consisting of forward-modeled variables. For this one should select a sequence of sector scans of the different elevation angles from the same radar, separated by minimal available time interval.

The data of the storm event of 24th of April, 2007 at a time around 17:31 UTC from the KSAO radar located at Chickasha, OC was selected for this test. The six data files representing sector scans at elevation 1, 2, 3, 5, 7, and 9 degrees are:

Table 9-1. Data files of the storm event of 24th of April, 2007 used for vertical continuity test.

Scan elevation, deg	CASA data file name
1	KSAO_20070424-173114.netcdf
2	KSAO_20070424-173119.netcdf
3	KSAO_20070424-173138.netcdf
5	KSAO_20070424-173142.netcdf
7	KSAO_20070424-173147.netcdf
9	KSAO_20070424-173152.netcdf

These sector scans were made during less than one minute, and scan at elevation of 2 deg was a full 360 deg scan. The next figure represents the reflectivity variable of these data files:

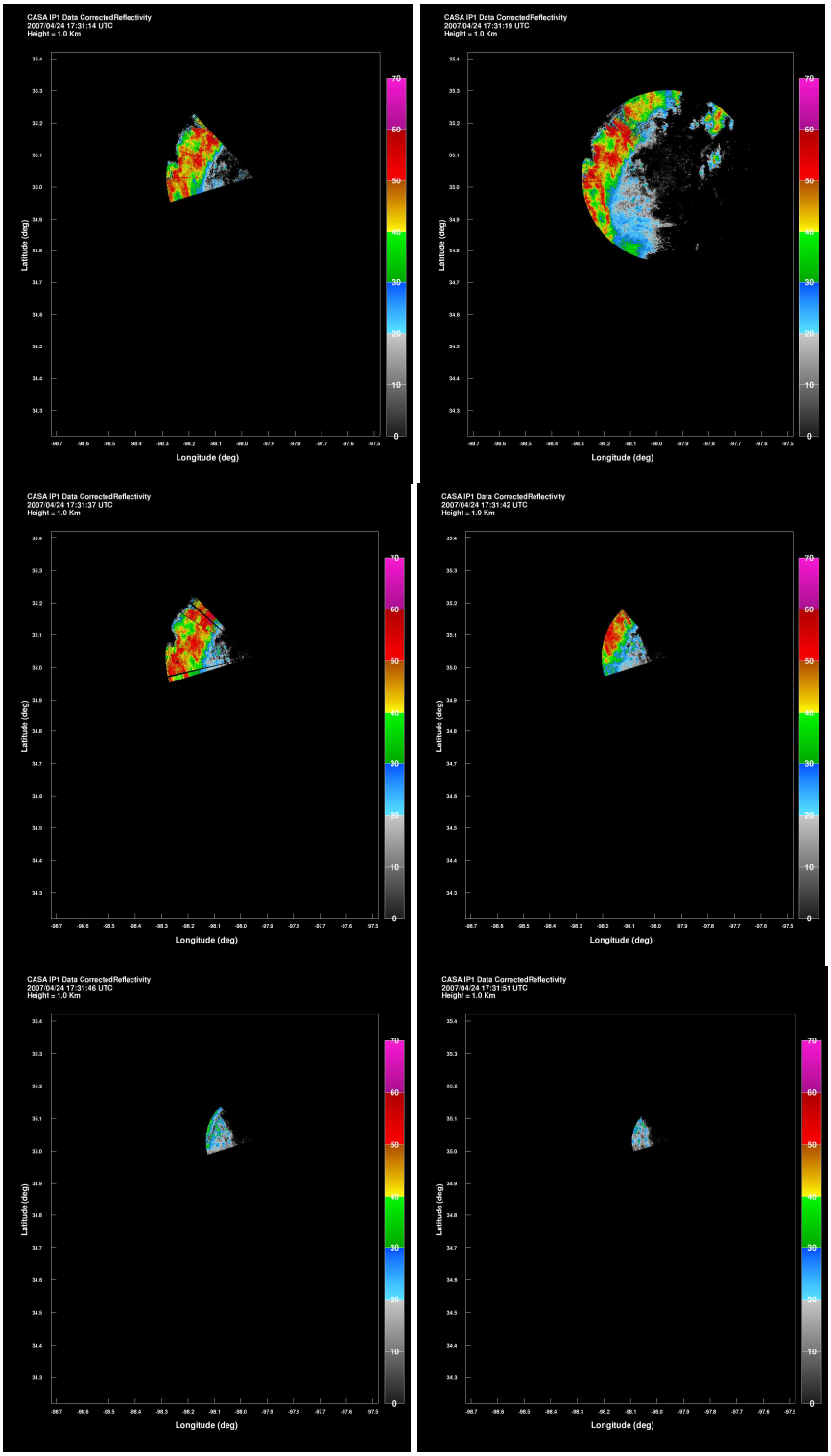

Figure 9-1. CASA data files of 24th of April, 2007, at elevations 1, 2, 3, 5, 7, 9 degrees. Shown is CorrectedReflectivity variable.

These sector scans overlap each other at the azimuth sector of 255-315 degrees. The data was collected in clockwise and counter-clockwise direction, as it can be seen from the next figure:

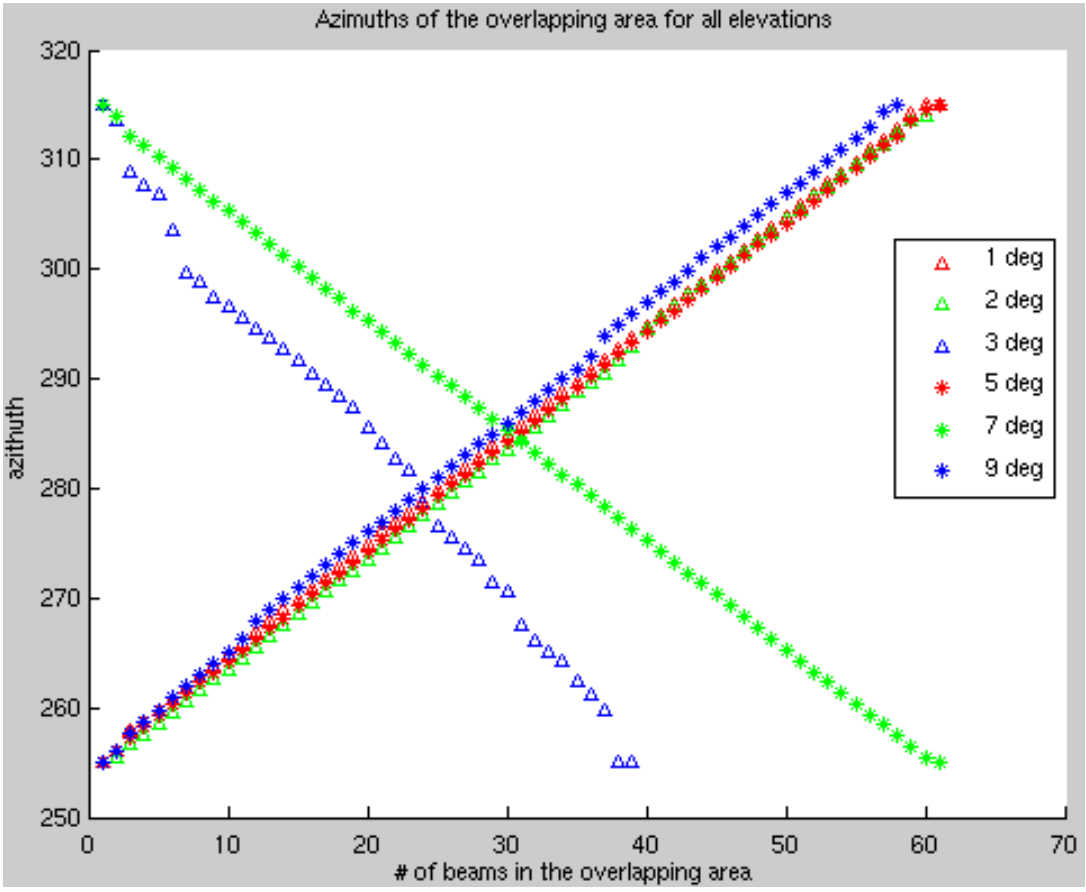

Figure 9-2. CASA data files of 24th of April, 2007, at elevations 1, 2, 3, 5, 7, 9 degrees. Shown are azimuths of the radar beams. It can be seen that azimuth intervals are not constant (3 deg elevation for example).

The azimuth intervals in the scans were not constant, so number of beams in the overlapping area changes from 40 to 60+ beams. So to create the fair 3-D dataset of the forward modeled variables, output data of the FM algorithm needs to be interpolated, as shown on the next figure:

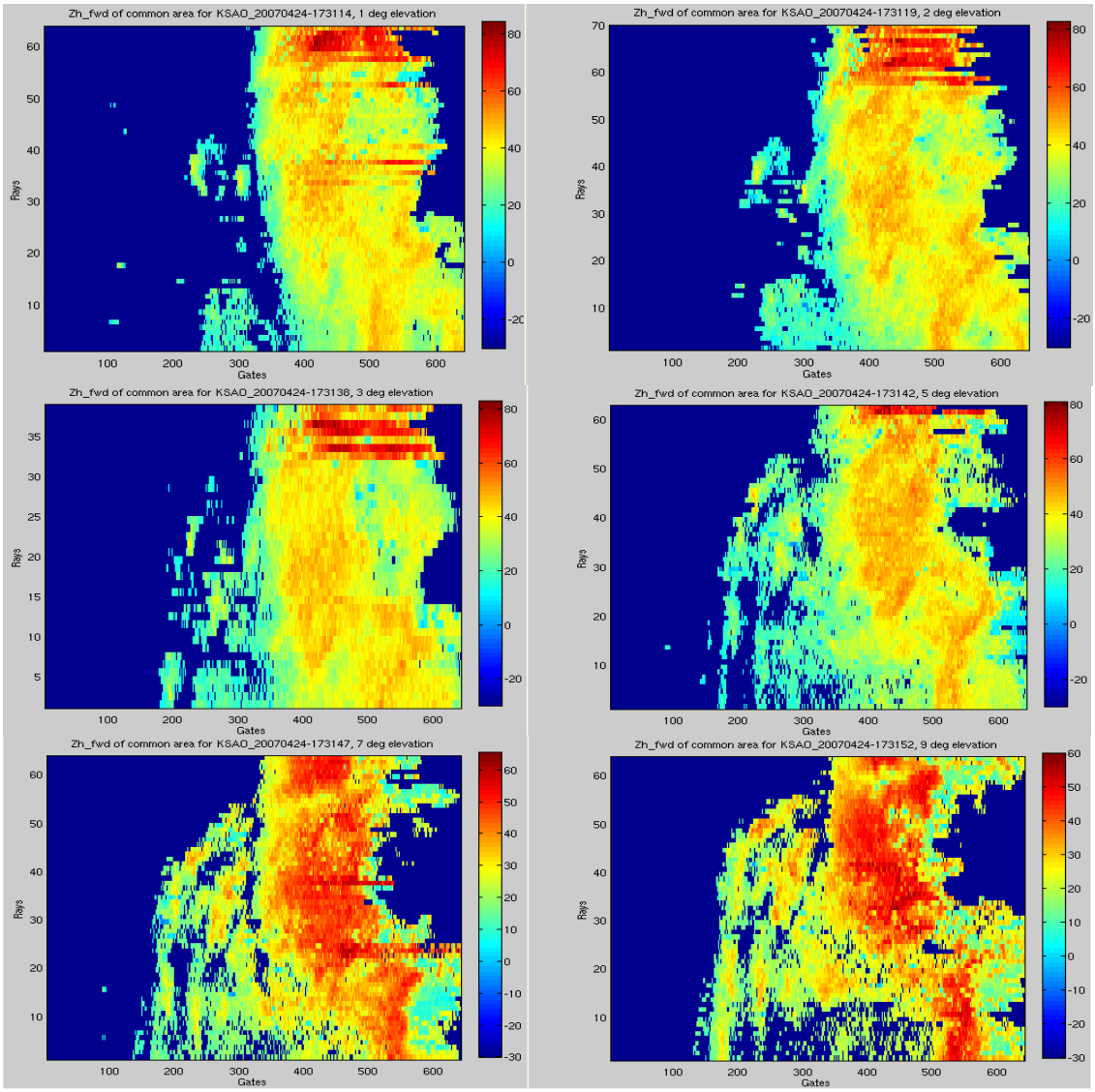

Figure 9-3. FM output for Zh variable for CASA data files of 24th of April, 2007, at elevations 1,2,3,5,7,9 degrees after interpolation.

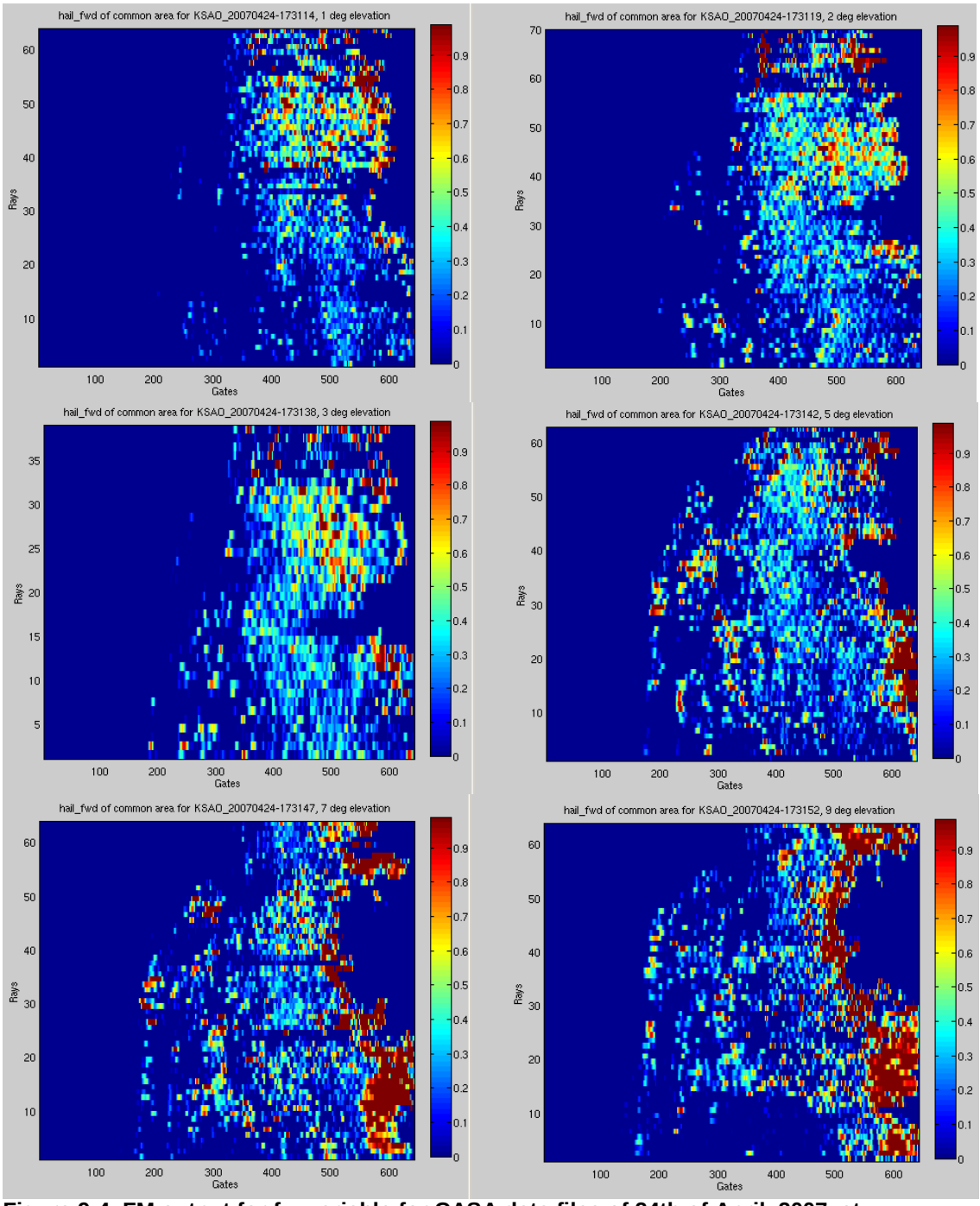

Figure 9-4. FM output for f_{ice} variable for CASA data files of 24th of April, 2007, at elevations 1,2,3,5,7,9 degrees after interpolation.

These scans can be combined into three-dimensional dataset which covers the overlapping area at azimuth 255-315 deg:

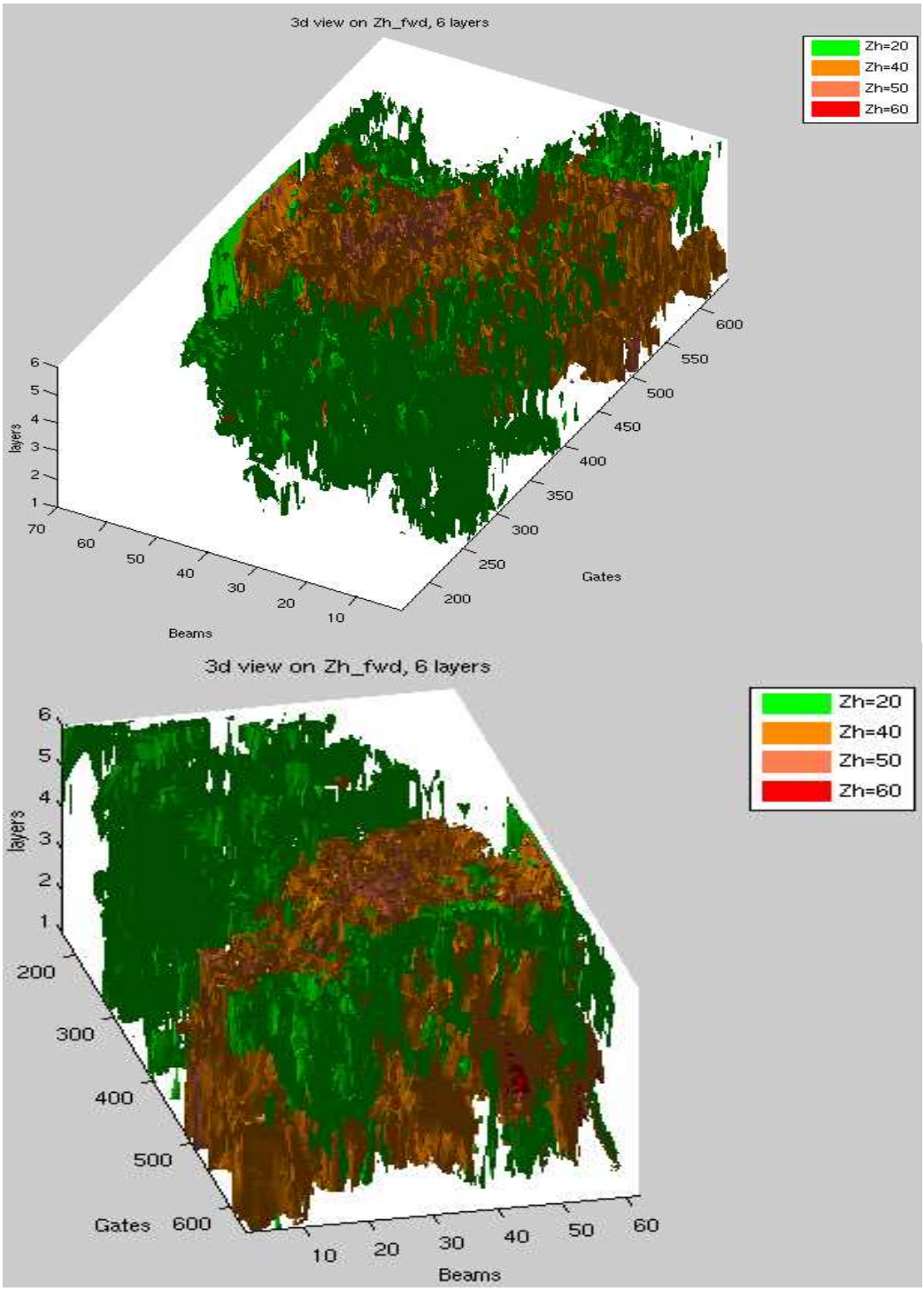

Figure 9-5. 3-D volume of the FM output data from different camera angles for Zh variable, for CASA data files of 24th of April, 2007. 6 layers correspond to scan elevations of 1,2,3,5,7,9 degrees. Shown are areas where forwarded reflectivity is equal to 20,40,50,60 dBz.

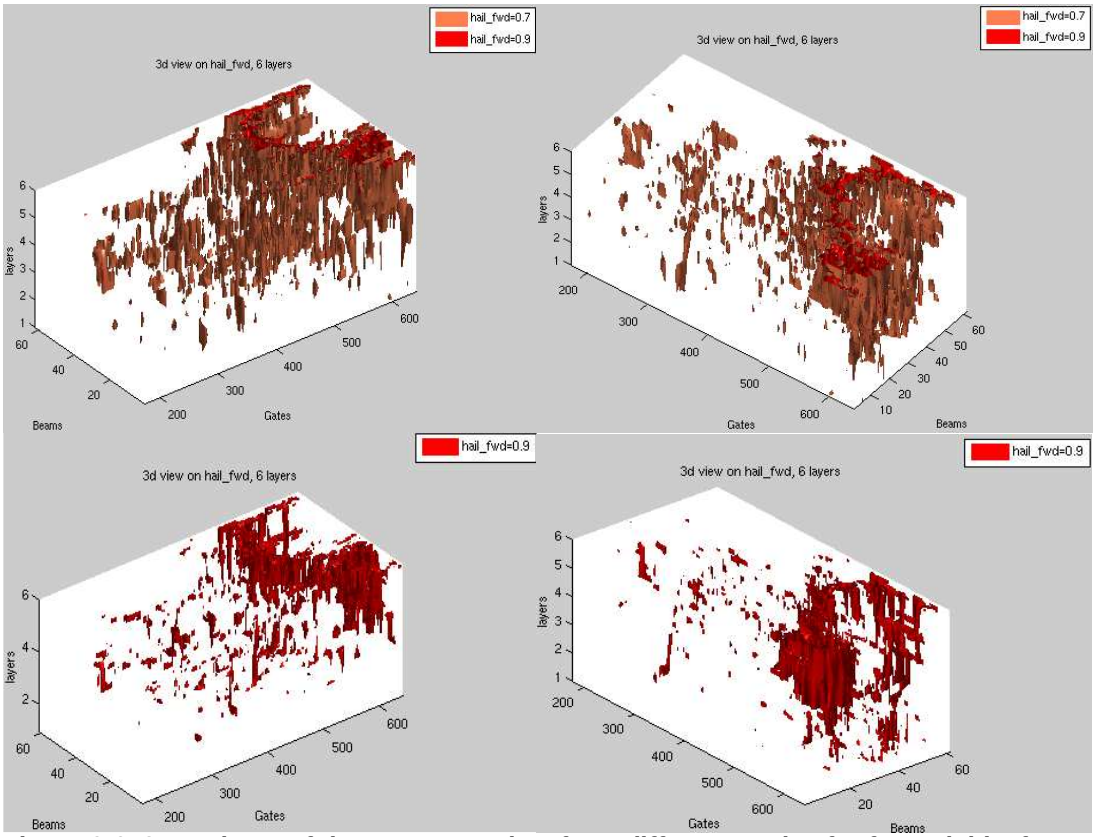

Figure 9-6. 3-D volume of the FM output data from different angles for f_{ice} variable, for CASA data files of 24th of April, 2007. 6 layers correspond to scan elevations of 1,2,3,5,7,9 degrees. Shown are areas where forwarded reflectivity f_{ice} is 0.7 and 0.9.

These figures show that the FM produces some systematic trend (not just random errors), there is correlation and continuity in vertical direction in all the data variables selected for inspection.

Chapter 10

COMPARISON OF THE RAIN RATE STATISTICS FROM FM AND TRADITIONAL METHODS

With the purpose to get some statistics on the OES output values, and to compare FM results to results achieved by other well known methods of radar data processing, one can collect the FM output for some significant amount of time (here 1 hour). For this the CASA data from the radar placed in Chikasha, collected at 10th of June 2007, from 22:12:57 to 23:19:00 was selected. This dataset consists of 27 files, each representing the full 360 degrees scan from CASA KCYR radar at 2 degrees elevation, with time intervals between scans around 3 min:

Table 10-1. CASA Chikasha radar files selected for the dataset

KCYR_20070610-221257.netcdf	KCYR_20070610-224127.netcdf
KCYR_20070610-221547.netcdf	KCYR_20070610-224418.netcdf
KCYR_20070610-221840.netcdf	KCYR_20070610-224724.netcdf
KCYR_20070610-222136.netcdf	KCYR_20070610-225015.netcdf
KCYR_20070610-222136.netcdf	KCYR_20070610-225306.netcdf
KCYR_20070610-222420.netcdf	KCYR_20070610-225556.netcdf
KCYR_20070610-222712.netcdf	KCYR_20070610-225840.netcdf
KCYR_20070610-222712.netcdf	KCYR_20070610-230135.netcdf
KCYR_20070610-223008.netcdf	KCYR_20070610-230424.netcdf
KCYR_20070610-223254.netcdf	KCYR_20070610-230715.netcdf

KCYR_20070610-223545.netcdf	KCYR_20070610-231021.netcdf
KCYR_20070610-223836.netcdf	KCYR_20070610-231311.netcdf
KCYR_20070610-223836.netcdf	KCYR_20070610-231558.netcdf
	KCYR_20070610-231900.netcdf

Figure10-1 shows the first and last of the dataset files:

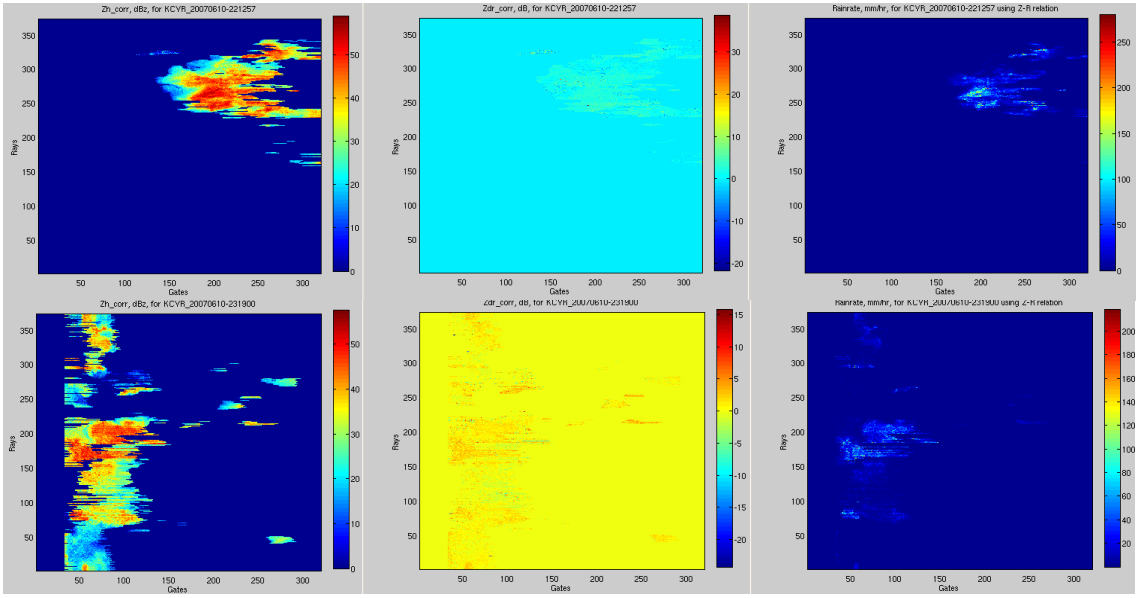

Figure 10-1.CASA dataset, first (KCYR_20070610-221257) and last (KCYR_20070610-231900) files. Shown are Zh_corr, Zdr_corr, and R (calculated using Z-R relation) for "good gates".

Rainrate values obtained from OES algorithm can be compared to values calculated using Z-R relation used in NEXRAD radars,

$R\_zr=(Z/300)^{1/1.4}$, mm/hr, (10.1)

where Z is reflectivity (in mm^6/m^3),

and to values R_kdp calculated using CASA specific differential phase (K_{dp}):

$R\_kdp=18.15*K_{dp}^{0.791}$, (10.2)

where this equation was developed for X-band using frequency scaling and presented in (Wang and Chandrasekar 2010). As K_{dp} is a noisy variable and can have positive and negative (not physical) values, R_kdp was calculated

$$R\_kdp=sign(Kdp)*18.15*(abs(K_{dp}))^{0.791}\ , \qquad (10.3)$$

to avoid non-physical complex values. Here R_kdp can have positive and negative values, but after summation and selection only positive values were used.

The comparison is done for the two intervals of Z_h, based on the value of corrected reflectivity of the CASA data. These two intervals are:

$$Z_{h\_corrected} > 0 \text{ dBZ} \qquad (10.4)$$

$$36 \text{ dBZ} < Z_{h\_corrected} < 40 \text{ dBZ},$$

where the second interval is the interval of “the most frequent” high values of $Z_{h\_corrected}$, which correspond to the core of the storm, as shown on the next figure:

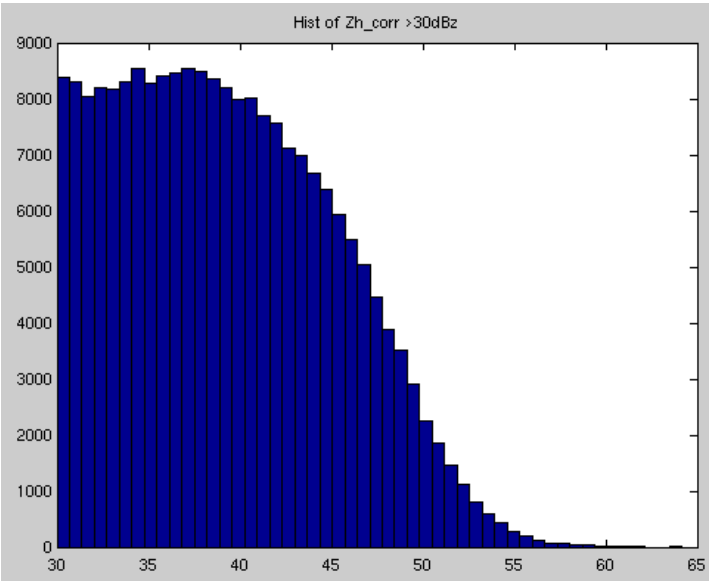

Figure 10-2. Histogram of high values of CASA corrected reflectivity variable Zh_corrected. “The most frequent” high values of Zh_corrected are in the interval 36-40 dBz.

Other limitations for the choice of the gates to compare are:

- gate has to be “good” , which means the CASA data file has “GateFlags”=1 for this gate;
- rain rate R has to be higher than 1 mm/hr for all three methods of calculation.

Figure 10-3 shows the histograms of the rain rate values obtained from FM algorithm:

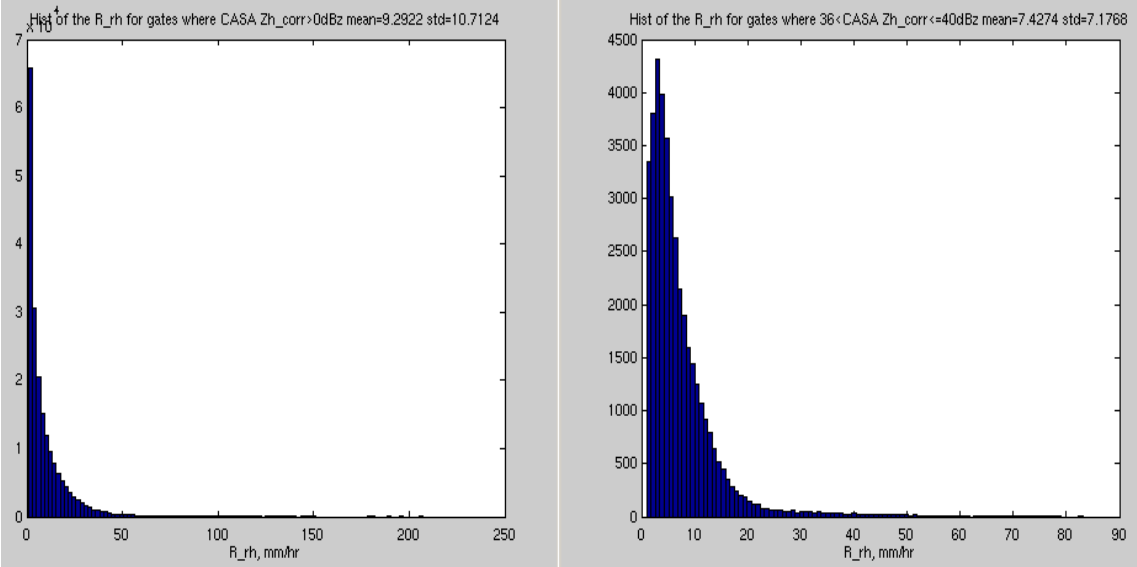

Figure 10-3. Histograms of the rainrate values for one hour CASA data from the KCYR radar, event of June 10, 2007, calculated using FM algorithm, for two selected intervals of corrected reflectivity.

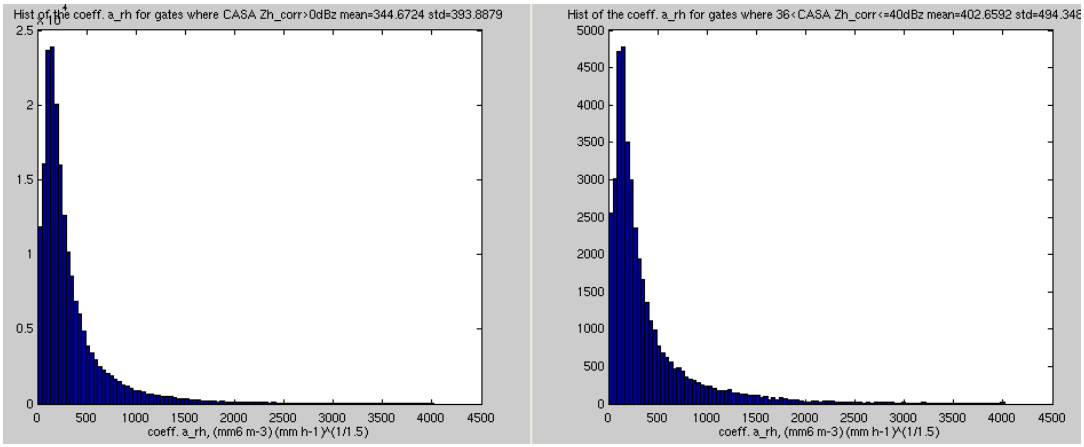

Figure 10-4. Histograms of the values of coefficient "*a*" for one hour CASA data from the KCYR radar, event of June 10, 2007, calculated using FM algorithm, for two selected intervals of corrected reflectivity.

Figure 10-4 shows that the values of coefficient "*a*" calculated using FM are generally higher than *a priori* value (200). Figure10-5 shows the normalized histograms of all three sets of rain rates:

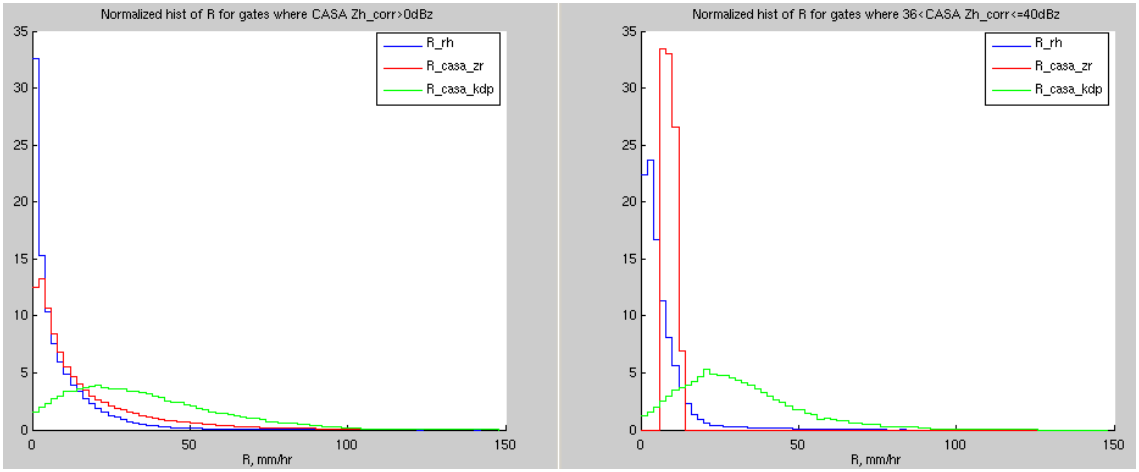

Figure 10-5. Normalized histograms of the rainrate values for one hour CASA data from the KCYR radar, event of June 10, 2007, calculated using FM algorithm, Z-R relation, and Kdp, for two selected intervals of corrected reflectivity.

This figure shows that there is a difference in PDFs of the rain rates calculated using different methods. Generally, the PDF of rain rate should be

similar for the FM and NEXRAD Z-R based methods (since FM is based on the Z-R relation with variable coefficient "*a*"). When the Z interval is fixed between 36-40 dBZ, the mode (the value that occurs most frequently in a data set) from the NEXRAD R is higher than for the FM method (implying that the "*a*" coefficient might be too high relative to 300). The PDF of $R(K_{dp})$ is very different for either case of Z>0 dBZ or for 36<Z<40 dBZ. The shape does not conform to what might be observed by a rain gauge or disdrometer, for example. This is most likely because of spatial smoothing of the derived rain rate from K_{dp} especially within narrow cores of precipitation < 3 km in scale. The peak R is reduced within the core, and moreover the profile of R is "stretched" on either side of the peak because of the filtering technique used to derive K_{dp}. This tends to distort the PDF of R (normally it is exponential or log-normal in shape). However, it does not mean that $R(K_{dp})$ cannot be used to estimate the rain rate (especially the moderate-to-intense rates that contribute most to the rain accumulations). As shown by Wang and Chandrasekar (2010), the $R(K_{dp})$ performs very well when hourly accumulations are compared against a large rain gage network in central Oklahoma.

A different manner of interpreting the PDF is to compute the exceedance probability which is defined as 1-CDF (where CDF is the cumulative distribution function). It is widely used in the radio wave propagation community. Figure 10-6 compares the exceedance probability that R > "abscissa value" for the three algorithms. We show the results which uses all data with Z>0 dBZ. If one considers a moderate R value of 10 mm h^{-1}, then the exceedance probability is

highest for R(K_{dp}), next is the NEXRAD Z-R and then the FM. This trend occurs at all rain rates and the differences are significant. It shows that the "*a*" coefficient in the FM method is frequently estimated as too "high" relative to the NEXRAD fixed coefficient of 300 giving lower R for the same reflectivity value. At this point without comparing the R from the FM method against a rain gage network (for example, using the same dataset as used by Wang and Chandrasekar 2010), the quantitative advantage of using the FM scheme is not clear, for rain rate estimation at X-band using the CASA radars.

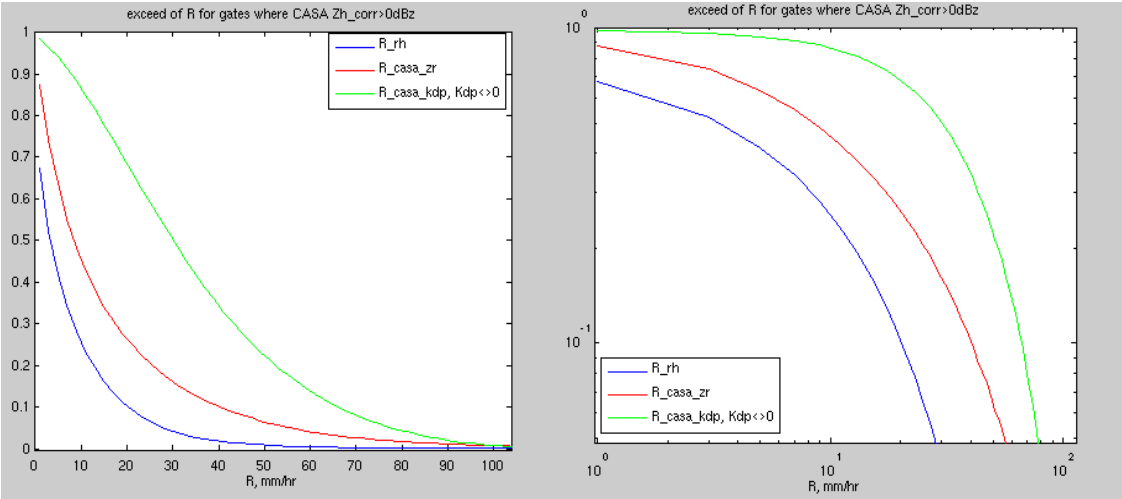

Figure 10-6. Exceedance probability curves of the rain rate values for one hour of CASA data from the KCYR radar, event of June 10, 2007, calculated using FM algorithm, Z-R relation, and Kdp, for Z>0 dBZ. Shown are the curves in linear (left) and log-log scale (right).

The histograms of the differences between rain rate values obtained from FM algorithm and values calculated using R(K_{dp}) and the NEXRAD Z-R methods are shown in Figure 10-7.

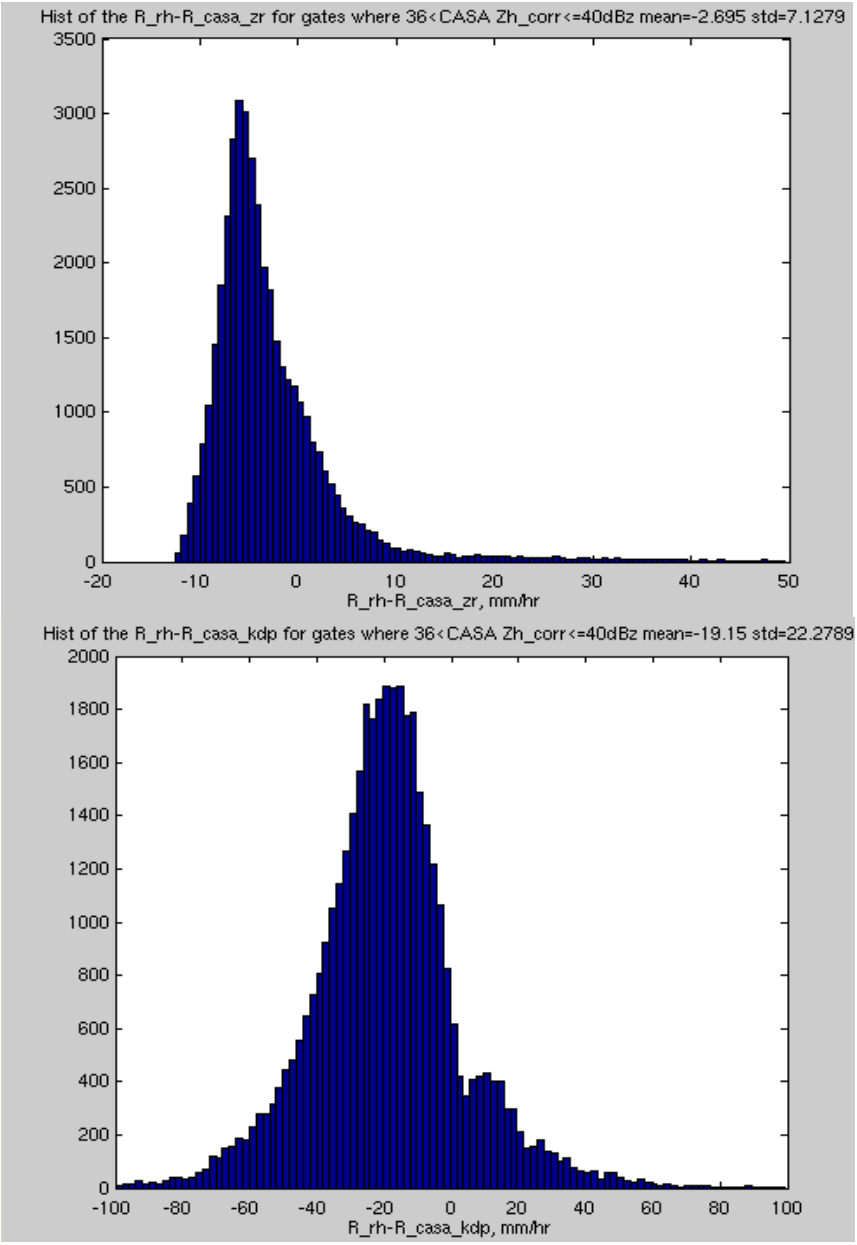

Figure 10-7. The histograms of the differences between rainrate values for one hour CASA data from the KCYR radar, event of June 10, 2007, calculated using FM algorithm and Z-R relation, FM algorithm and Kdp, for 36<Z<40 dBZ.

The histogram of the rain rate differences (R_rh - R_zr) (shown as (R_rh – R_casa_zr) on the Figure 10-7) and (R_rh - R_ kdp) (shown as (R_rh – R_casa_kdp) on the Figure 10-7) are both skewed and the mode is much more negative for (R_rh-R_kdp) relative to (R_rh - R_zr). Also, the standard deviation

of (R_rh - R_kdp) is much larger (22 mm h^{-1}) than for (R_rh - R_zr) (7 mm h^{-1}). The histogram of (R_rh - R_kdp) will appear to be more symmetric if the bias is removed which is not the case for (R_rh - R_zr). The implication of this feature is not clear at the moment.

Table 10-2 shows the normalized bias (NB) and fractional standard deviation (or coefficient of variation, CV) assuming that R_zr is the "truth". The definitions of NB and CV are given below:

$$CV = \text{std}(X)/\text{mean}(R\_zr), \quad (10.5)$$

here X = difference of two rain rates, (R_rh - R_zr) or (R_kdp - R_zr).

$$NB = \text{mean}(X)/\text{mean}(R\_zr) \quad (10.6)$$

Table 10-2. Coefficients of variation and normalized bias data for the "most frequent" Zcorrected interval

R_kdp – R_zr case		**R_rh – R_zr case**	
NB for "most frequent" Zh	1.97	NB for "most frequent" Zh	-0.3
CV for "most frequent" Zh	2.57	CV for "most frequent" Zh	0.8

From Table 10-2 it is clear that NB is very high for R_kdp (overestimate by factor of 2), whereas for R_rh it is more modest but in opposite direction (underestimate by 30%). The CV is very large for R_kdp implying very low correlation between R_kdp versus R_zr. Even the CV for R_rh is still quite high (0.8) but not unreasonably so.

One can divide R_zr range into 4 intervals:

Interval 1: R_zr in range 0-10 mm h^{-1}

Interval 2: R_zr in range 10-20

Interval 3: R_zr in range 20-30,

Interval 4: R_zr in range >30

and calculate mean values of the differences (R_rh-R_zr) (i.e., the bias) and corresponding standard deviations (σ), for these intervals, as shown in figure 10-8:

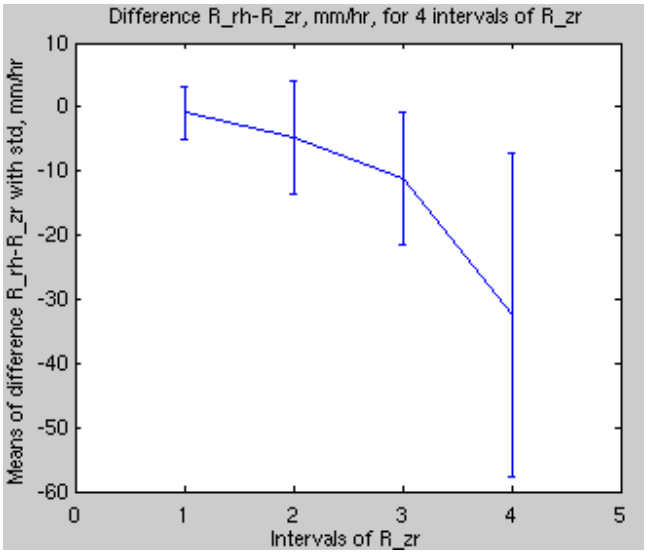

Figure 10-8. Mean values of the difference R_rh-R_zr with corresponding standard deviation values, for 4 intervals of R_zr

Figure10-8 is another way of showing the underestimation of R_rh relative to the R_zr (the latter is considered as "truth" as mentioned earlier). Clearly, the underestimation becomes more as the interval of R_zr increases and so does the standard deviation. At the lower rain rate intervals (<interval #3), the underestimate is not so significant suggesting that the coefficient "a" in the FM is not so different from the NEXRAD coefficient of 300 (recall *a priori* "a" value is

200). But at interval #4 (R_zr>30 mm h^{-1}), the underestimate becomes much larger and the standard deviation is also much larger. This suggests that the *a priori* "a" values are being changed according to the FM in general being too large (>200).

For the other difference, R_rh-R_kdp, and 4 intervals, these calculations are shown in Figure 10-9. In this case, for all intervals the underestimate of R_rh relative to R_kdp is quite large but only increasing slowly with rain rate interval (as compared with Figure 10-8).However, there is no real increase in the standard deviation which is different from Figure 10-8.

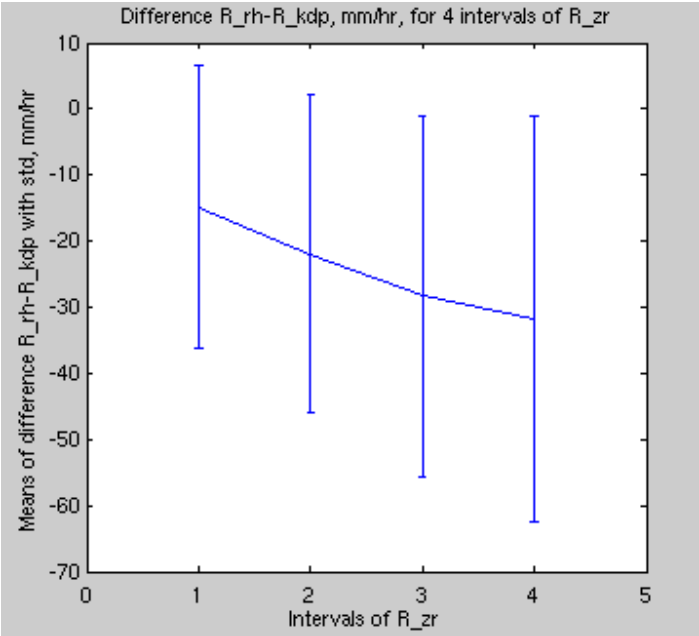

Figure 10-9. Mean values of the difference R_rh-R_kdp with corresponding standard deviation values, for 4 intervals of R_zr

Chapter 11

SUMMARY, CONCLUSIONS AND SUGGESTIONS FOR FUTURE WORK

The variational algorithm (also forward model or FM) was tested for three different dual-polarization radars, with measurements under different meteorological conditions at S- and X-bands. It was shown that this method is able to use information from Φ_{dp} and Z_{dr} variables in an optimal way, to correct for rain and mixed phase attenuation, and to locate areas where hail is present using the combination of Z, Z_{dr}, K_{dp}. It is able to estimate the fraction of the observed reflectivity which is due to hail. It is shown that this method is not only sensitive to the calibration of input variables but also on the pre-processing steps "tuned" for each radar system.

The performance of the original method for X-band CASA data was improved in several ways. The observational errors in the cost function were changed according to empirically established equations to re-balance the effect of corresponding variables, which improves the quality of the algorithm output. The ability of the FM to work in case of mixed phase, wet ice and hail precipitation was also improved, by supplying the "first guess" of the hail location and fraction of reflectivity due to hail at these locations into the algorithm, which then uses this data to automatically converge to the optimal state and makes final decision

about hail location and attenuation. It was shown that FM is able to produce some systematic trend, continuity of the variables values in vertical direction, which makes it possible to show the core of the storm and hail area in 3D.

After modifications, the attenuation correction of Z_h using the FM method works well even in the presence of the hail and mixed rain-hail precipitation, provided that absolute calibration of the input variable Z_h is accurate. For case of pure rain the attenuation correction results of FM method are comparable to other methods (based on differential propagation phase).

We have evaluated the estimation of rain rate by the FM and compared with the NEXRAD Z-R relations as well as with a R-K_{dp} relation. This evaluation is done in several different ways including histograms of rain rate differences, exceedance probabilities and statistics within different rain rate intervals. In general, the rain rates estimated by FM are lower than estimated by the two other selected methods. The reason for this underestimation is likely related to the absolute calibration state of the CASA radar used, in effect the measured reflectivity being too “cold” by several dB.

Future work is to use OES algorithms for the same cases described in (Wang and Chandrasekar 2010) and compare the results to the data from gauge networks (and disdrometer networks as they become more widely deployed). It is important to improve the data quality (using newer fuzzy logic schemes to classify echoes from non-precipitation targets) and to improve absolute calibration of reflectivity via external instruments (such as disdrometer networks).

REFERENCES

Andsager, K., K. V. Beard, and N. F. Laird, 1999: Laboratory measurements of axis ratios for large raindrops*. J. Atmos. Sci*., **56**, 2673–2683.

Atlas, D., W. G. Harper, F. H. Ludlam, W. C. Macklin, 1960: Radar scatter by large hail. *Quart. J. Roy. Meteor. Soc.,* **86**, 468.

Atlas, D. and F. H. Ludlam, 1961: Multi-wavelength radar reflectivity of hailstorms. *Quart. J. Roy. Meteor. Soc.*, **87**, 523-534.

Austin, R. T., and G. L. Stephens, 2001: Retrieval of stratus cloud microphysical parameters using millimeter-wave radar and visible optical depth in preparation for CloudSat. 1. Algorithm formulation. *J. Geophys. Res*., **106**, 28 233–28 242.

Aydin, K., Seliga, T.A., Balaji,V., 1986: Remote sensing of hail with a dual linear polarization radar. *J. Clim. Appl. Meteorol*., **25**, 1475-1486.

Aydin, K., Zhao,Y., Seliga, T.A., 1990: A differential reflectivity radar hail measurement technique; Observations during the Denver hailstorm of 13 June 1984*. J. Atmos. And Oceanic Tech*. **7**, 104-113.

Balakrishnan, N. and Zrnic, D.S. 1990a. Estimation of rain and hail rates in mixed-phase precipitation*. J. Atmos. Sci*., **47**: 565–583, 1990a.

Balakrishnan, N. and Zrnic, D.S. 1990b. Use of polarization to characterize precipitation and discriminate large hail. ***J. Atmos. Sci***., **47**: 1525–1540, 1990b.

Battan, L. J., 1973. “Radar attenuation of the Atmosphere.” Univ. of Chicago Press, Chicago, Illinois.

Battan, L. J., S. R. Browning and B. M. Herman, 1970: Attenuation by microwaves by wet ice spheres*. J. Appl. Meteor*., **9**, 832-834.

Battan, L. J., 1971: Radar attenuation by wet ice spheres. *J. Appl. Meteor*., **10**, 247-252.

Bringi V. N., R. M. Rasmussen, and J. Vivekanandan, 1986a: Multiparameter radar Measurements in Colorado convective storms. Part I: Graupel melting studies. *J. Atmos. Sci.,* **43**, 2545–2563.

Bringi V. N., J. Vivekanandan, and J. D. Tuttle, 1986b: Multiparameter radar measurements in Colorado convective storms. Part II: Hail detection studies. *J. Atmos. Sci.*, **43**, 2564–2577.

Bringi, V.N., V. Chandrasekar, N. Balakrishnan, and D.S. Zrnic, 1990: An examination of propagation effects in rainfall on radar measurements at microwave frequencies. *J. Atmos. Oceanic Technol*., **7**, 829 840.

Bringi, V.N. and A. Hendry: Technology of Polarization Diversity Radars for Meteorology. In *Radar in Meteorology*. D. Atlas, Ed., 153 190, Boston, MA, American Meteorological Society, 1990.

Bringi, V.N. and V. Chandrasekar, 2001: Polarimetric Doppler Weather Radar: Principles and Applications. Cambridge.

Brotzge, J., K. Brewster, B. Johnson, B. Philips, M. Preston, D. Westbrook, and M. Zink, 2005: CASA's first test bed: Integrative Project #1 (IP1). *32nd Conference on Radar Meteorology*, Albuquerque, NM.

Cheng, L. and English, M. 1983: A relationship between hailstone concentration and size. *J. Atmos. Sci.*, **40**: 204–213.

Depue, T., P. Kennedy, and S. Rutledge, 2007: Performance of the hail differential reflectivity (HDR) polarimetric hail indicator. *J. Appl. Meteor. Clim*. **46**, 1290 – 1301.

Doviak, R.J. and Zrnic, D.S. Doppler Radar and Weather Observations. 2nd edition, San Diego, CA, Academic Press, 1993.

Eccles, P. J. 1975: Developments in Radar Meteorology: National Hail Research Experiment to 1973. *Atmos. Technol*., Winter, 1974-75, 34-35.

Goddard, J. W. F., J. Tan, and M. Thurai, 1994: Technique for calibration of meteorological radars using differential phase. *Electron. Lett*., **30**, 166–167.

Golestani, Y., Chandrasekar, V., and Bringi, V. N. 1989: Intercomparison of multiparameter radar measurements. Prep., Radar Meteorol. Conf., 24th, 1989, 309-314.

Gunn, K. L. S., and T.W. R. East, 1954: The microwave properties of precipitation particles. *Quart. J. Roy. Meteor. Soc*., **80**, 522 545.

Heymsfield A. J., A. R. Jameson, and H. W. Frank, 1980: Hail growth mechanisms in a Colorado storm: Hail formation processes. *J. Atmos. Sci*., **37**, 1779–1807.

Hitschfeld W., and J. Bordan, 1954: Errors inherent in the radar measurements of rainfall at attenuating wavelengths. *J. Meteor*, **11**, 58–67.

Huang, G.J., V.N. Bringi, S. van den Heever, and W. Cotton, 2005: Polarimetric radar signatures from RAMS microphysics. *32nd Conference on Radar Meteorology*, Albuquerque, NM, Amer. Meteor. Soc., 24-29.

Hogan R.J., 2007: A Variational Scheme for Retrieving Rainfall Rate and Hail Reflectivity Fraction from Polarization Radar. *J. Appl. Meteor. and Climat*., **46**, 1544.

Keeler, R.J., B.W. Lewis and G.R. Gray, 1989: Description of NCAR/FOF CP 2 Meteorological Doppler Radar. *24th Conf. on Radar Meteorology*, Tallahassee, Florida, Amer. Meteor. Soc., 589-592

Liu, Y., G.J. Huang, V.N. Bringi and S. van den Heever, 2006: Estimation of X band radar attenuation due to wet hail: A simulation study using RAMS supercell case and dual wavelength (S/X band) radar. ERAD06, 49-52.

Liu, Y., V. N. Bringi, and M. Maki, 2006: Improved Rain Attenuation Correction Algorithms with Adaptation to Drop Shape Models, *IEEE International Geoscience and Remote Sensing Symposium 2006*, Denver, Colorado.

Liebe, H. J., T. Manabe, and G. A. Hufford, 1989: Millimeter-wave attenuation and delay rates due to fog/cloud conditions. *IEEE Trans. Antennas Propag*., **37**, 1617–1623.

Löhnert, U., S. Crewell, and C. Simmer, 2004: An integrated approach toward retrieving physically consistent profiles of temperature, humidity, and cloud liquid water. *J. Appl. Meteor.*, **43**, 1295–1307.

Meyers, M.P., R.L. Walko, J.Y Harrington, and W.R. Cotton, 1997: New RAMS cloud microphysics parameterization. Part II: the two moment scheme. *Atmos. Res*., **45**, 3-39.

McLaughlin, D. J. et al., 2005: Distributed Collaborative Adaptive Sensing (DCAS) for improved detection, understanding, and predicting of Atmospheric hazards, in *Proc. of 85th AMS Annual Meeting*, San Diego, California.

Marshall, J. and W. Palmer, 1949: The distribution of raindrops with size. *J. Meteorology*, **5**, 165-166.

Matrosov, S.Y., K.A. Clark, B.E. Martner, and A. Tokay: X-band polarimetric radar measurements of rainfall. *J. Appl. Meteor.*, **41**, 941-952, 2002.

Park, S.G., V.N. Bringi, V. Chandrasekar, M. Maki and K. Iwanami, 2005: Correction of radar reflectivity and differential reflectivity for rain attenuation at X band. Part I: theoretical and empirical basis. *J. Atmos. Oceanic Technol*., **22**, 1621-1632.

Park, S.G., M. Maki, K. Iwanami, V.N. Bringi and V. Chandrasekar, 2005: Correction of radar reflectivity and differential reflectivity for rain attenuation at X band. Part II: evaluation and application. *J. Atmos. Oceanic Technol*., **22**, 1633-1655.

Sadiku, M. N., 1985: Refractive index of snow at microwave frequencies. *Applied Optics*, **24**, No. 4.

Smyth, T. J., and A. J. Illingworth, 1998a: Correction for attenuation of radar reflectivity using polarization data. *Quart. J. Roy. Meteor. Soc*., **124**, 2393–2415.

Smyth, T. J., and A. J. Illingworth, 1998b: Radar estimates of rainfall rates at the ground in bright band and non-bright band events. *Quart. J. Roy. Meteor. Soc*., **124**, 2417–2434.

Smyth, T. J., T. M. Blackman, and A. J. Illingworth, 1999: Observations of oblate hail using dual-polarisation radar and implications for hail-detection schemes. *Quart. J. Roy. Meteor. Soc*., **125**, 993–1016.

Tabary, P., G. Vulpiani, J. J. Gourley, A. J. Illingworth and O. Bousquet, 2008: Unusually large attenuation at C band in Europe: How often does it happen? What is the origin? Can we correct for it?. ERAD08.

Testud, J., E.L. Bouar, E. Obligis, and M. Ali Mehenni, 2000: The rain profiling algorithm applied to polarimetric weather radar. *J. Atmos. Oceanic Technol*., **17**, 322-356.

Vulpiani, G., P. Tabary, J. Prent du Chatelet, O. Bouquet, M. L. Segond, and F. S. Marzano, 2007: Hail detection using a polarimetric algorithm at C band: Impact on Attenuation Correction. *33rd Conference on Radar Meteorology*, Cairns, Australia, Amer. Meteor. Soc.

Waterman, P., 1969: Scattering by dielectric obstacles. Alta Freq., **38**, 348–352.

Wilson, D. R., A. J. Illingworth, and T. M. Blackman, 1997: Differential Doppler velocity: A radar parameter for characterizing hydrometeor size distributions. *J. Appl. Meteor*., **36**, 649–663.